

Modelling with Hysteresis

for Oil Reservoir Simulation

Eric Baruch Gutierrez Castillo

Technische Universiteit Delft

MODELLING WITH HYSTERESIS

FOR OIL RESERVOIR SIMULATION

by

Eric Baruch Gutierrez Castillo

in partial fulfilment of the requirements for the degree of

Master of Science
in Applied Mathematics

at the Delft University of Technology,
to be defended publicly on Monday October 31, 2016.

Supervisor: Dr. ir. J. E. Romate
Thesis committee: Prof. dr. ir. C. Vuik, TU Delft
Dr. ir. J. E. Romate, TU Delft/Shell Global Solutions
Dr. B. J. Meulenbroek, TU Delft

An electronic version of this thesis is available at <http://repository.tudelft.nl/>.

CONTENTS

1	Introduction	1
1.1	Permeability	1
1.2	Scanning Curves	3
2	Preliminaries	5
2.1	Transport Equations	5
2.1.1	General Formulation	5
2.2	Formulations for incompressible fluid	6
2.2.1	Convection-Diffusion Equation	7
2.2.2	Buckley-Leverett Equation	7
2.3	Rarefaction and Shock Waves	8
2.3.1	Non-Linear Flux Function	8
2.3.2	Rarefaction Waves	9
2.3.3	Shock Waves	10
3	Finite Volume Methods	11
3.1	Discretized Flow Equations	11
3.1.1	Space Discretization	11
3.1.2	Time Discretization	12
3.1.3	Matrix Formulation	13
3.1.4	Source Term and Boundary Conditions	14
3.2	The Implicit Pressure Explicit Saturation (IMPES) Method	16
3.3	Dealing with Non-Linearity	17
3.3.1	Weighting Transmissibilities	17
3.3.2	Local Linearization of Transmissibilities	17
4	Relative Permeability Hysteresis & Capillary Pressure	19
4.1	Physical Background	19
4.1.1	Phase Saturations	19
4.1.2	Wettability	19
4.1.3	Land's Theory	20
4.2	Carlson	21
4.2.1	Estimating the trapping	22
4.2.2	Estimating C	24
4.3	Killough	25
4.3.1	Wetting Phase Hysteresis	26
4.4	The Scanning Hysteresis Model	27
4.4.1	The SHM Equations	28
4.5	Larsen & Skauge	29
4.5.1	Three-phase systems	29
4.5.2	The WAG Model	30
4.6	Capillary Pressure	32
4.6.1	Killough	32
4.6.2	Kleppe et al	33
5	Modelling with Hysteresis	35
5.1	The Buckley-Leverett Solution	35
5.2	The Buckley-Leverett Solution with History	37
5.2.1	Primary Imbibition	37
5.2.2	Secondary Drainage	40
5.2.3	Hysteresis Cycles	44

6	Time Dependent Bounding Curves with History	47
6.1	An Example	47
6.1.1	Low Salinity Water Injection	48
6.2	Time Dependency of Scanning Curves	50
6.2.1	Killough and Carlson.	50
6.2.2	Scanning Hysteresis Model	51
6.2.3	Option 3	53
6.2.4	Capillary Pressure	54
6.3	General Methodology	56
7	Numerical Implementation	59
7.1	Numerical Algorithms.	59
7.1.1	IMPES vs FIM	59
7.1.2	Scanning Curves Algorithm	60
7.1.3	Capillary Pressure	62
7.1.4	Land's Constant	63
7.1.5	Extended Bounding Curves	65
7.2	Numerical Examples	66
7.2.1	Sharp Salinity Drop	66
7.2.2	Gradual Salinity Increment	68
7.2.3	Sharp Salinity Surge	69
8	Overall Remarks	71
8.1	Classification of Hysteresis Models	71
8.2	Classification of Time-Dependent Hysteresis Models	72
8.3	Final Remarks.	73
	Bibliography	75

1

INTRODUCTION

In petroleum reservoir engineering various techniques are used to enhance the oil recovery from a reservoir. Practices such as water and gas injection have the secondary effect of changing the internal configuration of the fluids inside the reservoir. Afterwards the system behaves differently, depending not only on the present state of the reservoir but also on its previous history. Several variables presenting this “memory”, known as hysteresis, must be integrated properly into the simulation.

Such variables are usually determined empirically, but it is also possible to predict these functions using analytic models. Hysteretic variables and their modelling are the main topic of this document. In particular, models to predict the values of the relative permeabilities and capillary pressure of a system in porous media will be studied.

1.1. PERMEABILITY

Before describing hysteresis, let us first review the definition of permeability. It represents the capacity for flow through porous material, with higher permeability representing higher capacity. The relation between the permeability k of a fluid and its flow q (per square unit) is specified by Darcy’s law:

$$q = -\frac{k \Delta P}{\mu L} \quad (1.1)$$

where μ is the viscosity of the fluid, ΔP is the pressure gradient, and L the length of the material through which the fluid moves.

Permeability in this case is determined by the porous material alone. However for multiple phase flow, that is, a system containing two or more fluids, the presence of one fluid affects the flow of the others. The capacity of one phase to flow with respect to the others is called the relative permeability. We call absolute or intrinsic permeability the one determined by the solid material, and it is generally considered constant. The total permeability is the product of the absolute and relative permeabilities.

As explained in chapter 4, the fluids in a system are often characterized by their wettability. Since water has higher wettability than oil, in a two phase system they are usually referred to as the wetting and the non wetting phase, respectively.

The fraction of the pore space occupied by each phase in the control volume is called its saturation. The saturations of the wetting phase and non wetting phase in a two phase system are denoted s_w and s_n , respectively. If the system consists of only these two fluids, then

$$s_w + s_n = 1 \quad (1.2)$$

holds at all times. Since we can always recover $s_n = 1 - s_w$, it suffices to look at variables as functions of one saturation only. It is important to mention that the saturation s_w , and hence also s_n , never physically attains

the values 0 nor 1, not even asymptotically. The actual range of the saturation goes from s_{wc} , called the critical saturation, to the maximum saturation s_w^{max} .

The usual shape of the water relative permeability function k_w , with respect to the water saturation s_w , is as follows

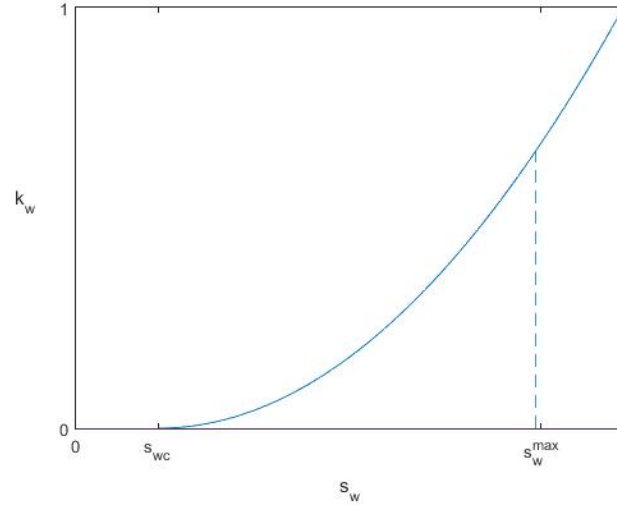


Figure 1.1: Relative permeability of the wetting phase vs wetting phase saturation.

This figure agrees with the intuition that the less oil there is in the volume, the easier the water will flow. Conversely, one would expect oil relative permeability k_n to increase as the water saturation drops.

This is in fact what occurs, the curve of k_n is always a decreasing function of s_w . However, a mayor anomaly is observed every time this is measured: the shape of the function k_n changes depending on whether the water saturation is increasing or decreasing. Indeed, this means we have two different shapes for this curve (figure 1.2).

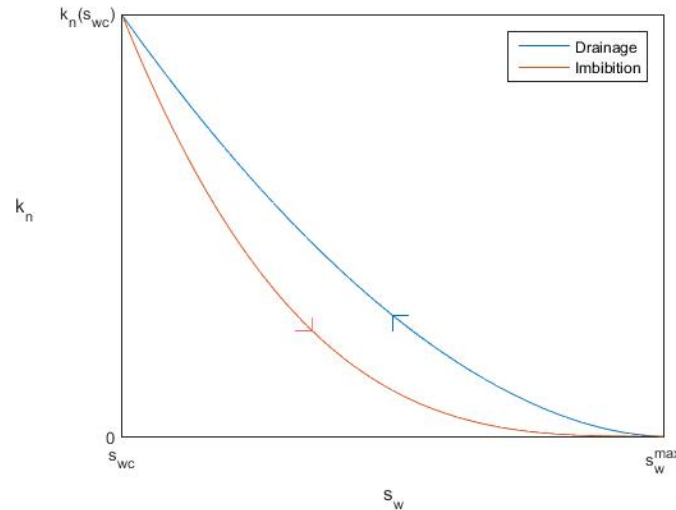


Figure 1.2: Relative permeability of the non-wetting phase vs water saturation.

The value of k_n depends on both the saturation s_w and the direction in which it is moving. When the water saturation is decreasing, i.e. when $\frac{\partial s_w}{\partial t} < 0$, then k_n follows the first curve, which is called the *drainage* curve, since water is being “drained” from the volume. Conversely when $\frac{\partial s_w}{\partial t} > 0$, we are in the case of the

second curve, called the *imbibition* curve.

This is explained by the fact that oil and water move differently through porous media, hence as one phase forces the other out, the distribution of the saturations inside the volume changes significantly, which in turn affects the phases capacity to flow, producing a process that is not exactly reversible.

The result is that k_n is a function not only of s_w but also of the previous state of the system, i.e. its history. This dependence on the past of the system is called hysteresis. Other variables such as capillary pressure also exhibit hysteretic behaviour when plotted against water saturation.

1.2. SCANNING CURVES

Figure 1.2 shows two cases where the derivative $\frac{\partial s_w}{\partial t}$ does not change sign at any time. Let us consider the alternative:

Assume water saturation is at its minimum, i.e. s_{wc} , and water starts being pumped into the reservoir, then k_n should follow the imbibition curve until the saturation reaches s_w^{max} . If, after reaching its maximum, the water starts being drained, k_n will now follow the drainage curve until $s_w = s_{wc}$ again.

However, if the draining process is interrupted before the saturation reaches s_{wc} , for instance at s_{wi} such that $s_{wc} < s_{wi} < s_w^{max}$, and water starts being pumped back into the volume, now k_n needs to stop following the drainage curve and follow the imbibition curve instead. But the imbibition and drainage curve do not intersect at almost any point, so for the transition from one to the other to be continuous, we need another curve starting at point $(s_{wi}, k_n(s_{wi}))$. These transition curves are called *scanning* curves.

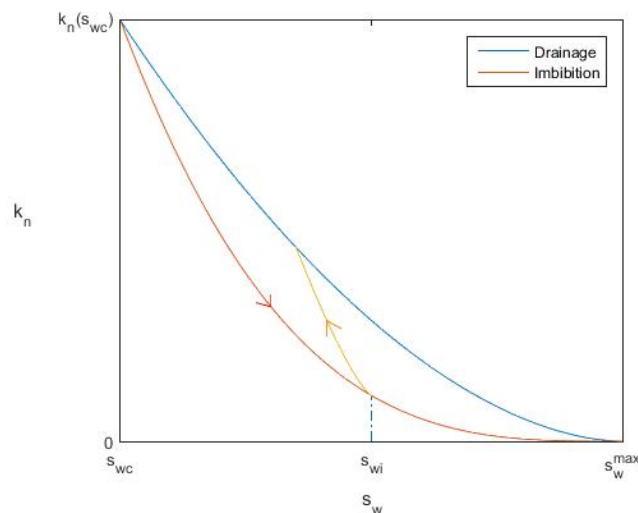


Figure 1.3: Imbibition process for k_n reversed at s_{wi} .

Figure 1.3 shows an imbibition process that has been reversed, hence the scanning curve goes in the opposite direction, i.e. the direction of decreasing wetting saturation, until it reaches the drainage curve. At this point, k_n follows the drainage curve again. Analogously, the drainage process can also be reversed at any point, which would result in a scanning curve going in the direction of increasing saturation, until it reaches the imbibition curve again.

In fact, any model that wishes to accurately describe k_n would need an infinite number of scanning curves, at any point s_{wi} where the process may be reversed. In general the drainage and imbibition curves, also called bounding curves, are empirically known and the scanning curves are predicted based on this information. On this document, several models describing different methods of constructing these scanning curves will be examined.

2

PRELIMINARIES

As stated before, various techniques are common practice for enhanced oil recovery. In water-flooding, water is injected in one or more places (injection wells) in a reservoir under high enough pressure for the oil in the reservoir to be pushed by the injected water towards the producing wells of the reservoir (oil displacement). In water alternating gas (WAG) injection water and gas are injected in turn for the same effect.

Consider a water-flooding in one space dimension. On one end water is injected and on the other end oil and water are produced. Both oil and water are assumed to be incompressible. In one spatial dimension, the flow is described by variables depending on (x, t) , the space and time coordinates. The main variables driving the model are phase saturation s_l and phase pressure p_l , where l represents both phases $l = w, n$.

2.1. TRANSPORT EQUATIONS

The two-phase model of fluid flow through a porous medium in one spatial dimension is given by the transport equations for oil and water mass [1]:

$$\frac{\partial}{\partial t}(\phi\rho_w s_w) + \frac{\partial}{\partial x}(\rho_w v_w) = 0. \quad (2.1)$$

$$\frac{\partial}{\partial t}(\phi\rho_o s_o) + \frac{\partial}{\partial x}(\rho_o v_o) = 0. \quad (2.2)$$

where v_l is the seepage velocity for phase l . This is not the actual velocity of a phase but its apparent velocity through the reservoir. Actual velocity is higher because of the tortuosity of the actual path of the flow through the pore space. According to Darcy's law for two phase flow in a porous medium, seepage velocity is given by

$$v_l = -K \frac{k_l}{\mu_l} \frac{\partial p_l}{\partial x} \quad \text{for } l = w, n \quad (2.3)$$

As before, p_l represents the pressure of each phase and k_l the relative permeability. Two properties of the fluids, the mass density ρ_l and the viscosity μ_l will be assumed constant. The permeability K and the porosity ϕ , i.e. the fraction of the total volume occupied by pores, are properties of the porous rock and are also taken as constants.

2.1.1. GENERAL FORMULATION

The conservation equations resulting of substituting seepage velocity (2.3) into the transport equations (2.1) and (2.2) are

$$\frac{\partial}{\partial x} \left[\frac{K k_l}{\mu_l} \rho_l \frac{\partial p_l}{\partial x} \right] = \frac{\partial}{\partial t} (\phi \rho_l s_l) \quad l = w, n \quad (2.4)$$

To follow the notation from [1], define the volume rates

$$B_w = \frac{[V_w]_{RC}}{[V_w]_{STC}}$$

$$B_n = \frac{[V_n]_{RC}}{[V_n]_{STC}}$$

where $[V_l]_{RC}$ is the volume occupied by a fixed mass of component l at reservoir conditions and $[V_l]_{STC}$ is the volume occupied by the same mass at stock tank (standard) conditions.

It follows from the definition of density that the densities ρ_l of the phases in the reservoir are related to the densities at stock tank conditions by:

$$\rho_w = \frac{1}{B_w} \rho_{wSTC}$$

$$\rho_n = \frac{1}{B_n} \rho_{nSTC}$$

Divide both sides of (2.4) by ρ_{lSTC} to obtain

$$\frac{\partial}{\partial x} \left[\frac{K k_l}{\mu_l B_l} \frac{\partial p_l}{\partial x} \right] = \frac{\partial}{\partial t} \left(\phi \frac{s_l}{B_l} \right) \quad l = w, n$$

The mobility λ_l of phase l is defined as

$$\lambda_l = K \frac{k_l}{\mu_l B_l}$$

For convenience, the numerical methods will also include the source terms q_l into our conservation equations:

$$\frac{\partial}{\partial x} \left[\lambda_l \frac{\partial p_l}{\partial x} \right] = \frac{\partial}{\partial t} \left(\phi \frac{s_l}{B_l} \right) + q_l \quad l = w, n \quad (2.5)$$

The source terms q_l are defined negatively, hence any sink will be represented by positive values of q_l and any productive source by negative values.

This formulation is convenient because all terms are in the units

$$\left(\frac{RC \text{ volume}}{STC \text{ volume}} \frac{1}{\text{time}} \right)$$

Hence q_l represents volume at stock tank condition produced per unit time per unit volume at reservoir condition.

2.2. FORMULATIONS FOR INCOMPRESSIBLE FLUID

Incompressibility of the two phases translates into constant density ρ_l . Define the total velocity as

$$v = v_o + v_w$$

Dividing equations (2.1) and (2.2) by ρ_w and ρ_o respectively, adding the resulting equations, and using the fact that $s_w + s_o = 1$, we obtain

$$\frac{\partial v}{\partial x} = 0 \quad (2.6)$$

Thus v is a function solely of t and is determined by boundary conditions. For simplicity, it is taken to be nonzero and independent of time.

2.2.1. CONVECTION-DIFFUSION EQUATION

The water and oil fractional flow functions are defined, respectively, by

$$f_w = \frac{k_w/\mu_w}{k_w/\mu_w + k_o/\mu_o} \quad \text{and} \quad f_o = \frac{k_o/\mu_o}{k_w/\mu_w + k_o/\mu_o} \quad (2.7)$$

Clearly $f_w + f_o = 1$. It is easy to see that

$$v f_w = -K \frac{k_w}{\mu_w} \left(f_w \frac{\partial p_w}{\partial x} + f_o \frac{\partial p_o}{\partial x} \right) \quad (2.8)$$

We define the capillary pressure as the difference in pressures $P_c = p_o - p_w$. Using the fact that $f_w + f_o = 1$, we obtain

$$v f_w = v_w - K \frac{k_w}{\mu_w} f_o \frac{\partial}{\partial x} P_c \quad (2.9)$$

Substituting v_w from equation (2.9) into equation (2.1) yields the convection diffusion equation for the water phase

$$\frac{\partial}{\partial t} (\phi s_w) + \frac{\partial}{\partial x} (v f_w) = \frac{\partial}{\partial x} \left[K \varepsilon \frac{\partial s_w}{\partial x} \right]$$

where

$$\varepsilon = -\frac{k_w}{\mu_w} f_o \frac{\partial P_c}{\partial s_w}$$

is the capillarity-induced diffusion coefficient. For $v \neq 0$, we can set

$$t = \frac{\phi K}{v^2} \tilde{t} \quad \text{and} \quad x = \frac{K}{v} \tilde{x}$$

in order to remove constants K , ϕ and v from our equation. For simplicity, we drop the tildes:

$$\frac{\partial}{\partial t} (s_w) + \frac{\partial}{\partial x} (f_w) = \frac{\partial}{\partial x} \left[\varepsilon \frac{\partial s_w}{\partial x} \right] \quad (2.10)$$

An analogue expression is found for the oil phase. Notice how the terms f_w and ε are subjected to hysteresis, as they depend on k_w , k_o and P_c .

2.2.2. BUCKLEY-LEVERETT EQUATION

Let us assume further that the capillary pressure changes almost insignificantly along the reservoir, i.e. $\frac{\partial P_c}{\partial x} = 0$. This implies

$$\frac{\partial p_n}{\partial n} = \frac{\partial p_w}{\partial p_n}$$

Using this in the definition of v_l (2.3), we can rewrite the fractional flow functions as

$$f_w = \frac{v_w}{v} = \frac{v_w}{v_w + v_n} \quad f_o = \frac{v_o}{v} = \frac{v_o}{v_w + v_o}$$

This definition of the flow functions is equivalent to our previous one when $\frac{\partial P_c}{\partial x}$ is negligible. This can easily be seen by setting $\frac{\partial P_c}{\partial x} = 0$ in equation (2.9).

Substituting $v_w = v f_w$ in equation (2.1) and dividing both sides by $\phi \rho_w$ yields

$$\frac{\partial s_w}{\partial t} + \frac{v}{\phi} \frac{\partial f_w}{\partial x} = 0$$

Using the chain rule we obtain the convection equation

$$\frac{\partial s_w}{\partial t} = - \left(\frac{v}{\phi} \frac{\partial f_w}{\partial s_w} \right) \frac{\partial s_w}{\partial x} \quad (2.11)$$

Where $u = \frac{v}{\phi} \frac{\partial f_w}{\partial s_w}$ is the characteristic speed of the system. The behaviour of solutions to (2.11) will be discussed in chapter 5.

2.3. RAREFACTION AND SHOCK WAVES

Consider a scalar conservation law of the form

$$s_t + f(s)_x = 0 \quad (2.12)$$

If the flux function f is linear, $f(s) = us$, then 2.12 is simply the advection equation with constant speed u , and its solution

$$s(x, t) = s^0(x - ut)$$

is simply the initial state $s^0(x) = s(x, 0)$ transported uniformly at speed u . The characteristic curves of the system, i.e. curves $x(t)$ along which s remains constant, are straight parallel lines in the x, t plane (figure 2.1).

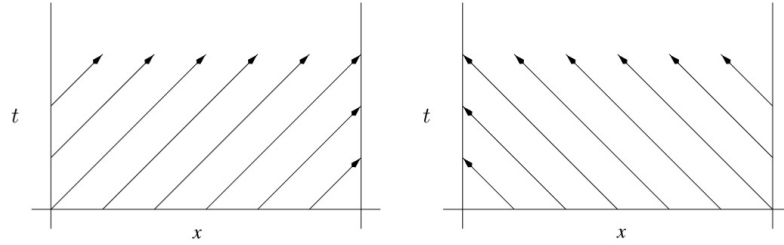


Figure 2.1: Characteristic lines of s for constant velocity $u > 0$ (left) and $u < 0$ (right).

When f is non-linear on s , however, the solution no longer translates identically over time. Instead it deforms as it goes on, and shock waves can also form, i.e. curves along which the solution is discontinuous.

2.3.1. NON-LINEAR FLUX FUNCTION

Consider a nonlinear flux function f , so that characteristic velocities f' are no longer constant but rather they depend on s . We may write (2.12) in its quasilinear form

$$s_t + f'(s)s_x = 0 \quad (2.13)$$

Thus, for any curve $x(t)$ satisfying the ODE

$$x'(t) = f'(s(x(t), t))$$

we have, by (2.13),

$$\begin{aligned} \frac{\partial}{\partial t} s(x(t), t) &= x'(t)s_x + s_t \\ &= 0 \end{aligned}$$

Hence s is constant along the curve $x(t)$, and consequently $x'(t)$ is also constant along the curve, and so the characteristic curve $x(t)$ must be a straight line.

Since characteristic velocities depend on s , these lines are not necessarily parallel. Rather, they may spread out or eventually collide. This is an essential feature of hyperbolic problems, which generates shock waves.

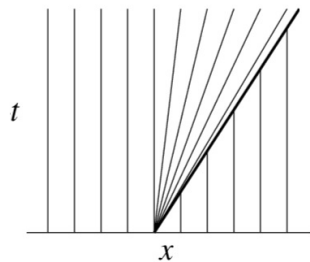


Figure 2.2: Characteristic lines of s for non constant characteristic velocity f' .

Assume that the initial state s^0 is smooth, and that the solution $s(x, t)$ remains smooth for some time, Then constant values of s propagate along characteristic curves. Using the fact that these curves are straight lines, it is possible to determine the solution:

$$s(x, t) = s^0(\xi)$$

where ξ solves the equation

$$x = \xi + f'(s^0(\xi))t \tag{2.14}$$

However, this reasoning is only valid as long as the solution $s(x, t)$ remains smooth.

2.3.2. RAREFACTION WAVES

Consider an initial saturation

$$s^0(x) = \begin{cases} 1 & x < 0 \\ 0 & x > 0 \end{cases} \tag{2.15}$$

as shown in figure 2.3. We are interested on tracking this state over the half space $x > 0$ over time. It is possible to build a solution by following the individual movement of each saturation, since we know their respective velocities.

Assume the flow function has monotonic derivative $f'(s)$, for instance $f(s) = s(1 + \varepsilon - s)$, with ε a positive constant. In that case the characteristic velocities corresponding to each saturation can be mapped as in figure 2.3:

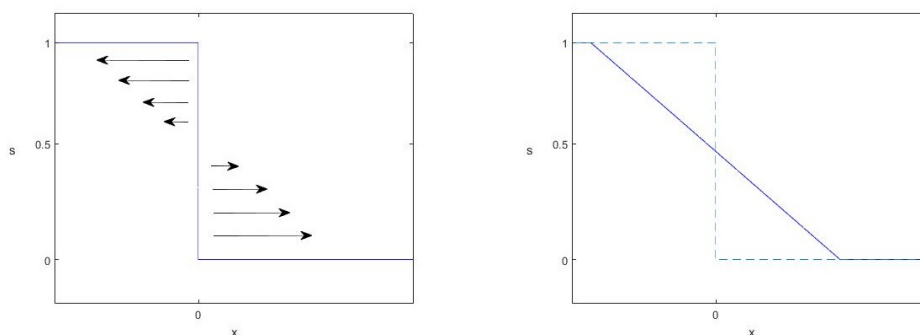


Figure 2.3: Initial saturation 2.15 with monotonic characteristic velocities is shown on the left. After any positive time t , each saturation has followed its own characteristic curve (right).

Notice how after a positive time the different saturation values move further apart from each other, i.e. the solution becomes rarefied. We call this a rarefaction wave.

2.3.3. SHOCK WAVES

Assume now an initial saturation

$$s^0(x) = \begin{cases} 0 & x < 0 \\ 1 & x > 0 \end{cases} \quad (2.16)$$

If we allow each saturation s to follow their respective characteristic curve, after a positive time we would obtain a triple value solution (figure 2.4). This is because equation (2.14) only has unique solution while s is smooth.

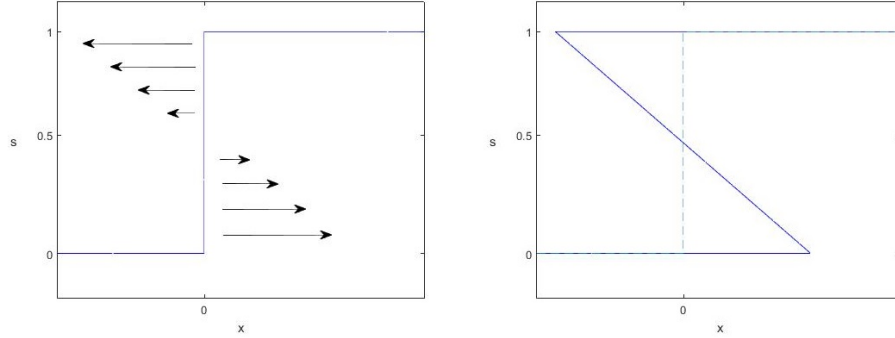


Figure 2.4: Initial saturation 2.16 with monotonic characteristic velocities is shown on the left. On the right an incorrect solution is shown where each saturation has followed its own characteristic curve.

This solution is physically incorrect. The actual observed behaviour is that all saturations advance at the same time, transporting the discontinuity along the half space. The advancing discontinuity is called a shock wave.

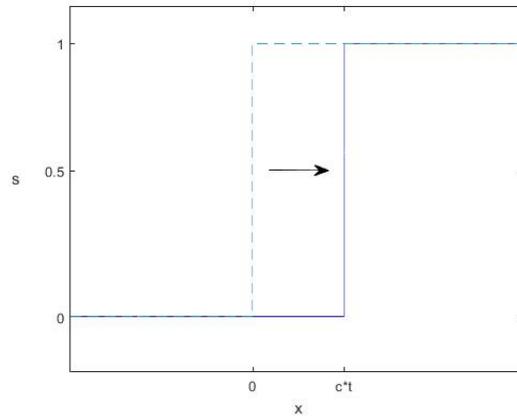


Figure 2.5: A shock wave after positive time t . Speed is determined by 2.17. For this case, $c = \varepsilon$.

The speed c of the whole shock wave, and hence also its direction, is given by the Rankine-Hugoniot condition [2]:

$$c = \frac{f(s_L) - f(s_R)}{s_L - s_R} \quad (2.17)$$

where s_L and s_R denote the values of the saturation at the left and right side of the discontinuity, respectively. Since this values can change over time hence so does the shock speed c . However, for a piecewise constant initial state such as 2.16, all shock waves travel at constant speed.

3

FINITE VOLUME METHODS

This section is meant to explain the numerical methods described in [1] for simulating phase flow in a reservoir. The reader familiar with the IMPES method and Newton's iterative method may skip it entirely. All schemes were written using Matlab and the resulting simulations are presented in chapters 5, 6 & 7.

3.1. DISCRETIZED FLOW EQUATIONS

Let us recall equation (2.5) of mass conservation:

$$\frac{\partial}{\partial x} \left[\lambda \frac{\partial p}{\partial x} \right] = \frac{\partial}{\partial t} \left(\phi \frac{s}{B} \right) + q \quad (3.1)$$

For simplicity let us ignore the phase indexes l for now. Variables p and s are discretized over the spatial domain $x \in [0, L]$ as vectors of length N using a block-centred uniform grid.

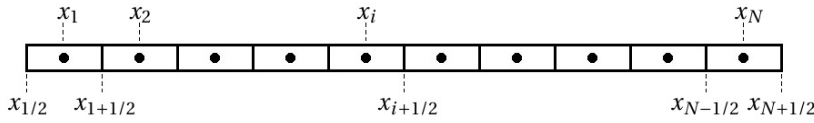


Figure 3.1: 1D block-centred grid of size N .

3.1.1. SPACE DISCRETIZATION

We wish to give a linear operator T that approximates the left hand side of (3.1), so that

$$T(P) \approx \frac{\partial}{\partial t} U + Q \quad (3.2)$$

Where $P = (p_1, \dots, p_N)^T$ and $Q = (q_1, \dots, q_N)^T$ are the discretization vectors of p and q , and U represents the vector

$$U_i = \left(\phi \frac{s}{B} \right) \Big|_{x_i}$$

Since (3.1) expresses mass conservation, it can be written in its integral form

$$A_i \int_{x_{i-1/2}}^{x_{i+1/2}} \frac{\partial}{\partial x} \left[\lambda \frac{\partial p}{\partial x} \right] = A_i \int_{x_{i-1/2}}^{x_{i+1/2}} \frac{\partial}{\partial t} \left(\phi \frac{s}{B} \right) + A_i \int_{x_{i-1/2}}^{x_{i+1/2}} q \quad (3.3)$$

where the integration has been carried over the block volume i and A_i represents the area of the cross section. Using Green's theorem, the left-hand side becomes

$$\int_{x_{i-1/2}}^{x_{i+1/2}} \frac{\partial}{\partial x} \left[\lambda \frac{\partial p}{\partial x} \right] = \lambda \frac{\partial p}{\partial x} \Big|_{x_{i+1/2}} - \lambda \frac{\partial p}{\partial x} \Big|_{x_{i-1/2}}$$

Approximating the function by central finite difference on $x_{i+1/2}$ means

$$\begin{aligned} b'_l &= \frac{db_l}{dp_l} \\ S'_l &= \frac{dS_l}{dP_c} \\ \phi' &= \frac{d\phi}{dp} \end{aligned}$$

When ϕ is not constant, i.e. if the reservoir rock is also subject to compression, ϕ can be assumed to depend on $p = \frac{1}{2}(p_n + p_w)$. In this case, we can write

$$\begin{aligned} \Delta_t \phi &= \phi' \Delta_t p \\ &= \phi' \frac{1}{2} (\Delta_t p_n - \Delta_t p_w) \end{aligned}$$

Similarly,

$$\begin{aligned} \Delta_t S_l &= S'_l \Delta P_c \\ &= S'_l (\Delta_t p_n - \Delta_t p_w) \end{aligned}$$

Hence (3.8) can be expressed as

$$\Delta_t \left(\phi \frac{S_l}{B_l} \right) = (\phi S_l)^n b'_l \Delta_t p_l + (\phi b_l)^{n+1} S'_l (\Delta_t p_n - \Delta_t p_w) + \frac{1}{2} b_l^{n+1} S_l^n \phi' (\Delta_t p_n - \Delta_t p_w) \quad (3.9)$$

Equations (2.5) are then discretized using the backward difference approximation:

$$\begin{aligned} [\Delta T_w (\Delta p_w)_i]^{n+1} &= [d_{11} \Delta_t p_w + d_{12} \Delta_t p_n]_i + Q_{wi} \\ [\Delta T_n (\Delta p_n)_i]^{n+1} &= [d_{21} \Delta_t p_w + d_{22} \Delta_t p_n]_i + Q_{ni} \end{aligned} \quad (3.10)$$

Where coefficients d_{ij} are found from (3.9), using the fact that $S'_w = -S'_n$,

$$\begin{aligned} d_{11} &= \frac{V}{\Delta t} [(\phi S_w)^n b'_w - (\phi b_w)^{n+1} S'_w + \frac{1}{2} b_w^{n+1} S_w^n \phi'] \\ d_{12} &= \frac{V}{\Delta t} [(\phi b_w)^{n+1} S'_w + \frac{1}{2} b_w^{n+1} S_w^n \phi'] \\ d_{21} &= \frac{V}{\Delta t} [(\phi b_w)^{n+1} S'_w + \frac{1}{2} b_w^{n+1} (1 - S_w^n) \phi'] \\ d_{22} &= \frac{V}{\Delta t} [(\phi (1 - S_w^n) b'_n - (\phi b_n)^{n+1} S'_w + \frac{1}{2} b_n^{n+1} (1 - S_w^n) \phi'] \end{aligned}$$

3.1.3. MATRIX FORMULATION

Define the unknown pressure vector by

$$\mathbf{P} = [p_{1w}, p_{1n}, \dots, p_{iw}, p_{in}, \dots, p_{Nw}, p_{Nn}]$$

Then we can write the discretization (3.10) as

$$\mathbf{TP}^{n+1} = \mathbf{D}(\mathbf{P}^{n+1} - \mathbf{P}^n) + \mathbf{Q} \quad (3.11)$$

The i -th block of \mathbf{T} , corresponding to p_{iw} and p_{in} , has the non-zero elements:

$$\left[\begin{array}{cc|cc} T_{wi-1/2} & 0 & -(T_{wi-1/2} + T_{wi+1/2}) & 0 \\ 0 & T_{ni-1/2} & 0 & -(T_{ni-1/2} + T_{ni+1/2}) \end{array} \middle| \begin{array}{cc} T_{wi+1/2} & 0 \\ 0 & T_{ni+1/2} \end{array} \right]$$

The i -th block of matrix \mathbf{D} is the 2x2 matrix

RATE CONDITIONS

Rate conditions specify the incoming (or leaving) water or oil rate through one of our one-dimensional block boundaries. On this document, rate conditions will always be specified on the left boundary of the grid.

Rate conditions follow Darcy's law:

$$\tilde{q}_l = -K \frac{k_l}{B_l \mu_l} \frac{\partial p_l}{\partial x}$$

Discretization over the block boundary $i + 1/2$ yields

$$\tilde{Q}_l = -A \left(K \frac{k_l}{B_l \mu_l} \right)_{i+1/2} \frac{1}{\Delta x_{i+1/2}} [p_{li+1} - p_{li}]$$

The first equation of system (3.11) reads:

$$T_{w1+1/2}(p_{w2} - p_{w1}) - T_{w1-1/2}(p_{w1} - p_{w0}) = (d_{11}\Delta_t p_w + d_{12}\Delta_t p_n)_1 + Q_{w1} \quad (3.13)$$

where p_{w0} is a virtual point outside our domain. Since the left boundary of our grid is $i = 1/2$, we can write a water rate condition \tilde{Q}_w at this point, and replace the equivalent terms in 3.13 to obtain

$$T_{w1+1/2}(p_{w2} - p_{w1}) - \tilde{Q}_w = (d_{11}\Delta_t p_w + d_{12}\Delta_t p_n)_1 + Q_{w1}$$

Rearranging

$$T_{w1+1/2}p_{w2} - T_{w1+1/2}p_{w1} = (d_{11}\Delta_t p_w + d_{12}\Delta_t p_n)_1 + (Q_{w1} + \tilde{Q}_w)$$

A similar treatment befalls any oil rate condition \tilde{Q}_n . For simplicity, when using the notation (3.11), the source term \mathbf{Q} is meant to include the boundary conditions \tilde{Q}_l as well.

PRESSURE CONDITIONS

Pressure of one or both phases can also be specified at the boundaries. Assume oil pressure \tilde{p}_n is known at the right boundary at all times. We would like to include it into the last equation of (3.11):

$$T_{nN+1/2}(p_{nN+1} - p_{nN}) - T_{nN-1/2}(p_{nN} - p_{nN-1}) = (d_{21}\Delta_t p_w + d_{22}\Delta_t p_n)_N + Q_{IN} \quad (3.14)$$

Again, we find that p_{nN+1} is a virtual point outside the grid. However, \tilde{p}_n is specified at coordinate $N + 1/2$ and hence it can be expressed as

$$\tilde{p}_n = \frac{p_{nN+1} + p_{nN}}{2}$$

We may then solve for the virtual point

$$p_{nN+1} = 2\tilde{p}_n - p_{nN}$$

And replace it in equation (3.14):

$$T_{nN+1/2}(2\tilde{p}_n - 2p_{nN}) - T_{nN-1/2}(p_{nN} - p_{nN-1}) = (d_{21}\Delta_t p_w + d_{22}\Delta_t p_n)_N + Q_{IN}$$

Rearranging

$$\begin{aligned} -(2T_{nN+1/2} + T_{nN-1/2})p_{nN} + T_{nN-1/2}p_{nN-1} &= (d_{21}\Delta_t p_w + d_{22}\Delta_t p_n)_N \\ &+ (Q_{IN} - 2T_{nN+1/2}\tilde{p}_n) \end{aligned}$$

This involves a slight change in the last row of matrix \mathbf{T} and, as before, inclusion of the boundary condition in source term \mathbf{Q} .

The change in matrix \mathbf{T} is welcomed, since a system of incompressible phases with only rate conditions on both boundaries generally results in a singular matrix \mathbf{T} , which is an undesired complication. Taking a pressure condition on at least one of the two boundaries guaranties the existence of solution for the system, whether is incompressible or not.

3.2. THE IMPLICIT PRESSURE EXPLICIT SATURATION (IMPES) METHOD

The IMPES method solves the implicit system for the unknown pressure first, then computes the unknown saturation explicitly. To this purpose, let us recall discretization (3.6):

$$[\Delta T_l(\Delta p_l)]^{n+1} = \frac{1}{\Delta t} \Delta_t \left(\phi \frac{S_l}{B_l} \right) + Q_l$$

Expand the right hand side as in (3.9)

$$\Delta_t \left(\phi \frac{S_l}{B_l} \right) = (\phi S_l)^n b'_l \Delta_t p_l + (\phi b_l)^{n+1} \Delta_t S_l + \frac{1}{2} b_l^{n+1} S_l^n \phi' (\Delta_t p_n - \Delta_t p_w) \quad (3.15)$$

where we have not expressed $\Delta_t S_l$ in terms of P_c . Instead, substitution of (3.15) in (3.6) yields a system with unknowns S_w , S_n and p_n , as in (3.16) and (3.17) below.

The main assumption behind the IMPES method is that capillary pressure does not change significantly over a time step, that is $\Delta_t P_c \simeq 0$. This means we can assume P_c on the left hand of (3.16) to be at time level n instead of $n+1$, and also implies $\Delta_t p_w = \Delta_t p_n$. Therefore, we can denote $p = p_n$ and write:

$$[\Delta T_w(\Delta p - \Delta P_c)_i]^{n+1} = [c_{1p} \Delta_t p]_i + [c_{1w} \Delta_t S_w]_i + Q_{wi} \quad (3.16)$$

$$[\Delta T_n(\Delta p)_i]^{n+1} = [c_{2p} \Delta_t p]_i + [c_{2n} \Delta_t S_n]_i + Q_{ni} \quad (3.17)$$

where we have used $\Delta p_w = \Delta p - \Delta P_c$, and coefficients c are easily found from (3.15):

$$\begin{aligned} c_{1p} &= \frac{V}{\Delta t} [(S_w \phi)^n b'_w + S_w^n b_w^{n+1} \phi'] \\ c_{1w} &= \frac{V}{\Delta t} (\phi b_w)^{n+1} \\ c_{2p} &= \frac{V}{\Delta t} [(S_n \phi)^n b'_n + S_n^n b_n^{n+1} \phi'] \\ c_{2n} &= \frac{V}{\Delta t} (\phi b_n)^{n+1} \end{aligned}$$

First step is to combine equations (3.16) and (3.17) to obtain a single pressure equation. This is done by multiplying the first equation by α and adding the two equations. The right hand side of the resulting equation is

$$(\alpha c_{1p} + c_{2p}) \Delta_t p_n + (-\alpha c_{1w} + c_{2n}) \Delta_t S_n + \alpha Q_{wi} + Q_{ni}$$

where we have used $\Delta_t S_w = -\Delta_t S_n$. Coefficient α is then obtained from

$$(-\alpha c_{1w} + c_{2n}) = 0$$

Hence choosing $\alpha = c_{2n}/c_{1w}$ yields the pressure equation

$$[\Delta T_n(\Delta p)_i]^{n+1} + \alpha [\Delta T_w(\Delta p)_i]^{n+1} = (\alpha c_{1p} + c_{2p}) \Delta_t p_i + \alpha [\Delta T_w(\Delta P_c)_i]^n + Q_{ni} + \alpha Q_{wi} \quad (3.18)$$

Which can be written as

$$\mathbf{TP}^{n+1} = \mathbf{D}(\mathbf{P}^{n+1} - \mathbf{P}^n) + \mathbf{P}_c^n + \mathbf{Q} \quad (3.19)$$

Now \mathbf{P} is the non-wetting phase pressure vector, \mathbf{T} is a tridiagonal matrix and \mathbf{D} is diagonal.

Once the pressure is solved, it is advanced in time and used in (3.16) and (3.17) to explicitly update saturations S_l^{n+1} . When the new saturations are known, capillary pressure P_c is updated and used explicitly in the next time step.

Again, matrices \mathbf{T} and \mathbf{D} contain coefficients evaluated at time $n+1$, hence some method is required to linearize the system.

3.3. DEALING WITH NON-LINEARITY

Nonlinearities appear in systems (3.11) and (3.19) as functions in matrices \mathbf{T} and \mathbf{D} . In [1] they are divided into weak and strong nonlinearities.

Weak nonlinearities are all variables that are functions of the pressure of one phase only. These include μ_l, B_l and b_l . In general, it poses no problem to evaluate these variables one time step behind, i.e. as a function of p_l^n instead of p_l^{n+1} . For the approximation of coordinate $i + 1/2$ we can always use

$$\mu_{li+1/2} = \frac{1}{2}(\mu_{li+1} + \mu_{li})$$

Strong nonlinearities are coefficients that depend on saturation or capillary pressure, for instance k_l, S'_w and P_c . In particular, k_l introduces the principal non-linearity in (3.19). Approximating strong nonlinearities as $k_l^{n+1} \approx k_l^n$ is only conditionally stable ([1],5.4.1.2), hence other linearizations must be sought.

The question of how to approximate the $i + 1/2$ coordinate in space is called “weighting”, while the problem of approximating time step $n + 1$ is referred to as “local linearization” of the nonlinear system.

3.3.1. WEIGHTING TRANSMISSIBILITIES

Intuitively one would propose an approximation that makes sense analytically, such as the midpoint weighting

$$k_{li+1/2} = \frac{1}{2}(k_l(S_{wi+1}) + k_l(S_{wi}))$$

or the weighting

$$k_{li+1/2} = k_l \left(\frac{1}{2}(S_{wi+1} + S_{wi}) \right)$$

However, schemes such as the midpoint weighting may cause the solution to converge, as the mesh becomes finer, to a mathematically possible but physically incorrect solution ([1],5.5.1). For this reason, the commonly used scheme is the “upstream weighting” defined by

$$k_{li+1/2} = \begin{cases} k_l(S_{wi}) & \text{if flow is from } i \text{ to } i+1 \\ k_l(S_{wi+1}) & \text{if flow is from } i+1 \text{ to } i \end{cases} \quad (3.20)$$

This formula provides only first order approximation. An example of a second order approximation by Todd *et al.* ([3],1972) uses two stream points:

$$k_{li+1/2} = \begin{cases} \frac{1}{2}(3k_l(S_{wi}) + k_l(S_{wi-1})) & \text{if flow is from } i \text{ to } i+1 \\ \frac{1}{2}(3k_l(S_{wi+1}) + k_l(S_{wi+2})) & \text{if flow is from } i+1 \text{ to } i \end{cases}$$

3.3.2. LOCAL LINEARIZATION OF TRANSMISSIBILITIES

As stated before, IMPES treats saturation explicitly, by approximating $k_l(S_w^{n+1}) \approx k_l(S_w^n)$. However doing this does not guarantee stability. A good alternative is to use iterative methods. For this purpose recall equation (3.11)

$$\mathbf{T}^m \mathbf{P}^{n+1} = \mathbf{D}^m (\mathbf{P}^{n+1} - \mathbf{P}^n) + \mathbf{Q}$$

where m denotes the time level at which \mathbf{D} and \mathbf{T} are evaluated, and introduce the notation

$$\mathbf{R}_m^k = \mathbf{T}^m \mathbf{P}^k - \mathbf{D}^m (\mathbf{P}^k - \mathbf{P}^n) \quad (3.21)$$

Then (3.11) can be rewritten as

$$(\mathbf{T}^m - \mathbf{D}^m) (\mathbf{P}^{n+1} - \mathbf{P}^n) = -\mathbf{R}_m^n + \mathbf{Q}$$

BASIC ITERATIVE METHODS

The method of simple iteration consist on approximating \mathbf{P}^{n+1} by computing the iterations $\mathbf{P}^{(v)}$, $v = 0, 1, \dots$, by setting

$$(\mathbf{T}^{(v)} - \mathbf{D}^{(v)})(\mathbf{P}^{(v+1)} - \mathbf{P}^{(v)}) = -\mathbf{R}_{(v)}^{(v)} + \mathbf{Q} \quad (3.22)$$

with $\mathbf{P}^{(0)} = \mathbf{P}^n$, and iteration stops when convergence is achieved, i.e. when $\mathbf{P}^{(v+1)} - \mathbf{P}^{(v)}$ is small enough.

Another iterative method, Newton's method is defined by

$$\mathbf{DR}^{(v)}[\mathbf{P}^{(v+1)} - \mathbf{P}^{(v)}] = -\mathbf{R}_{(v)}^{(v)} + \mathbf{Q} \quad (3.23)$$

where \mathbf{DR} is the Jacobi matrix of $\mathbf{R}(\mathbf{P}) = \mathbf{TP} - \mathbf{D}(\mathbf{P} - \mathbf{P}^n)$, i.e.

$$\mathbf{DR} = \left[\frac{\partial \mathbf{R}_{li}}{\partial p_{kj}} \right]_{ij} \quad k, l = w, n$$

Equivalently,

$$\mathbf{DR} = \begin{bmatrix} \frac{\partial \mathbf{R}_{wi}}{\partial p_{wj}} & \frac{\partial \mathbf{R}_{wi}}{\partial p_{nj}} \\ \frac{\partial \mathbf{R}_{ni}}{\partial p_{wj}} & \frac{\partial \mathbf{R}_{ni}}{\partial p_{nj}} \end{bmatrix}_{ij}$$

PRESSURE AND SATURATION FORMULATION

The two-phase system described by (3.16) and (3.17) can be written as

$$\mathbf{T}^{n+1}\mathbf{P}^{n+1} + \mathbf{D}^{n+1}(\mathbf{S}^{n+1} - \mathbf{S}^n) = \mathbf{Q} \quad (3.24)$$

Equation (3.21) may also be expressed in terms of oil pressure p and water saturation S :

$$\mathbf{R}_m^k = \mathbf{T}^m \mathbf{P}^k + \mathbf{D}^m (\mathbf{S}^k - \mathbf{S}^n)$$

So that

$$\mathbf{T}^{n+1}(\mathbf{P}^{n+1} - \mathbf{P}^n) + \mathbf{D}^{n+1}(\mathbf{S}^{n+1} - \mathbf{S}^n) = -\mathbf{R}_{n+1}^n + \mathbf{Q}$$

We can write the two variables into one vector $\mathbf{X} = \begin{pmatrix} \mathbf{P} \\ \mathbf{S} \end{pmatrix}$, hence

$$[\mathbf{T}^{n+1}, \mathbf{D}^{n+1}](\mathbf{X}^{n+1} - \mathbf{X}^n) + \mathbf{R}_{n+1}(\mathbf{X}^n) - \mathbf{Q} = 0$$

If we write the left hand side of the equation as

$$\mathbf{f}(\mathbf{X}^{n+1}) = 0$$

Then the linear system can be solved using Newton's iterative method by setting

$$\mathbf{F}^{(v)}(\mathbf{X}^{(v+1)} - \mathbf{X}^{(v)}) = -\mathbf{f}^{(v)} \quad (3.25)$$

where $\mathbf{X}^{(0)} = \mathbf{X}^n$ and \mathbf{F} is the Jacobian matrix for \mathbf{f} :

$$\mathbf{F}^{(v)} = \begin{pmatrix} f_i \\ x_j \end{pmatrix}^{(v)}$$

4

RELATIVE PERMEABILITY HYSTERESIS & CAPILLARY PRESSURE

In reservoir modeling significant errors can result whenever hysteresis is ignored. In [4] an example is given where using drainage data instead of imbibition data in a gas reservoir with a strong water drive could result in predicted recoveries of as much as twice the amount actually observed .

Hysteresis in relative permeability affects systems where the porous rock exhibits a strong wettability preference for a specific phase. On a macroscopic level, when the system experiences a change in saturation from a drainage to an imbibition process, the non wetting phase is subject to entrapment by the wetting phase [6].

The best known models used in industry, including the models introduced by Killough ([5],1976) and Carlson ([6],1981), will be presented in this chapter. A brief description of the physical phenomenon is also explained.

4.1. PHYSICAL BACKGROUND

Land ([7],1968) formalized the concept of hysteresis by describing the behaviour of the trapping that the non wetting phase undergoes, and explaining its effect on the relative permeability. Ever since, almost every model builds upon his ideas to describe hysteresis.

4.1.1. PHASE SATURATIONS

The range in which the wetting phase saturation s_w varies goes from the critical saturation s_{wc} , the saturation at which this phase starts to flow; to the maximum saturation $s_w^{max} = 1 - s_{nr}$, where the irreducible saturation s_{nr} is the saturation at which the non wetting phase can no longer be displaced.

Formally, s_{nr} is the value at which the non wetting phase can no longer be displaced by the wetting phase, while s_{nc} is the value at which the non wetting phase can no longer be displaced by any kind of pressure gradient. Because of other variables, s_{nc} and s_{nr} may be different but clearly $s_{nr} \geq s_{nc}$ at all times. Furthermore, while s_{nc} usually remains constant, s_{nr} may change due to hysteresis. This will become clear as we go through this chapter.

Analogously, the range of the non wetting phase saturation s_n goes from s_{nc} to $1 - s_{wr}$. When considering water, it can often be assumed that $s_{wc} = s_{wr}$.

4.1.2. WETTABILITY

Wetting is the ability of a liquid to maintain contact with a solid surface. The degree of wetting, known as wettability, is determined by a force balance between adhesive and cohesive forces. Adhesive forces between a liquid and solid cause a liquid drop to spread across the surface. Cohesive forces within the liquid cause the drop to ball up and avoid contact with the surface.

The contact angle θ is the angle at which the liquid interface meets the solid interface. The contact angle is determined by the result between adhesive and cohesive forces. As the tendency of a drop to spread out over a flat, solid surface increases, the contact angle decreases. Thus, the contact angle provides a useful characterization of wettability.

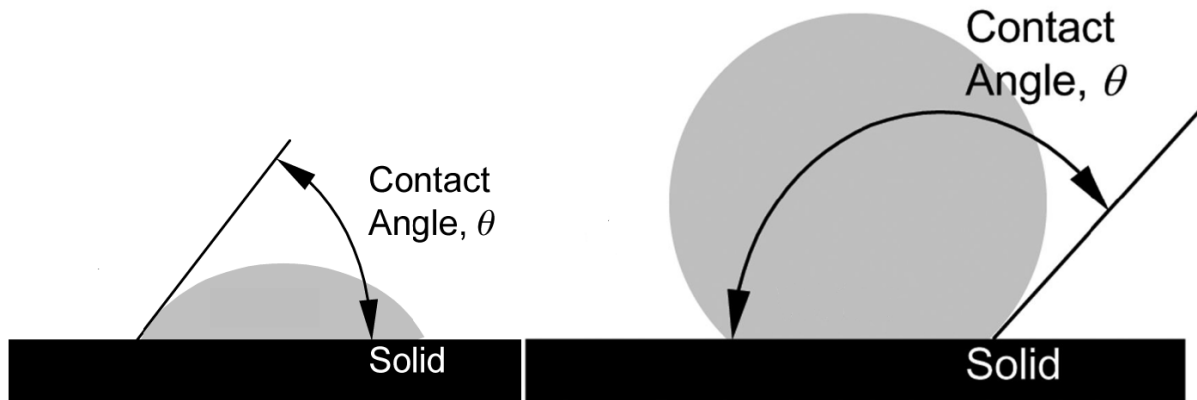


Figure 4.1: Different fluids exhibiting different wettability. The contact angle θ serves as an inverse measure of wettability, [19].

Capillary pressure and relative permeabilities depend on the interaction between the phases, which in turn depend on the size and shape of the pores and the wettability of the phases. Different rocks exhibit different wetting levels for each phase, but in general water-wet systems, i.e. surface with preference to be coated with water, are far more common.

4.1.3. LAND'S THEORY

In a water-wet system, water inside the pore space tends to gather close to the surface of the rock, while the oil stays further away from the rock walls. Hence in the smaller pores and pore throats, which have a larger surface/volume ratio, water is generally more present than oil and tends to flow easier.

According to Land's experiments, as the oil begins to flow into the medium, it invades first the bigger pores. As the oil saturation continues to increase, the smaller the size of the pores it starts to occupy. During this process k_r follows the primary drainage curve, until the process is reversed. When this happens, the wetting phase enters the system, pushing the main bulk of the oil phase first, and trapping a portion of the non wetting phase in the smaller pores.

Since the variables of interest are mostly dependent on the saturation, this trapped volume will play a role in describing their behaviour. We will see more details of Land's work as they come up in some of the following models.

4.2. CARLSON

Let us now consider the model proposed by Carlson ([6], 1981). It focuses on the relative permeability of the non wetting phase k_n in a two phase system and it assumes that the relative permeability of the wetting phase k_w exhibits no hysteretic behaviour. Furthermore, k_n follows two bounding curves, the primary drainage curve k_n^D and the primary imbibition curve k_n^I .

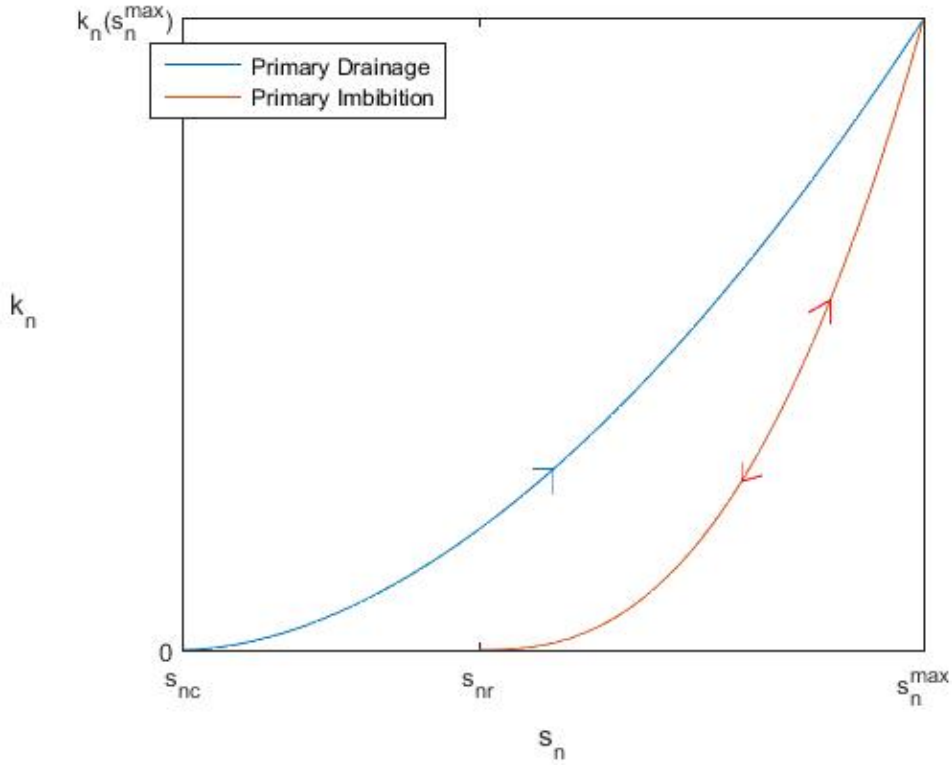


Figure 4.2: Relative permeability of oil vs oil saturation, according to Land's experiments.

As suggested by Land, it is assumed that trapping only occurs during imbibition, hence if the imbibition process is reversed then the imbibition curve will be retraced exactly, as shown in figures 4.2 and 4.4. Hence, instead of scanning curves, what we have is different imbibition curves k_n^I , as in figure 4.4.

Let s_{nt} be the "trapped" fraction of the saturation described by Land, and s_{nf} the "free" fraction, so that

$$s_n = s_{nf} + s_{nt} \quad (4.1)$$

Following Carlson's reasoning, we can predict the imbibition curve by using the drainage curve and adjusting for the trapping. The values of imbibition curve that k_n follows must be the values of the drainage curve evaluated on the free saturation only, equivalently

$$k_n^I(s_n) = k_n^D(s_{nf}) \quad (4.2)$$

This states that if no trapping occurred the imbibition and drainage curves would be identical.

Consider figure 4.3. At the beginning of the imbibition, at s_n^{max} , both curves have the same value, since no trapping has taken place yet. As the imbibition process goes on, and water starts trapping the oil, the trapped saturation s_{nt} grows and the curves drift further apart. Hence in order to predict the curve k_n^I we need to know the value of s_{nt} for any given saturation s_n .

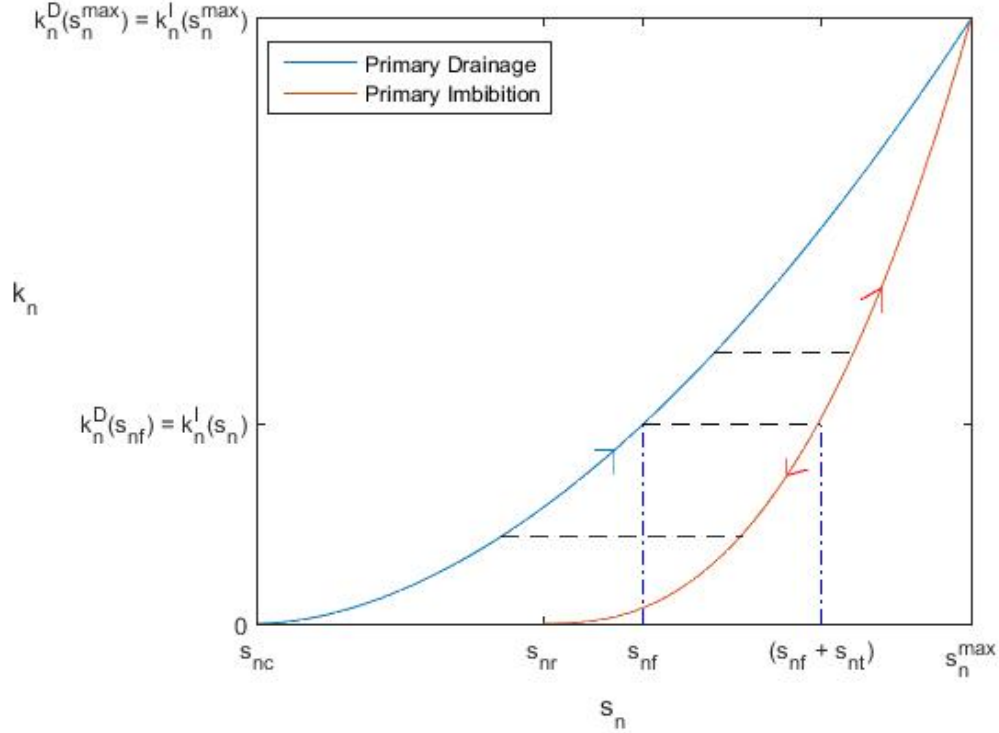


Figure 4.3: Relative permeability of oil vs oil saturation.
Equation (4.2) explains the distance between the two curves caused by the trapped saturation s_{nt} .

4.2.1. ESTIMATING THE TRAPPING

Since part of the non wetting fluid was trapped by the incoming wetting fluid, the irreducible saturation s_{nr} is strictly greater than the original saturation s_{nc} , as it contains all the trapped oil that could not be displaced. In fact, the later the drainage process is reversed, the more trapping occurs, which results in a larger residual saturation s_{nr} .

Land [7] formalized this through his experiments and established the relation between the saturation at which the drainage is reversed, s_{ni} , and the irreducible saturation s_{nr} :

$$\frac{1}{s_{nr}} - \frac{1}{s_{ni}} = C \quad (4.3)$$

where C is a constant.

Hence s_{nr} increases along with the historical maximum s_{ni} , as shown in figure 4.4. Intuitively, the more non wetting phase enters our volume before we start forcing it back out, the harder it will be for the wetting phase to push it all out, as more non wetting volume will be trapped in the smaller pores.

Land computed the value of the free saturation s_{nf} as a function of s_n , s_{nr} and C . To show this, let us recall equation (4.1):

$$s_n = s_{nf} + s_{nt}$$

It is clear that $s_{nt} = 0$ when $s_n = s_{ni}$, and that $s_{nf} = 0$ when $s_n = s_{nr}$. At any other value s_n , $s_{ni} > s_n > s_{nr}$, it is possible, using equation (4.3), to determine the distribution of s_n between s_{nt} and s_{nf} .

At s_n , exactly s_{nt} has already been trapped. The free saturation s_{nf} is subject to further entrapment according to equation (4.3). The amount in s_{nf} that is yet to be trapped, s_{nfr} , is determined by substituting s_{nf} for s_{ni} and s_{nfr} for s_{nr} in equation (4.3):

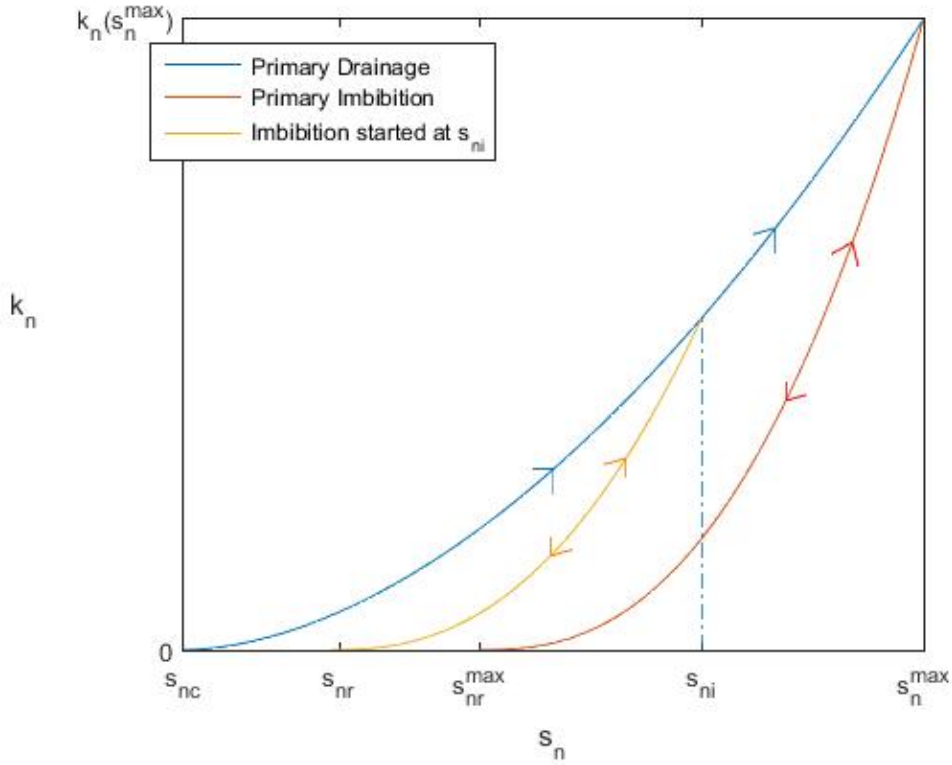


Figure 4.4: Relative permeability k_n vs s_n . The drainage process has been reversed at s_{ni} . Equation (4.3) states the relation between s_{ni} and s_{nr} .

$$\frac{1}{s_{nfr}} - \frac{1}{s_{nf}} = C$$

Equivalently

$$s_{nfr} = \frac{s_{nf}}{1 + Cs_{nf}} \quad (4.4)$$

Eventually s_{nt} will reach s_{nr} , but at the moment the trapped saturation is the future total trapped saturation minus the saturation yet to be trapped, i.e.

$$s_{nt} = s_{nr} - s_{nfr}$$

Substituting (4.4) into this last equation yields

$$s_{nt} = s_{nr} - \frac{s_{nf}}{1 + Cs_{nf}}$$

Replacing s_{nt} by $s_n - s_{nf}$,

$$s_n - s_{nf} = s_{nr} - \frac{s_{nf}}{1 + Cs_{nf}}$$

Solving for s_{nf} yields

$$s_{nf} = \frac{1}{2} \left[(s_n - s_{nr}) + \sqrt{(s_n - s_{nr})^2 + \frac{4}{C}(s_n - s_{nr})} \right] \quad (4.5)$$

This equation allows us to determine s_{nf} at any given moment. The value of s_{nf} can then be used in equation (4.2) to predict the unknown imbibition curve from the empirically known drainage curve.

However, we need the right input to compute s_{nf} . If s_{ni} is known and C can be predicted, then s_{nr} and s_{nf} can be computed using (4.3) and (4.5).

4.2.2. ESTIMATING C

Let us assume s_{ni} is known exactly. In practice measurements of s_{nr} are difficult to obtain, but we can use the following procedure to compute it without experimental determination.

Let s_{nj} be N experimental imbibition data points, and s_{nfj} their respective free saturation fractions. Substituting equation (4.3) into (4.5) and solving for s_{nr} gives us

$$s_{nrj} = \frac{1}{2} \left[s_{nj} - s_{nfj} + \left((s_{nj} - s_{nfj})^2 + \frac{4s_{ni}s_{nfj}(s_{nj} - s_{nfj})}{s_{ni} - s_{nfj}} \right)^{\frac{1}{2}} \right]$$

A value s_{nrj} is computed for every experimental data point j , in order to deal with the uncertainties that may arise. An unbiased estimate of s_{nr} is then obtained by taking the average

$$\bar{s}_{nr} = \frac{1}{N} \sum_{j=1}^N s_{nrj}$$

Once \bar{s}_{nr} is obtained, it can be used in equation (4.3) to compute C . With C determined, we can use equation (4.3) to calculate the corresponding s_{nr} given any s_{ni} . The value of s_{nf} follows immediately from this using (4.5). Finally, by equation (4.2), the imbibition curve k_n^I will be given by the drainage curve k_n^D evaluated on s_{nf} .

The whole process requires exact knowledge of the primary drainage curve and the point s_{ni} , and at least one experimental value s_{nj} in the imbibition curve.

4.3. KILLOUGH

Killough's model [5] was introduced before Carlson's and it uses a simpler solution but requires more input data. As in Carlson's model, assume no trapping occurs during drainage. Hence any imbibition curves, when reversed, are retraced exactly until we arrive again at the primary drainage curve.

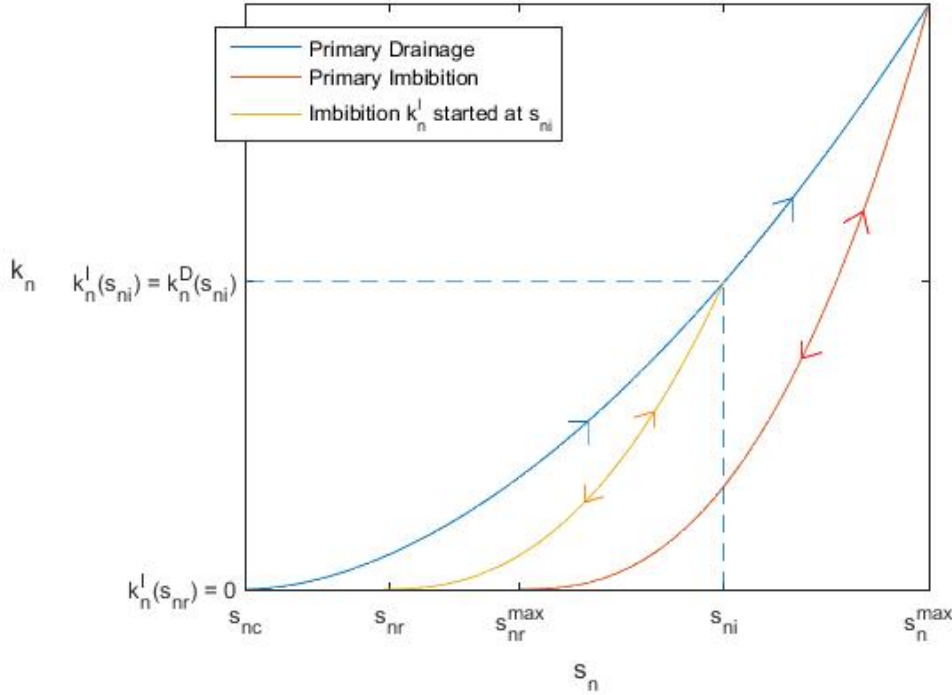


Figure 4.5: Relative permeability of oil k_n vs oil saturation s_n . Drainage process reversed at s_{ni} . The ensuing imbibition curve (yellow) results of interpolating its two extreme values.

Assume the primary drainage process is reversed at saturation s_{ni} . At this moment it is true that

$$k_n^I(s_{ni}) = k_n^D(s_{ni}) \quad (4.6)$$

However we know that the new imbibition curve will reach $k_n = 0$ when saturation arrives at s_{nr} , which depends on s_{ni} by equation (4.3).

$$k_n^I(s_{nr}) = 0 \quad (4.7)$$

To predict the intermediate curve k_n^I lying between (4.6) and (4.7), Killough considered two methods: a) parametric interpolation and b) normalized experimental data.

a) Using parametric interpolation on (4.6) and (4.7) yields

$$k_n^I(s_n) = k_n^D(s_{ni}) \left(\frac{s_n - s_{nr}}{s_{ni} - s_{nr}} \right)^\lambda \quad (4.8)$$

where λ is a given parameter. Clearly it is satisfied that $k_n^I = k_n^D$ at s_{ni} and $k_n^I = 0$ at s_{nr} .

Notice that in order to obtain the corresponding value of s_{nr} , this method requires computing parameter C from equation (4.3), although Killough described it simply as

$$C = \frac{1}{s_{nr}^{max}} - \frac{1}{s_{ni}^{max}} \quad (4.9)$$

i.e. defined by the extreme values of the saturation, corresponding to the end of the primary drainage process and the end of the primary imbibition process. This requires measuring s_{nr}^{max} , which can be difficult in practical situations.

b) Alternatively to (4.8), using normalized experimental data results in

$$k_n^I(s_n) = k_n^D(s_{ni}) \left[\frac{k_n^{I*}(s_n^*) - k_n^{I*}(s_{nr}^{max})}{k_n^{I*}(s_n^{max}) - k_n^{I*}(s_{nr}^{max})} \right]$$

where k_n^{I*} is the experimental or analytical primary imbibition curve, which lies between the maximum possible s_n and s_{nr}^{max} , and s_n^* is given by

$$s_n^* = \left[\frac{(s_n - s_{nr})(s_n^{max}) - s_{nr}^{max}}{s_{ni} - s_{nr}} \right] + s_{nr}^{max} \quad (4.10)$$

For this last method, is clear that both boundary curves, drainage and imbibition, are assumed known at least empirically.

4.3.1. WETTING PHASE HYSTERESIS

Killough also considered the effect of trapping on the wetting phase relative permeability. The solution follows the same idea, with the scanning curve ranging from $k_w^I(s_{ni}) = k_w^D(s_{ni})$ to a maximum $k_w^I(s_{nr})$. This last value is approximated using

$$k_w^I(s_{nr}) = k_w^D(s_{nr}) + [k_w^{I*}(s_{nr}^{max}) - k_w^D(s_{nr}^{max})] \left(\frac{s_{nr}}{s_{nr}^{max}} \right)^a$$

where k_w^{I*} is defined analogous to k_n^{I*} , and a is a given parameter. The interpolation between $k_w^I(s_{ni})$ and $k_w^I(s_{nr}^{max})$ is given by

$$k_w^I(s_n) = k_w^D(s_{ni}) + \left[\frac{k_w^{I*}(s_n^*) - k_w^{I*}(s_{nr}^{max})}{k_w^{I*}(s_{nr}^{max}) - k_w^{I*}(s_n^{max})} \right] (k_w^I(s_{nr}) - k_w^D(s_{ni}))$$

where s_n^* is defined as in (4.10).

4.4. THE SCANNING HYSTERESIS MODEL

Generally denoted SHM, the model described in ([8],2001) is based on the experimental data gathered by Gladfelter and Gupta [9] and by Braun and Holland [10]. They did not consider horizontal flow as it is done in this document, but rather they studied vertical flow driven by gravity in porous media.

Consequently, the curves they registered for relative permeability are different that the ones used by Land. Also they do not borrow from Land's theory for oil trapping, but rather propose the following behaviour:

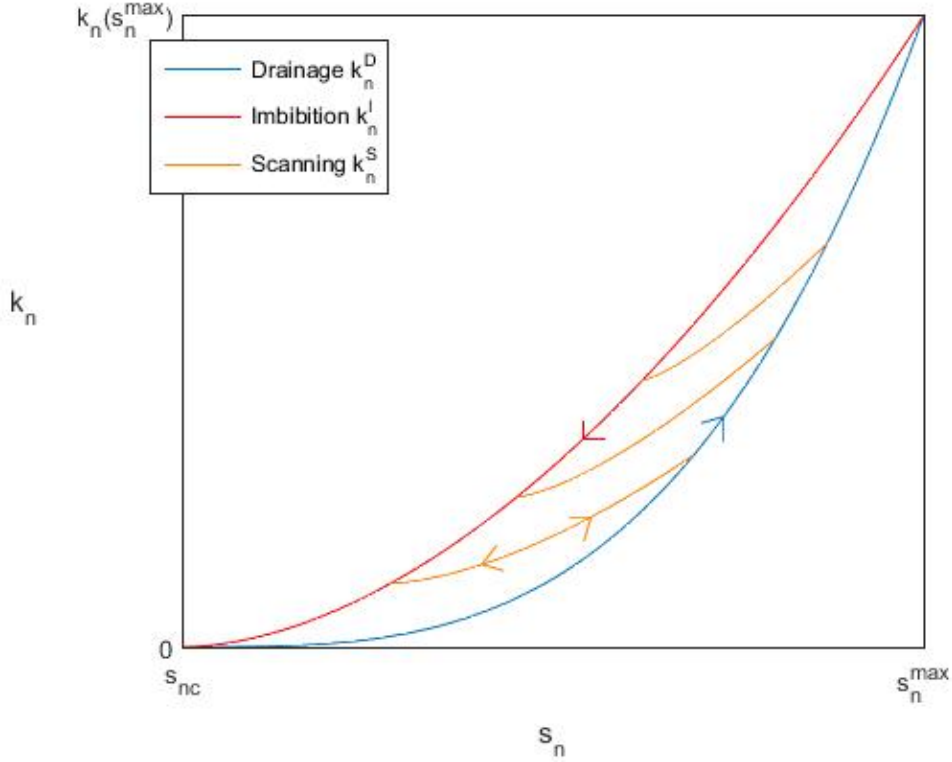


Figure 4.6: Relative permeability of oil vs oil saturation, as documented by [9] and [10]. In the SHM, the scanning curves are exactly reversible.

Notice how the boundary curves have inverted roles as compared to the previous models. This discrepancy is due to the different nature of the physical model considered. This diversity of scenarios helps illustrate why are there no well-established physical models around hysteresis.

In this model, whenever a primary process is reversed, a scanning curve is used to move from one primary curve to the other. If a process is reversed while on a scanning curve, the scanning curve is retraced exactly. The boundary curves are assumed known and denoted by

$$k_n^D(s_n) \quad \text{and} \quad k_n^I(s_n)$$

For the scanning curves, a parameter π is introduced to serve as the “memory” of the system:

$$k_n^S = k_n^S(s_n, \pi)$$

As we move along one of the boundary curves, i.e. drainage or imbibition, the memory state of the system changes, hence π changes accordingly. As soon as we enter a scanning curve, parameter π remains constant during the duration of the scanning process, until we reach another boundary curve.

For consistency, π is different for every scanning process, which implies scanning curves never touch. Since it is only a reference parameter, π values can be chosen arbitrarily. In this case, $\pi \in [0, 1]$.

For continuity, when following a primary curve, π must be modified in such a way that

$$k_n^D(s_n) = k_n^S(s_n, \pi) \quad \text{along the primary drainage curve}$$

and

$$k_n^I(s_n) = k_n^S(s_n, \pi) \quad \text{along the primary imbibition curve}$$

This, together with the smoothness and monotony of the relative permeability functions, uniquely determines π . Hence π can be solved as a function of the saturation s_n in any of both cases:

$$\pi = \pi^D(s_n) \quad (\text{drainage}) \quad \text{and} \quad \pi = \pi^I(s_n) \quad (\text{imbibition})$$

4.4.1. THE SHM EQUATIONS

Next, an expression for k_n^S must be chosen. Schaerer et al [11] use the following choices, defined as functions of $s = s_w$:

$$k_n^D(s) = (1 - s)^\eta$$

$$k_n^I(s) = (1 - s)^\theta$$

With $1 < \theta < \eta$, and

$$k_n^S(s, \pi) = \frac{(1 - \pi)^\xi}{(1 - \alpha\pi)^\zeta} (1 - \alpha s)^\zeta$$

Where ξ, ζ are also shaping parameters greater than 1. In [11], they use $\theta = 2, \eta = 3, \xi = 2$ and $\zeta = 1$.

Once π^D and π^I are defined, the convection-diffusion equation for the wetting phase (2.10) is modified to include the parameter π :

$$\frac{\partial s}{\partial t} + \frac{\partial}{\partial x} F(s, \pi) = \frac{\partial}{\partial x} \left[\varepsilon \frac{\partial s}{\partial x} \right] \quad (4.11)$$

where $s = s_w$, ε is taken as a small positive constant, and F is divided in three cases,

$$F(s, \pi) = f^D(s) = \frac{k_w(s)/\mu_s}{k_w(s)/\mu_s + k_n^D(s)/\mu_n} \quad \text{when} \quad \pi = \pi^D(s) \quad \text{and} \quad \frac{\partial s}{\partial t} < 0$$

$$F(s, \pi) = f^I(s) = \frac{k_w(s)/\mu_s}{k_w(s)/\mu_s + k_n^I(s)/\mu_n} \quad \text{when} \quad \pi = \pi^I(s) \quad \text{and} \quad \frac{\partial s}{\partial t} > 0$$

$$F(s, \pi) = f^S(s) = \frac{k_w(s)/\mu_s}{k_w(s)/\mu_s + k_n^S(s, \pi)/\mu_n} \quad \text{and} \quad \frac{\partial \pi}{\partial t} = 0 \quad \text{otherwise}$$

corresponding to the drainage, imbibition and scanning case, respectively.

The system is then supplied with appropriate initial and/or boundary conditions. Riemann solutions for this problem are presented in [8] and [11].

4.5. LARSEN & SKAUGE

Hysteresis is also present during changes in saturation during three phase flow. Most three-phase systems consist of a wetting phase (water), an intermediate phase (oil) and a non wetting phase (gas). In these processes, such as water alternating gas injection (WAG), the two-phase hysteresis models will generally not be able to describe relative permeabilities reported for the reservoirs.

Larsen and Skauge ([4],1998) present a representation for relative permeability that accounts for hysteresis in a three-phase scenario.

4.5.1. THREE-PHASE SYSTEMS

During two-phase flow, there is only one independent saturation, hence the system can only move in two directions, drainage or imbibition. In the three-phase system however, at least two saturations are independent, meaning there is an infinite number of directions the saturation distribution can take.

For instance a DDI process consists of decreasing water saturation, decreasing oil saturation, and increasing gas saturation. In order to be compatible with the two-phase case, relative permeabilities must be defined for every trajectory, as in figure 4.7:

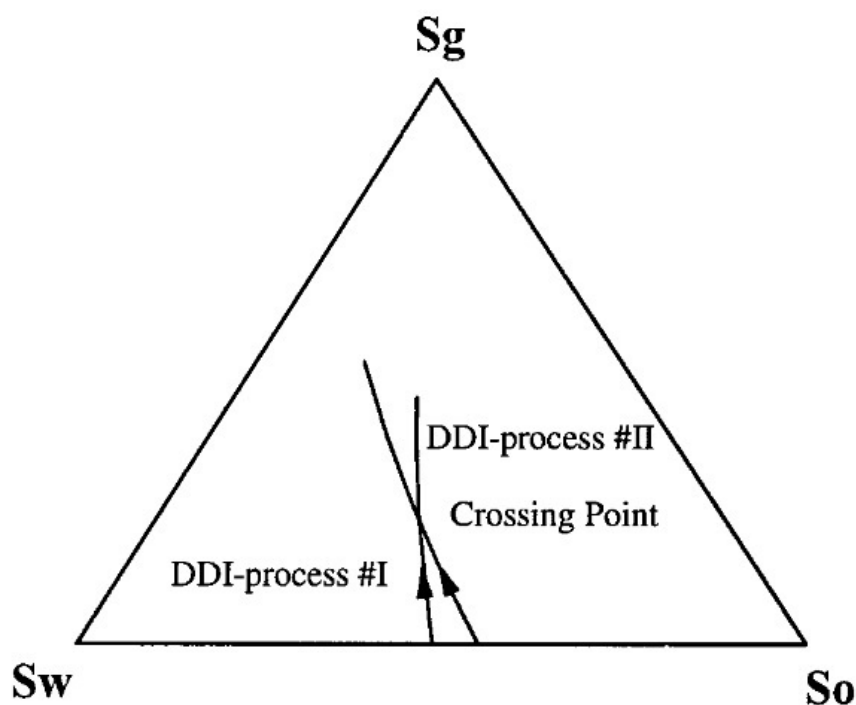


Figure 4.7: Two DDI process starting from different water and oil saturation. Due to hysteresis, at the crossing point relative permeabilities are in general not unique ([4],Figure 1).

For consistency, trajectories must be described by the three saturation directions. That is, no phase can change saturation direction during a trajectory. These are known as constrained trajectories and the model focuses on these processes only.

Like in the previous models, relative permeability of a trajectory will be a function of saturation and the starting point of a trajectory. In the two-phase case, we used s_{ni} to denote the point at which a process was reversed, i.e. when a new trajectory was started. Hence permeabilities were usually of the form

$$k = f(s_x, s_{xi})$$

where x represents either phase. In three-phase, at least two saturations are needed to determine the third one, and two initial saturations to determine the initial point of a trajectory, hence we will have

$$k = f(s_x, s_y, s_{xi}, s_{yi})$$

4.5.2. THE WAG MODEL

Consider a water alternating gas scenario. Every time both a water and a gas injection is complete, the cycle starts again, as shown in figure 4.8. These will result in hysteresis “loops”, each loop displaying overall less relative permeability, as trapping occurs on every cycle.

To estimate the trapping, Land’s formalism will be used. Only non wetting phase (gas) hysteresis will be explained.

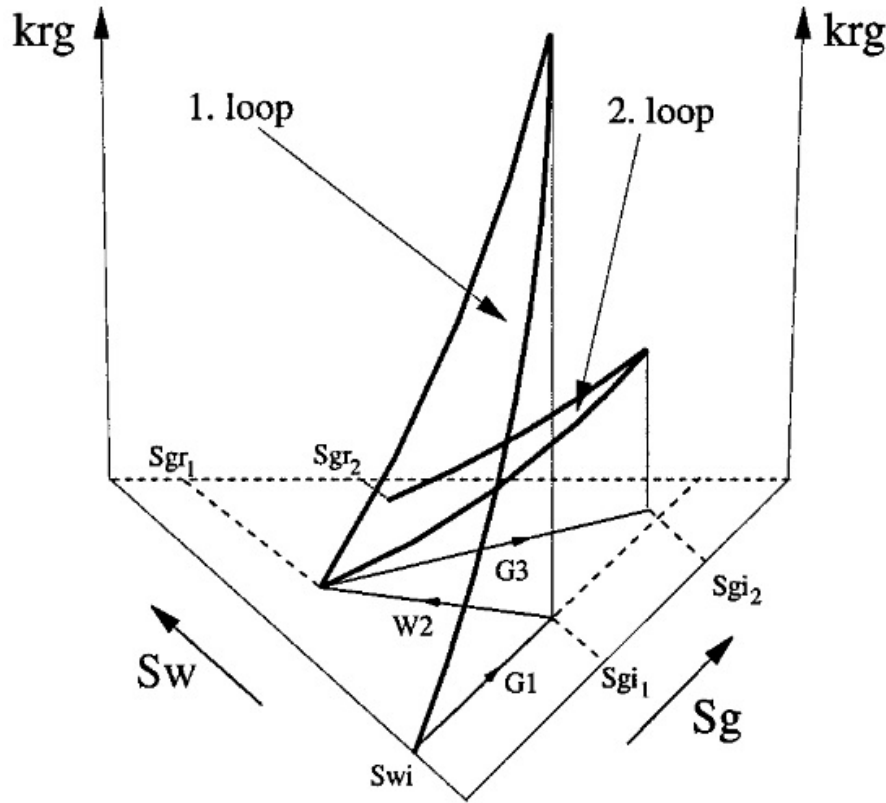


Figure 4.8: Gas relative permeability vs water and gas saturation, during a WAG process ([4], Figure 4).

DRAINAGE

During increasing gas saturation (drainage), k_g^D for loop n is calculated by

$$[k_g^D(s_g, s_w^I, s_g^{start})]_n = \left\{ [k_g^{input}(s_g) - k_r^{input}(s_g^{start})] \left(\frac{s_{wi}}{s_w^I} \right)^\alpha \right\}_n + [k_g^I(s_g^{start})]_{n-1} \quad (4.12)$$

where $s_g \in [s_g^{start}, 1]$. The primary gas relative permeability curve, G_1 , exists from $s_g = 0$ to the maximum gas saturation. The first set of parenthesis on equation (4.12) represents a transformation of the G_1 curve at $s_g = s_g^{start}$.

The second set accounts for reduction of gas relative permeability in presence of moving water. The last term is the stopping point of the last hysteresis loop. This term ensures continuity between hysteresis loop n and $n - 1$. When $n = 1$, this term is zero.

IMBIBITION

Decreasing gas saturations (imbibition) obey the trapped gas model of Land. For every loop, this involves a small transformation of the gas saturation

$$(s_g^{trans})_n = (s_g)_n - (s_g^{end})_{n-1}$$

where $(s_g)_n \in [(s_g^{end})_{n-1}, (s_{gi})_n]$. In the same way, we have

$$(s_{gr}^{trans})_n = (s_{gr})_n - (s_g^{end})_{n-1}$$

$$(s_{gi}^{trans})_n = (s_{gi})_n - (s_g^{end})_{n-1}$$

and

$$(C^{trans})_n = \frac{1}{(s_{gr}^{trans})_n} - \frac{1}{(s_{gi}^{trans})_n}$$

Now equation (4.5) can be used with transformed saturations. Note that the $(s_g^{end})_{n-1}$ term cancels out in the resulting equation:

$$(s_{gf})_n = \frac{1}{2} \left[(s_g - s_{gr}) + \sqrt{(s_g - s_{gr})^2 + \frac{4}{C^{trans}} (s_g - s_{gr})} \right]_n$$

The transformed free saturation can then be calculated as

$$(s_{gf}^{trans})_n = (s_{gf})_n + (s_g^{end})_{n-1}$$

The relative permeability can now be computed using equation (4.2), with s_{gf} replaced by s_{gf}^{trans}

$$[k_g^I(s_g) = k_g^D(s_{gf}^{trans})]_n$$

where $s_{gf}^{trans} \in [(s_g^{start})_n, (s_{gi})_n]$.

4.6. CAPILLARY PRESSURE

Two models to represent P_c hysteresis are presented in this section.

4.6.1. KILLOUGH

A model proposed by Killough [5] exists where the bounding curves behave asymptotically at the extreme saturations s_{wc} and $1 - s_{nc}$, as in figure 4.9. If a reversal happens at point s_{wi} , then a scanning curve is produced with starting point $(s_{wi}, f(s_{wi}))$, and the ending point is one of the two asymptotic saturations. The shape of the scanning curve is interpolated from the two bounding curves and it depends on the direction of the curve.

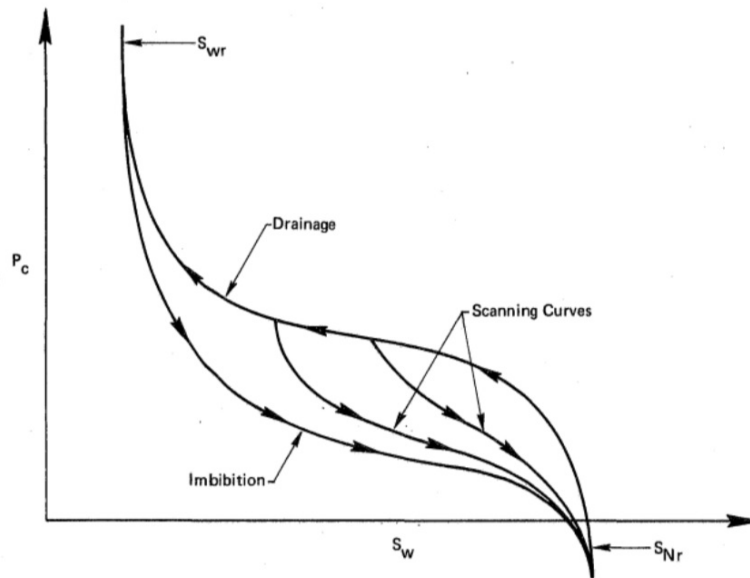


Figure 4.9: Bounding curves and scanning curves for capillary pressure as a function of s_w ([5], Figure 1).

Any other reversal may happen while on a scanning curve (figure 4.10). This is treated in the same fashion, i.e. a new scanning curve starts at the new reversal point $s_{wi}^{(2)}$ and ends at the last remembered reversal point s_{wi} , after which it rejoins the bounding curve again.

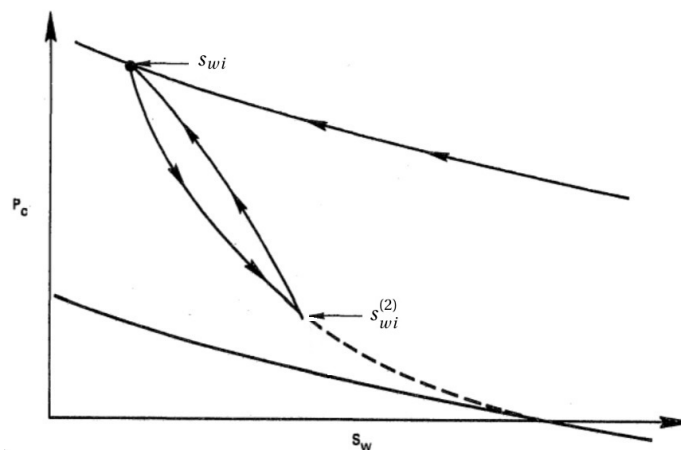


Figure 4.10: Scanning curve reversed at point $s_{wi}^{(2)}$, which generates a second scanning curve which ends at the original reversal point s_{wi} ([5], Figure 2).

As with relative permeability, each scanning curve depends on the reversal point s_{wi} , and each point s_{wi} yields a different scanning curve. As before, scanning curves going in the same direction will not intersect.

Notice how the ending point for any scanning curve going in the imbibition direction is s_{nr} . Hence, in order for this model to be compatible with the relative permeability hysteresis model, Land's prediction of trapped oil s_{nr} must be respected and, as before, dependent on the reversal point s_{wi} by equation (4.3).

4.6.2. KLEPPE ET AL

An alternate model is proposed by J. Kleppe, P. Delaplace, R. Leonormand, G. Hamon and E. Chaput for capillary pressure as a function of gas saturation. In [12] they describe an experiment with gas-oil drainage and imbibition where oil acts as the wetting phase, which exhibits no effects from hysteresis, and gas takes the role of the non wetting phase with hysteresis. Analogously to a water-oil system, one may assume

$$s_g + s_o = 1$$

In their experiment, Land's equation (4.3) was not able to adequately describe the residual saturation of the non wetting phase, i.e. the gas saturation s_{gr} . Their results showed that the relation between s_{gi} and s_{gr} was approximately linear. Compatible with their measurements is the formula:

$$s_{gr} = \frac{s_{gi}}{s_g^{max}} s_{gr}^{max} \quad (4.13)$$

In their model scanning curves are not interpolated but rather each depends on only one bounding curve. For instance, if a reversal occurs at saturation s_{gi} while on the drainage curve, i.e. while the gas saturation is increasing, the new scanning curve is exactly the imbibition curve scaled down to the domain of the scanning curve, i.e. to $[s_{gr}, s_{gi}]$, with the residual saturation s_{gr} determined by s_{gi} by equation (4.13):

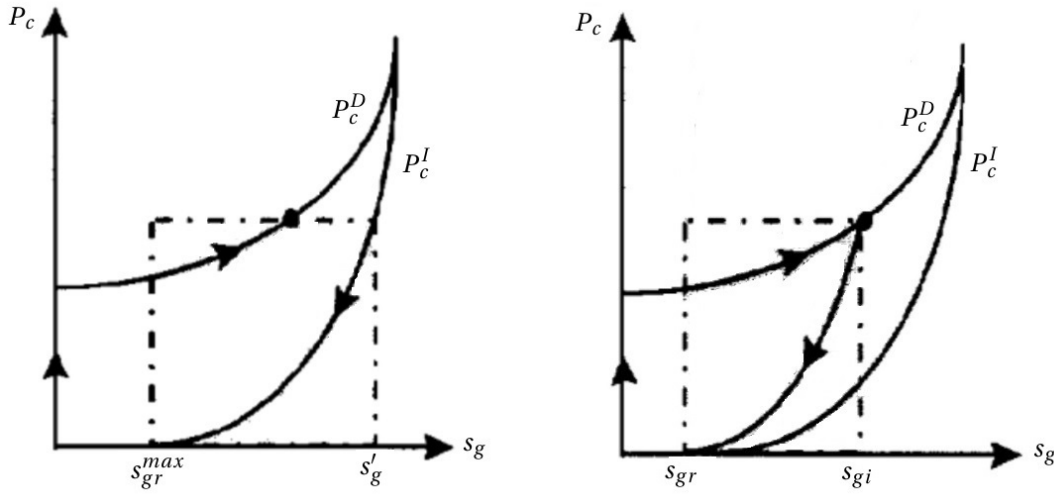


Figure 4.11: Capillary pressure P_c as function of gas saturation s_g . Drainage process reversed at point s_{gi} generating a scanning curve which ends at s_{gr} ([12], Figure 9).

In this case, the scanning curve is given by

$$P_c(s_g) = P_c^I(s_g^I)$$

with $s_g \in [s_{gr}, s_{gi}]$ and $s_g^I \in [s_{gr}^{max}, s_g^I]$ defined as

$$s_g^I = (s_g' - s_{gr}^{max}) \left(\frac{s_g - s_{gr}}{s_{gi} - s_{gr}} \right) + s_{gr}^{max}$$

where s_g^I is the saturation that satisfies $P_c^I(s_g^I) = P_c(s_{gi})$.

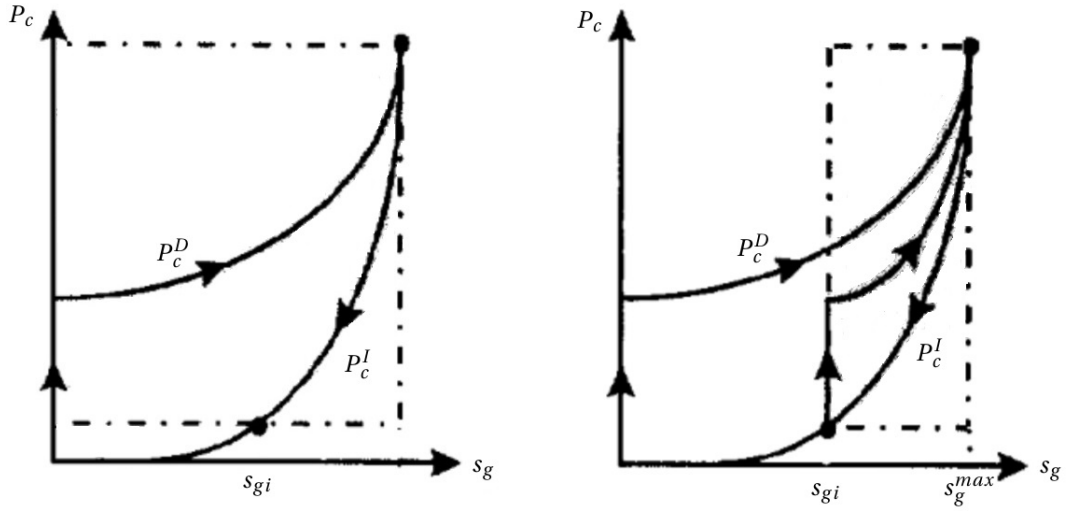


Figure 4.12: Imbibition process reversed at point s_{gi} generating a scanning curve which ends at s_g^{max} ([12], Figure 9).

Similarly for the reversal of an imbibition process the scanning curve is given by the drainage curve P_c^D scaled from $[s'_g, s_g^{max}]$ to $[s_{gi}, s_g^{max}]$, equivalently

$$P_c(s_g) = P_c^D(s_g^D)$$

with $P_c^D(s'_g) = P_c(s_{gi})$ and

$$s_g^D = (s_g^{max} - s'_g) \left(\frac{s_g - s_{gi}}{s_g^{max} - s_{gi}} \right) + s'_g$$

Reversals may happen not only on bounding curves but rather anywhere in the P_c graph. In this case the algorithm remains the same, since we can always find s'_g such that $P_c^\delta(s'_g) = P_c(s_{gi})$, for $\delta = I, D$ and $P_c(s_{gi})$ the starting point of the scanning curve, whichever it may be.

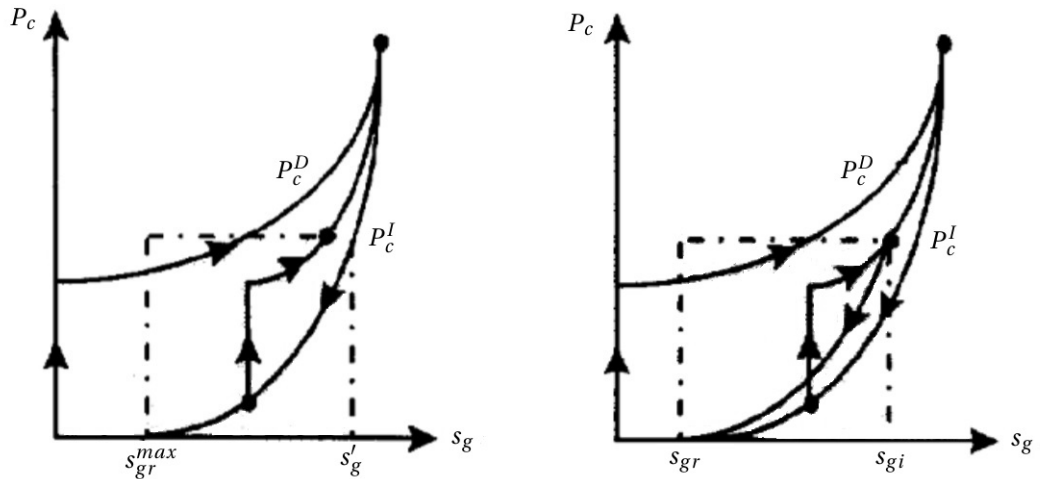


Figure 4.13: Secondary drainage process reversed at point s_{gi} generating a second scanning curve which ends at s_{gr} ([12], Figure 9).

Notice that, as opposed to Killough's method, any new scanning curve will not depend on the history of all previous scanning curves. It depends solely on the last reversal point and direction.

5

MODELLING WITH HYSTERESIS

5.1. THE BUCKLEY-LEVERETT SOLUTION

Recall the Buckley-Leverett equation 2.11 for two-phase systems:

$$s_t + f(s)_t = 0 \quad (5.1)$$

where $s = s_w$ and $f(s) = \frac{v}{\phi} f_w(s)$. If we assume the solution $s(x, t)$ to be smooth, we may write this in its quasilinear form

$$s_t + f'(s)s_t = 0$$

and the characteristic velocities are given by

$$f'(s) = \frac{v}{\phi} \frac{\partial f_w}{\partial s} \quad (5.2)$$

For f_w defined as in 2.7 the characteristic velocities have the following shape:

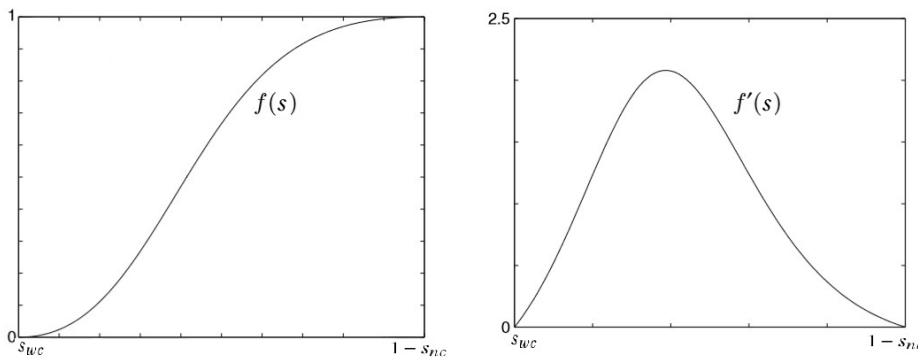


Figure 5.1: Flow function $f(s)$ as in equation 5.1 and the characteristic velocities described by $f'(s)$.

For such a flow function, Buckley and Leverett found a solution to the hyperbolic equation 5.1. Consider initial conditions similar to (2.15), namely

$$\begin{aligned} s(x, 0) &= s_{wc} \\ s(0, t) &= 1 - s_{nc} \end{aligned}$$

then the solution consists of an advancing shock wave followed by a rarefaction wave. This is known as a compound wave (figure 5.2).



Figure 5.2: Water saturation profile for the Buckley-Leverett solution of a water injection. The correct solution is built from the triple-valued solution by setting the shock wave at the front of the advancing water.

Since the speed of the shock must be given by the Rankine–Hugoniot condition (2.17), the value of s at the left side of the shock is the saturation that travels at that specific characteristic speed, i.e. the saturation that satisfies

$$f'(s) = \frac{f(s) - f(s_R)}{s - s_R} \quad (5.3)$$

Let the shock saturation be denoted by s_k . All saturations below it move at the same speed, thus forming a shock of height s_k . The saturations above s_k move at their respective characteristic speeds in a rarefaction wave. Figures 5.3 and 5.4 show the Buckley-Leverett solution compared to the simulations obtained by the IMPES method.

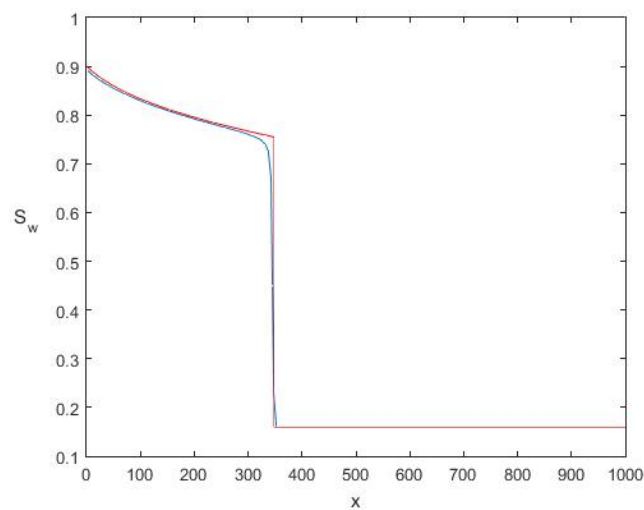


Figure 5.3: Buckley Leverett solution (red) and the numerical solution by IMPES (blue) after $t = 200$ days. For comparison to be possible, velocity v in equation 5.2 must be coherent with the boundary conditions used in the simulation.

Notice the physical interpretation of figure 5.3: As water moves in it displaces a certain fraction s_k of the oil immediately, but it cannot push all of it at once. Behind the shock, there is a mixture of oil and water, with less and less oil as time goes on.

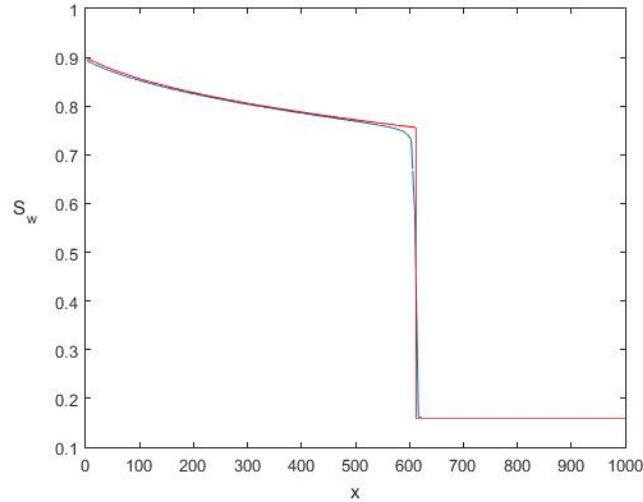


Figure 5.4: Buckley Leverett solution (red) and the numerical solution by IMPES (blue) after $t = 400$ days.

At the production well at the right boundary, one obtains the maximum saturation of oil steadily until the shock arrives, after which comes the mixture. After the shock, the oil production is diminished at each time step. Notice how it is impossible to recover all the oil in a finite amount of time.

5.2. THE BUCKLEY-LEVERETT SOLUTION WITH HISTORY

The previous section presented an example of a primary drainage only. With no reversals occurring and no initial trapping $s_{nt} = 0$, no further trapping could happen, and hysteresis was not a factor.

5.2.1. PRIMARY IMBIBITION

To show how history affects flow, consider a primary imbibition process. According to Land’s theory, as imbibition goes on oil saturation gets trapped thus decreasing oil relative permeability. This results in different flow functions f_w for the drainage and imbibition case.

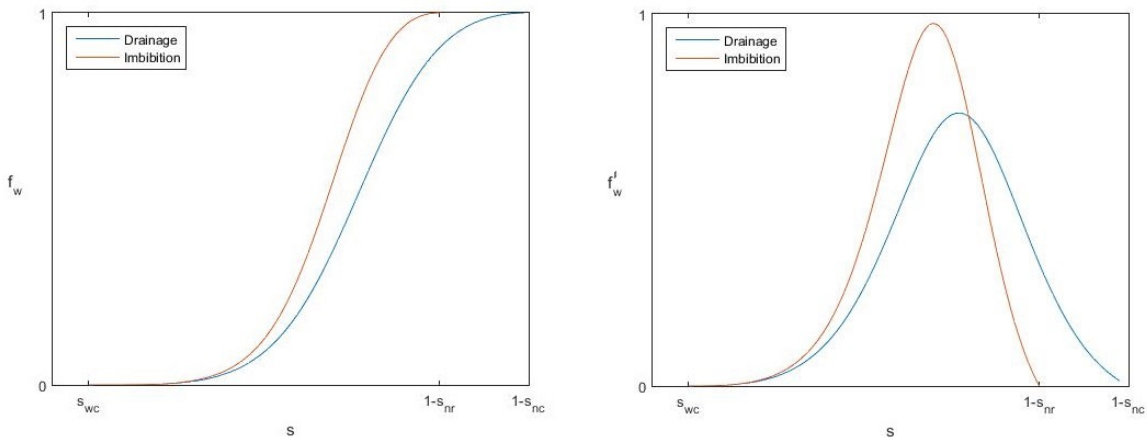


Figure 5.5: Fractional water flow f_w for the imbibition (red) and drainage case (blue), and their derivatives f'_w .

The flow function defines the shock speed and the shock saturation by the Rankine-Hugoniot condition (5.3). Notice this condition is satisfied if and only if speed $c(s)$, in this case given by

$$c = \frac{f_w(s_R) - f_w(s_L)}{s_R - s_L} = \frac{f_w(s)}{s - s_{wc}} \tag{5.4}$$

matches the slope of the tangent to $f_w(s)$, as in figure 5.6:

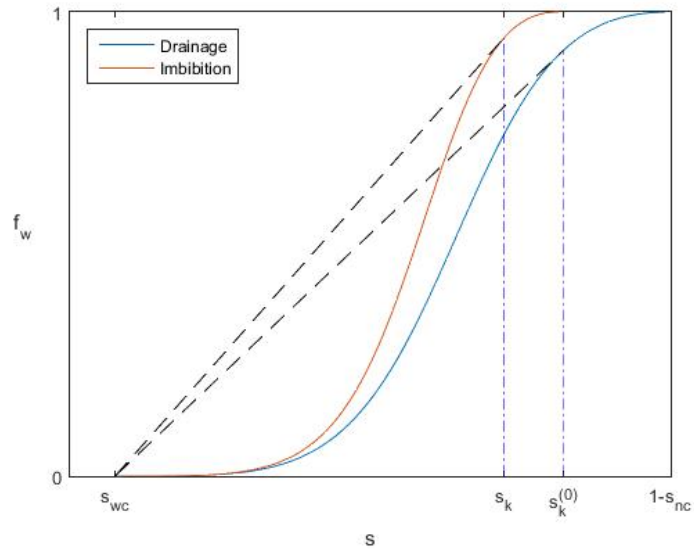


Figure 5.6: The shock saturation $s_k^{(0)}$ for a water injection with no hysteresis taken into account, and the real shock saturation s_k obtained from the imbibition curve.

The expected solution under Buckley-Leverett's reasoning changes when history is taken into account. Figure 5.7 shows the solution for the imbibition process with and without hysteresis effect:

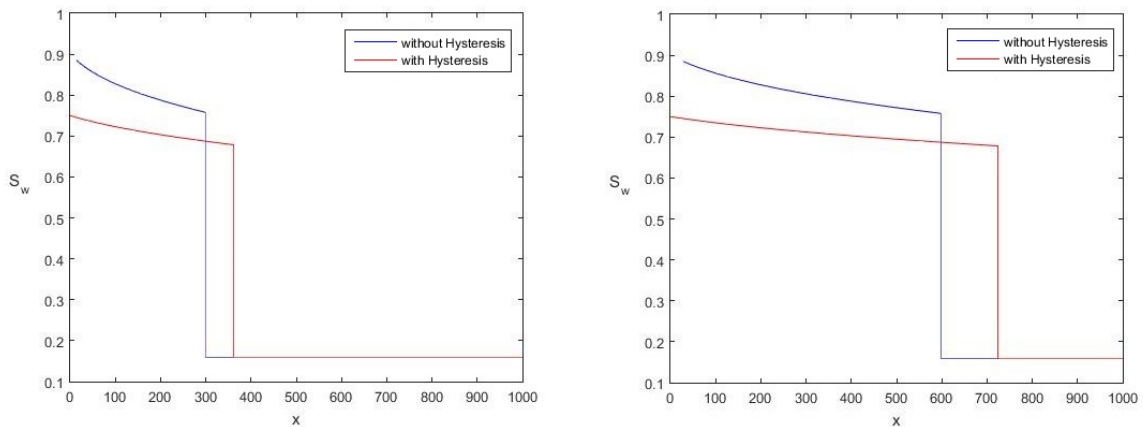


Figure 5.7: Water saturation profile for a water injection without any oil trapping (blue) and the correct solution with reduced oil mobility due to trapping (red).

Trapped oil results in a faster advancing water front which pushes less oil out of the reservoir. The pure oil production that one observes before the shock will last less, since the shock advances faster due to reduced oil mobility. Even after an infinite amount of time, the imbibition process will only manage to push out $1 - s_{nr}$ oil out, instead of the expected $1 - s_{nc}$ if hysteresis is ignored.

KILLOUGH

On this last example Killough's model was used to determine the oil relative permeability for the correct solution. In figure 5.8, Killough's model was used again for both the analytical Buckley-Leverett and the numerical solution obtained with the IMPES method:

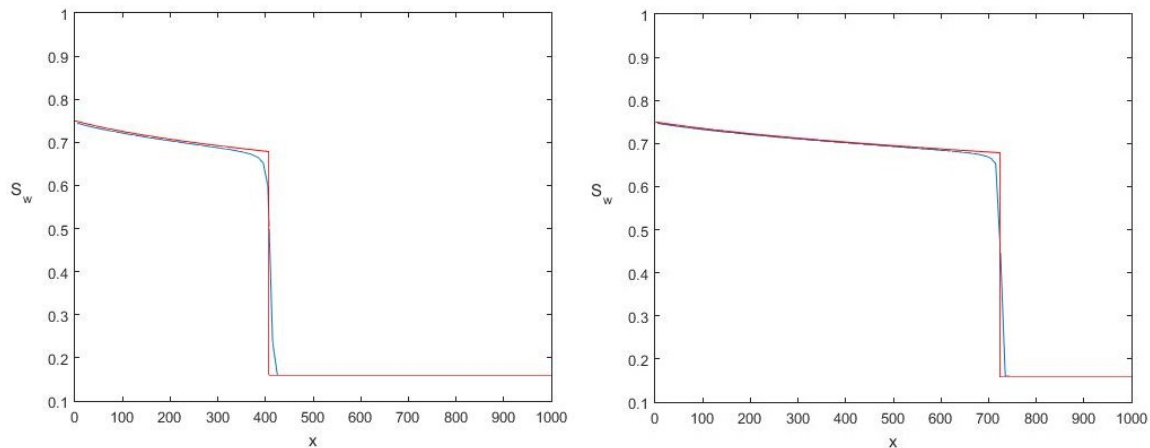


Figure 5.8: Buckley-Leverett solution for a water injection with history (red) and the numerical solution with history obtained by IMPES (blue). Both solutions consider Killough's hysteresis model.

Compare these results with figures 5.3 and 5.4. Notice how the actual solutions move faster than the ones where history was ignored. Oil is produced more slowly and in less quantity due to trapping, and the maximum theoretical amount of oil that can be recovered is also reduced.

CARLSON

By the same process, the solution can also be built from the imbibition curve described by Carlson's model. Imbibition curves for the models of Carlson and Killough are different and this implies slightly different flow curves that those shown in figure 5.5.

Nevertheless, both models behave similarly and we can expect the final results to be similar. The numerical and analytical solutions for Carlson's reasoning agree with these expectations:

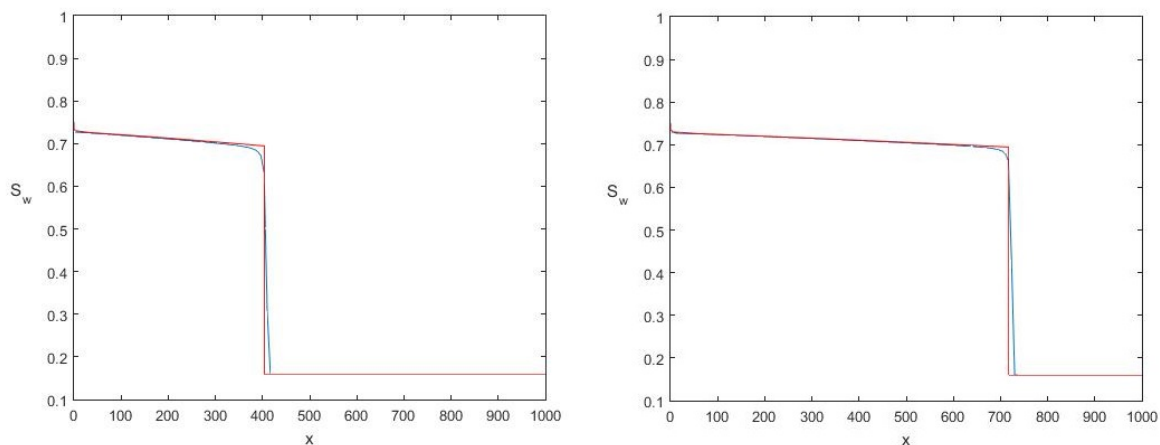


Figure 5.9: Following Carlson's model, the Buckley-Leverett solution for a water injection with history (red) is presented, as well as the numerical solution with history obtained by IMPES (blue).

Figures 5.8 and 5.9 show numerical solutions s_w discretized over a grid of size $N = 200$. In both cases, as the mesh becomes finer the solution approaches the analytical Buckley-Leverett solution.

5.2.2. SECONDARY DRAINAGE

Consider now a secondary drainage with historical turning point s_{ni} , i.e. the primary drainage was reversed at $s_{wi} = 1 - s_{ni}$, then primary imbibition followed, and finally imbibition was reversed again into a second drainage process.

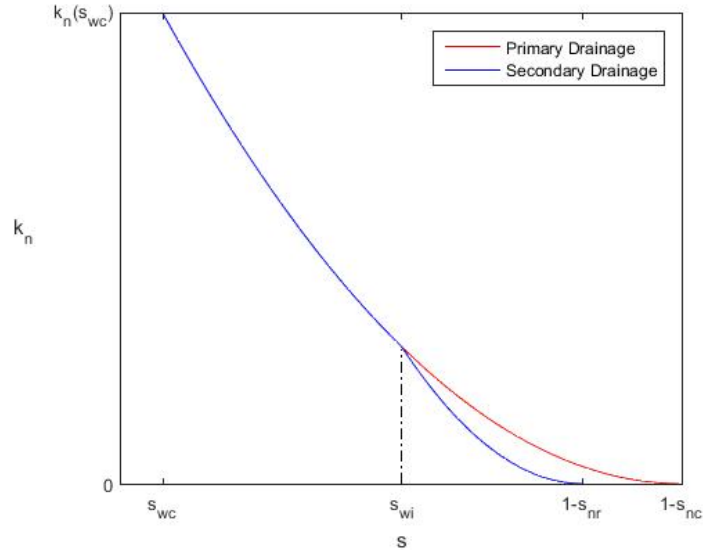


Figure 5.10: Oil relative permeability k_n vs water saturation s . First a primary drainage (red) occurred until $s = s_{wi}$. At this point, an imbibition process started and ended at $s = 1 - s_{nr}$. Finally, a secondary drainage (blue) was started and finished at $s = s_{wc}$.

According to both Carlson's and Killough's model, relative permeability during secondary drainage must now follow the imbibition curve k_n^I until oil saturation reaches s_{ni} again, at which point k_n is now given by the primary drainage curve k_n^D (figure 5.10).

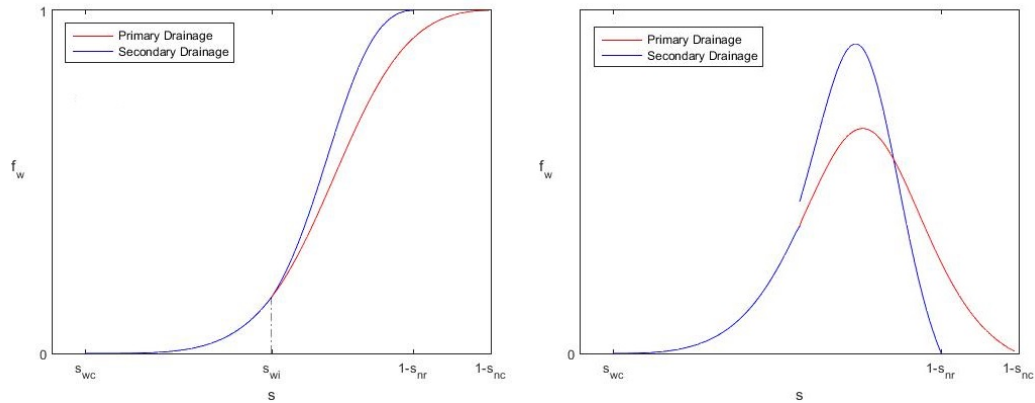


Figure 5.11: Fractional flow f_w vs water saturation s . According to Carlson and Killough, after secondary drainage reaches s_{wi} , permeabilities behave as in primary drainage.

During secondary drainage, oil relative permeability k_n is diminished due to trapped oil, thus f_w increases. When water reaches again the historical low saturation s_{wi} , the rising oil saturation has reconnected all trapped oil, hence k_n behaves as in primary drainage again and so does f_w .

Notice how the secondary drainage curve k_n is not differentiable at s_{wi} (figure 5.10), which in turn generates a discontinuity for f_w' at s_{wi} (figure 5.11). Physically, this represents the speed increase that water undergoes when oil trapping begins. Equivalently, if we choose to follow the secondary drainage curve, s_{wi} represents the historical point when oil becomes reconnected, hence gaining significant permeability.

A drainage scenario can be thought as the Buckley-Leverett equation (5.1) with initial conditions

$$\begin{aligned} s(x, 0) &= s_w^{max} \\ s(0, t) &= s_{wc} \end{aligned} \tag{5.5}$$

where the initial water saturation

$$s_w^{max} = \begin{cases} 1 - s_{nc} & \text{for primary drainage} \\ 1 - s_{nr} & \text{for secondary drainage} \end{cases}$$

depends on the kind of process. As before the solution consists of an advancing shock wave followed by a rarefaction wave. Now, however, saturations under s_k move at their respective velocities, while saturations above s_k move with the advancing shock at speed c . To show this, it is sufficient to turn figure 5.2 upside down:

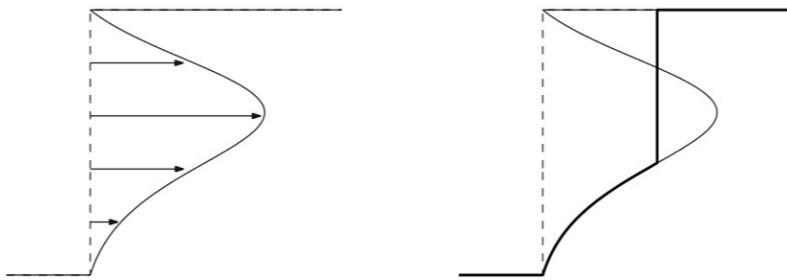


Figure 5.12: Buckley-Leverett solution built from the triple-valued solution with (5.5) as initial conditions .

In this scenario, shock speed c is given by

$$c = \frac{f_w(s_L) - f_w(s_R)}{s_L - s_R} = \frac{f_w(s) - 1}{s - s^{max}} \tag{5.6}$$

Figure 5.13 shows the shock saturation s_k obtained from equating (5.6) with f'_w .

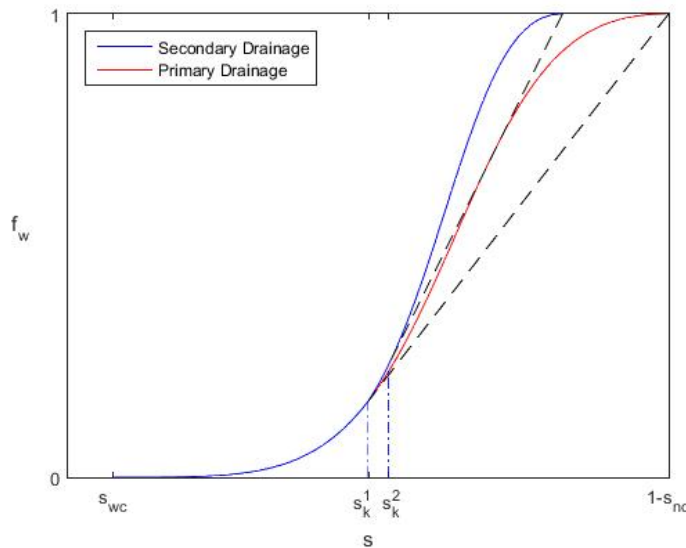


Figure 5.13: The Rankine-Hugoniot condition (5.3) is satisfied for primary drainage at s_k^1 and for secondary drainage at s_k^2 .

KILLOUGH

Following Killough's model, the resulting Buckley-Leverett solutions are:

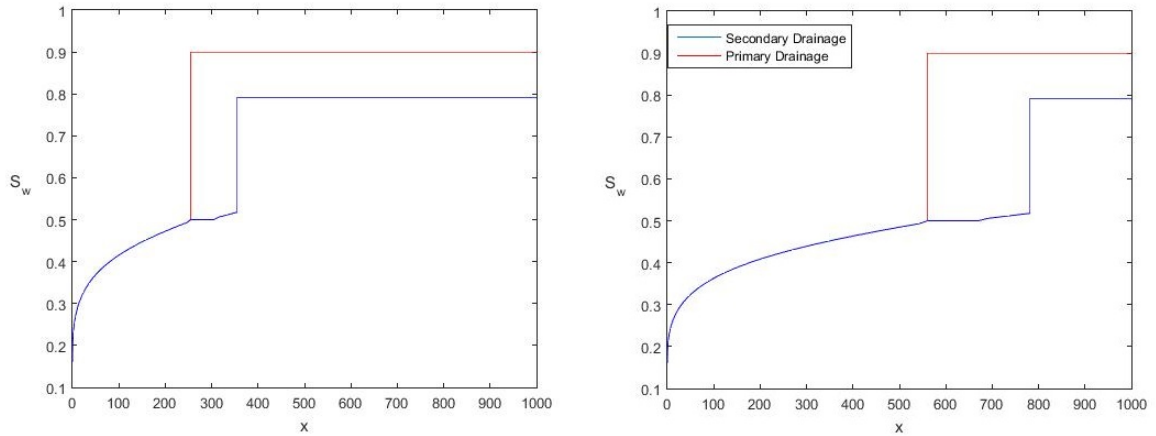


Figure 5.14: Buckley-Leverett solution for primary drainage (red) with the shock starting at saturation s_k^1 , and for secondary drainage (blue) with shock saturation s_k^2 , following Killough's model.

During secondary drainage oil advances more slowly due to its altered relative permeability curve, producing a smaller amount of water being displaced than in the primary process. By (2.6), total velocity must remain constant, hence slower oil implies that the water profile in the secondary case must move faster.

Notice as well how the discontinuity in velocity f_w' for the secondary case (figure 5.11) induces a sharp acceleration at saturation s_{wi} (which in this case coincides with s_k^1). This generates a constant region in the rarefaction wave, which grows larger as time goes on.

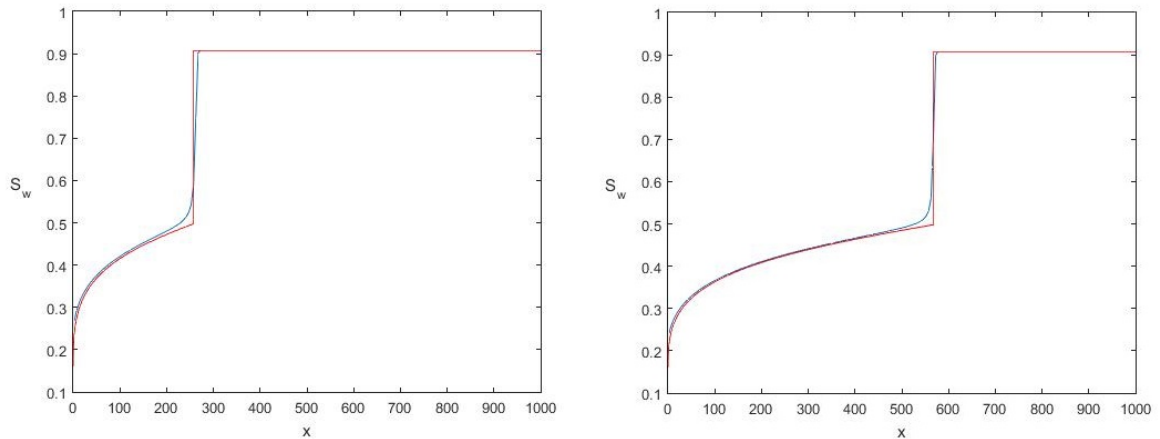


Figure 5.15: Water saturation of a primary drainage process, as described by its analytical solution (red) and its numerical solution (blue).

Figure 5.15 shows the primary drainage process analytical and numerical solutions. These curves are the same for both methods of Killough and Carlson, since they both take the same primary drainage relative permeability curve as input.

For secondary drainage process following Killough's curves, both kind of solutions are presented in figure 5.16:

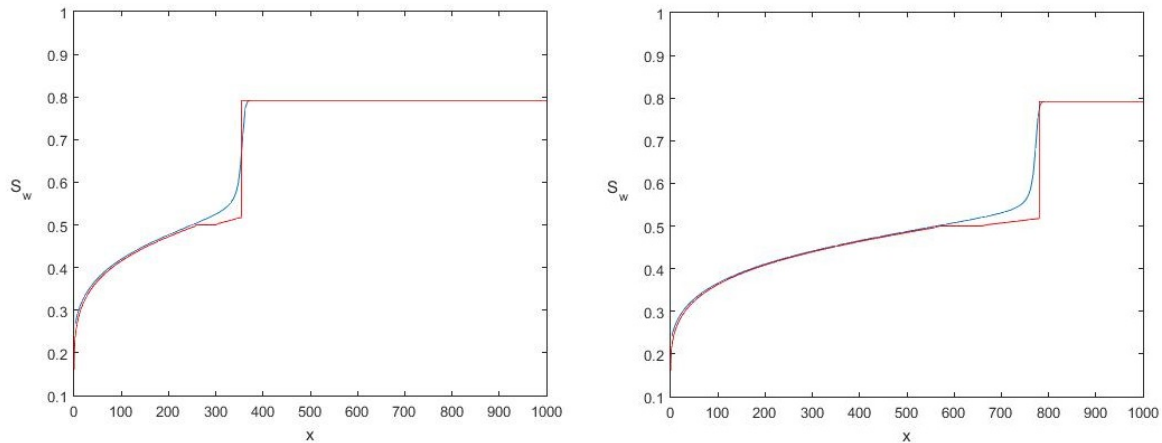


Figure 5.16: Water saturation profile of a secondary drainage process as described by Killough's method. Both the analytical (red) and numerical (blue) solutions are presented.

Drainage becomes slow immediately after breakthrough, i.e. when the shock reaches the right boundary, and grows slower as time goes on. Notice how neither one of the drainage processes, primary or secondary, manage to drain the totality of the water saturation.

CARLSON

Compare now figure 5.14 to the solutions built upon Carlson's model in figure 5.17. Notice that the same discontinuity in f_w^l at s_{wi} must be present, generating the speed gap visible in the rarefaction-wave part of the solution:

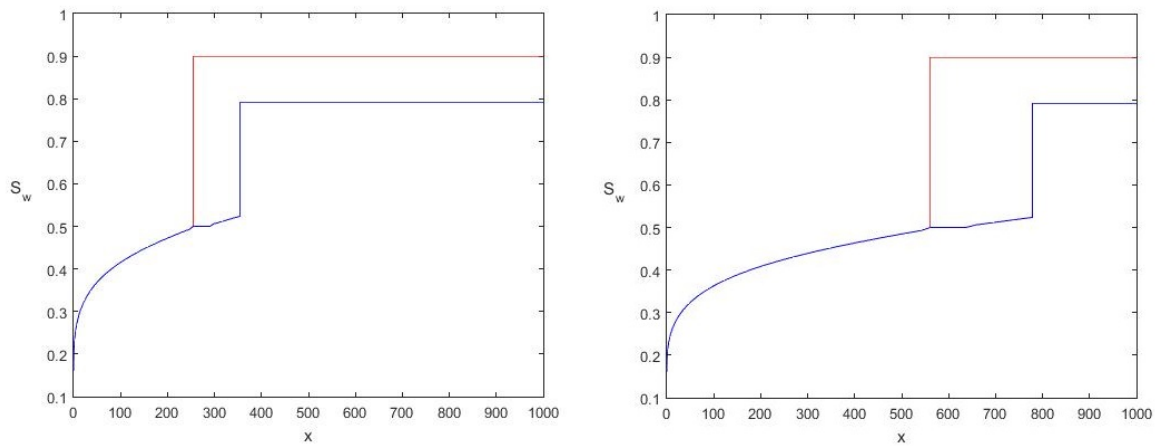


Figure 5.17: Buckley-Leverett solution for primary drainage (red) and for secondary drainage (blue) as determined by Carlson's hysteresis model.

Supplying the IMPES solution with the relative permeability curves described by Carlson, the numerical solution again behaves as the Buckley-Leverett solution:

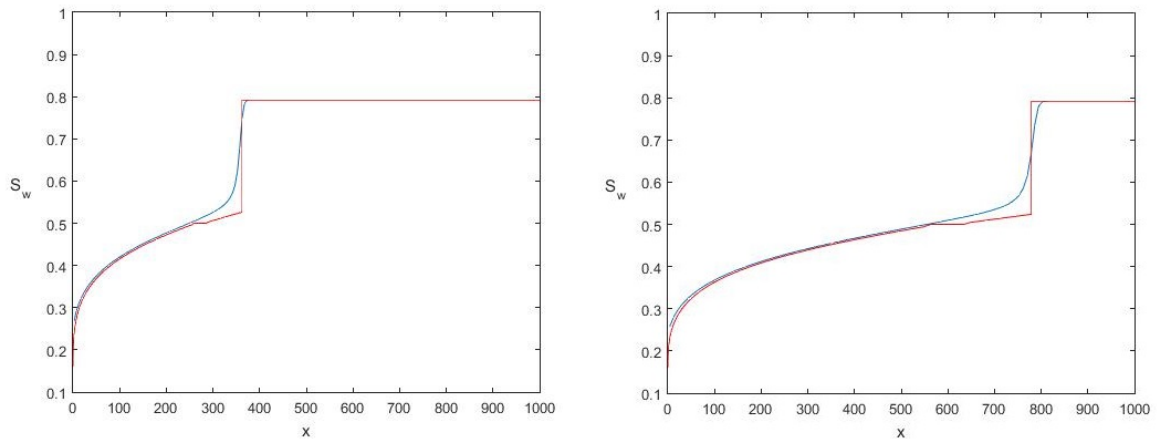


Figure 5.18: Secondary drainage process solutions, analytical (red) and numerical (blue), both exhibiting hysteresis as determined by Carlson.

As before, we find that the numerical solutions in figures 5.16 and 5.18 converge to their respective analytical solutions as the mesh becomes finer.

5.2.3. HYSTERESIS CYCLES

Assume a primary drainage process as described in figure 5.15, followed by a primary imbibition. Hence the initial state for the imbibition process will be the water saturation profile as it was at the end of the drainage. Following the solution of a primary drainage as described on figure 5.15 over time yields:

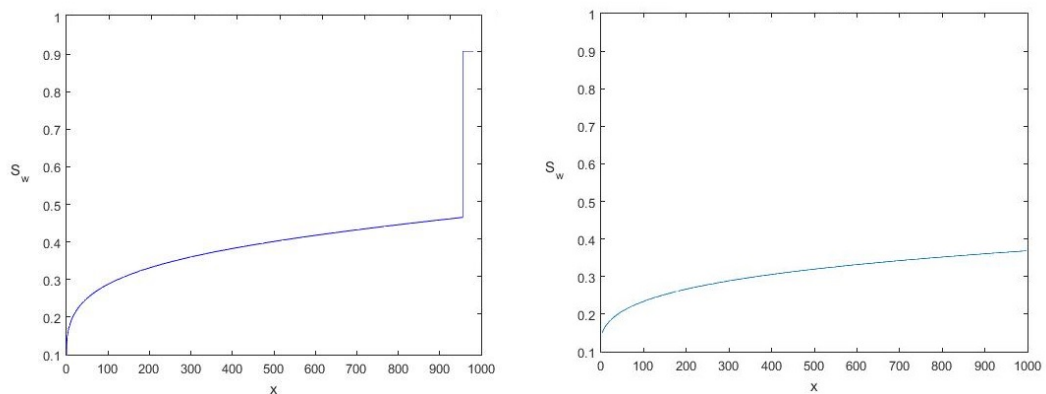


Figure 5.19: Water saturation profile for a primary drainage process, just before and after breakthrough.

After breakthrough the solution behaves as a rarefaction wave, with the water saturation slowly decreasing over time. After a finite time, when imbibition starts, saturation is not constant over the length of the reservoir. Hence the Buckley-Leverett solution will now consist of three parts: a rarefaction wave followed by a shock followed by a second rarefaction wave (figure 5.20).

The first rarefaction wave is due to the non-constant shape of the initial state. The shock and rarefaction wave that follow belong to the classic Buckley-Leverett solution described before. The shock speed c is still determined by the Rankine-Hugoniot condition (2.17), and the advancing shock saturation s_k is the value of s that satisfies (5.3):

$$f'(s) = \frac{f(s) - (s_R)}{s - s_R} = c \quad (5.7)$$

However, saturation s_R at the right side of the shock is not constant over x , hence as the shock moves along the reservoir its speed c will vary and, by (5.7), so will its shock saturation s_k .

KILLOUGH

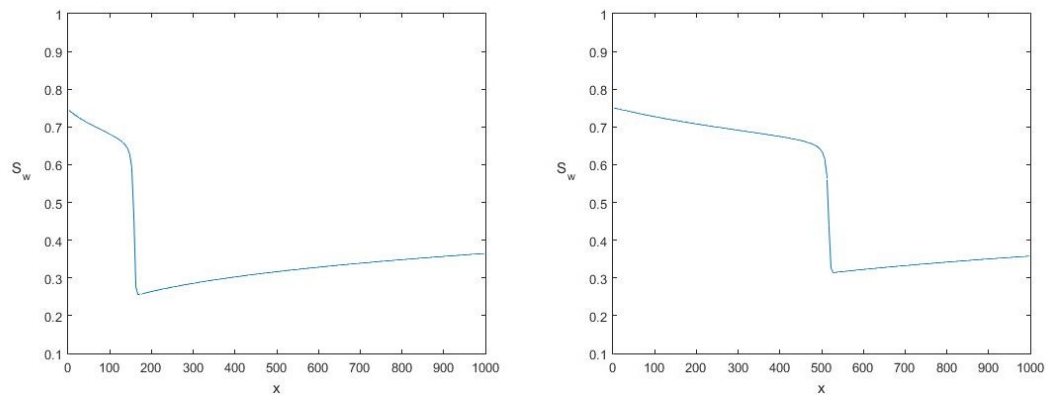


Figure 5.20: Water saturation profile for a primary imbibition process, with the end of the primary drainage as initial state.

The primary imbibition happens now faster than if performed on a constant initial state. As the shock advances, it comes across more water from the initially existing state, i.e. higher values for s_R and $f(s_R)$, causing the shock speed to increase. Shock speed continues to increase corresponding to the increase in water saturation it encounters along the reservoir.

Shock saturation also varies over time, decreasing as shock speed increases. Intuitively, as the water front encounters more water, the water in the shock gains increased relative permeability and flows easier. Since total seepage velocity must remain constant, equation (2.6), oil is displaced more slowly, which translates into less oil produced per time step at the right boundary. As we have seen in figure 5.7, lesser oil production is consistent with a smaller shock saturation s_k .

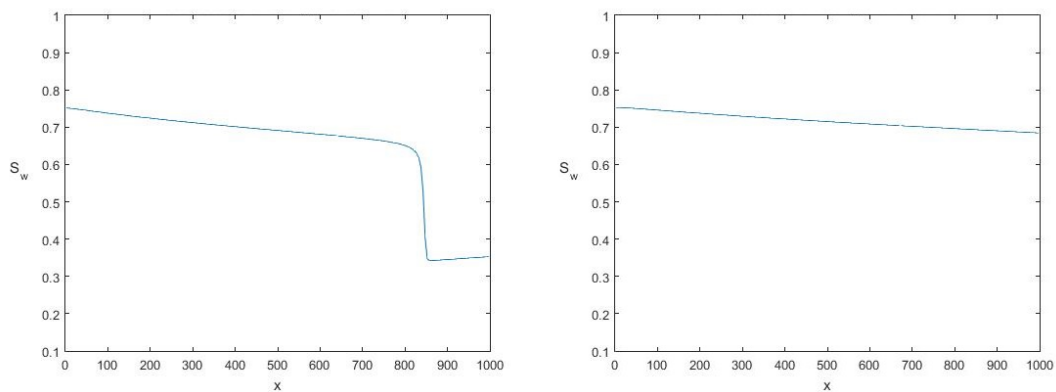


Figure 5.21: Water saturation profile for the primary imbibition process described in figure (5.20), just before and after breakthrough.

After breakthrough, we see again a water profile which is again not constant on x (figure 5.21). This is the initial state for the secondary drainage. As in the imbibition case, the solution will again consist of a rarefaction wave followed by a shock and a second rarefaction (figure 5.22).

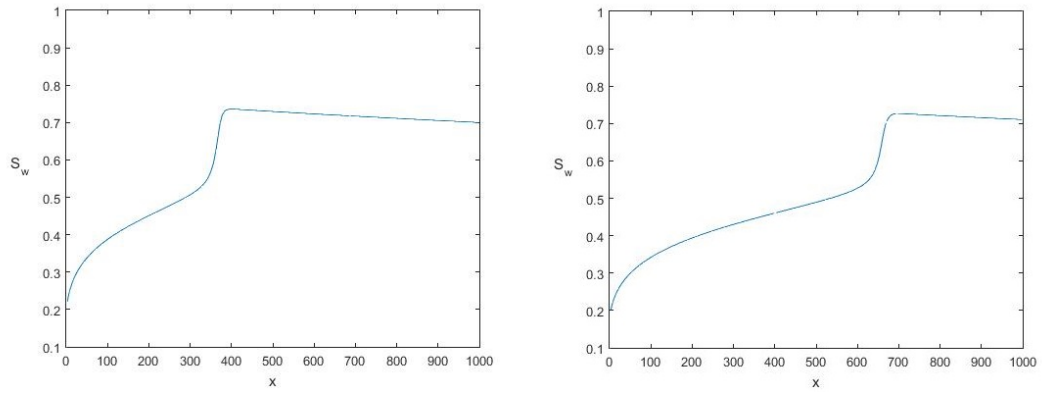


Figure 5.22: Water saturation profile for a secondary drainage process following the solution in (5.21).

CARLSON

Simulating the hysteresis cycle for Carlson's relative permeability curves yields similar results:

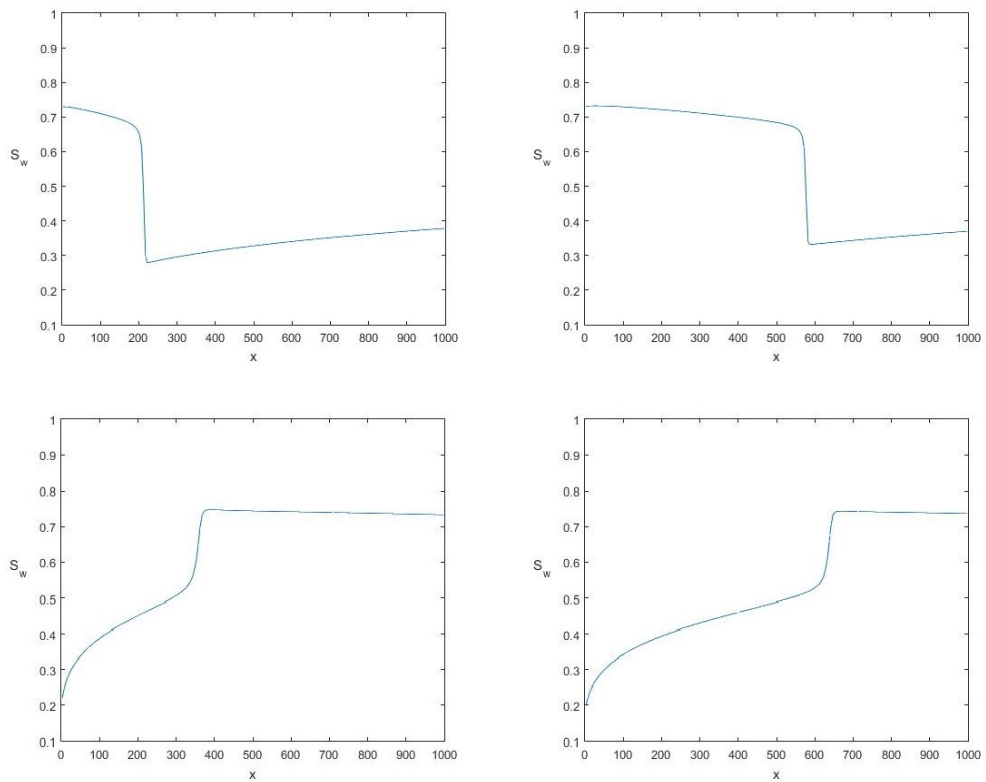


Figure 5.23: Water saturation profile for a primary imbibition process after a primary drainage (up) followed by a secondary drainage (down). Relative permeabilities are dictated by Carlson's model.

6

TIME DEPENDENT BOUNDING CURVES WITH HISTORY

The models presented so far for describing hysteresis have been using the primary drainage and primary imbibition curves, i.e. the bounding curves, as input. In these models, the bounding curves are assumed fixed. However, as mentioned in chapter 1, relative permeability functions depend on many chemical and physical properties of the reservoir.

Some of these properties like porosity, rock density, fluid viscosity, fluid composition; to mention a few, are subject to changes over time. The natural question of how the hysteresis models behave under time-dependent bounding curves is addressed in this chapter. To this purpose, let us introduce the concept of salinity as an example of time dependence.

6.1. AN EXAMPLE

The amount of dissolved salts in a body of water directly affects its viscosity, density and rock-wettability, and through these properties it also affects the relative permeability of both phases. While all these variables are needed to make accurate simulations, the interest of this document is on the effect of salinity on relative permeability hysteresis. Hence only relative permeabilities are assumed to be dependent on salt content. To further focus on hysteresis, only oil relative permeability curves are considered for these simulations.

To explain the effect of salinity on oil relative permeability curves, Jerauld, Webb & Lin [13] showed a direct relation between salt content in injected water and residual oil saturation s_{nr} . This dependence is linear and disappears after certain levels of concentration.

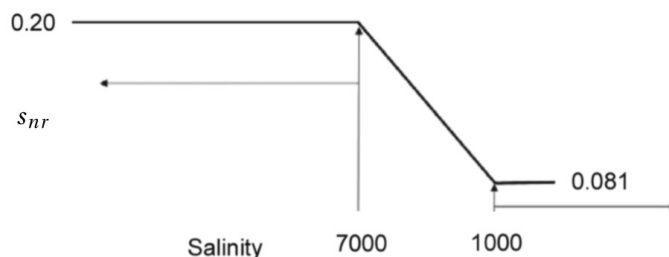


Figure 6.1: Residual oil saturation s_{nr} as a function of salinity in ppm, according to [13].

This means that the change in water viscosity and wettability imposed by the lower salinity levels produce less trapping of oil. Land's theory tells us that oil trapping is the phenomenon driving hysteresis. According to our two main models based on Land's work, Killough and Carlson, different values of s_{nr} translate into different behaviour of all the scanning curves.

6.1.1. LOW SALINITY WATER INJECTION

Low salinity water injection is usually performed to improve oil recovery. Generally, the existing connate water in the reservoir s_{wc} is displaced by the incoming water. Jerauld, Webb & Lin showed that this displacement is not always piston-like and that salt diffusion also occurs between the high salinity connate water and low salinity injected water, hence creating a double-front Buckley-Leverett solution [13].

On this document, however, the interest is on the time dependency of the bounding curves, hence piston-like displacement will be assumed with no salt exchange between the water bodies.

Assume water is continuously injected into the reservoir, and that the salinity levels of the injected water drop gradually at a constant rate. The effect on this phenomenon on the oil mobility can be expressed as a continuous function λ_n which depends explicitly on salt content $z(t)$ and implicitly on time. Hence flow function f_w varies as time goes on.

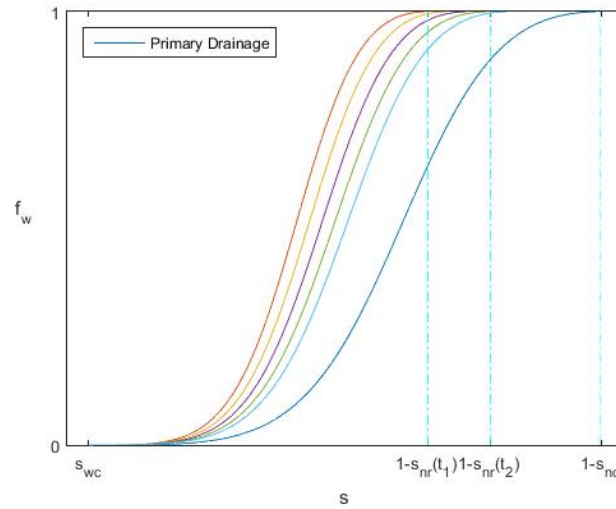


Figure 6.2: Fractional flow function f_w vs s_w corresponding to an imbibition process, for different values of trapped oil s_{nr} . The value of s_{nr} varies in time according to figure 6.1.

This makes the construction of the Buckley-Leverett solution more than challenging. Indeed, fractional flow now depends implicitly on time, hence we may write $f_w = f_w(s, t)$, and shock speed varies with time as well:

$$c(t) = \frac{f_w(s_L, t) - f_w(s_R, t)}{s_L - s_R}$$

Shock height (s_L in case of imbibition) and shock speed c are determined implicitly from equation (5.3):

$$f'_w(s) = \frac{f_w(s) - f_w(s_R)}{s - s_R} \quad (6.1)$$

Due to the time dependency of functions f_w and f'_w , equation (6.1) needs to be solved every time step, which is computationally expensive. Hence the analytical solution is not shown in this section. However, it is possible to build the numerical solution of an imbibition (or drainage) process that accounts for hysteresis with time dependent bounding curves.

We know that less residual oil saturation implies less trapping resulting in an imbibition process that displaces more oil. Results from section 5.2 showed that more displaced oil implies slower movement of the water profile, since total seepage velocity v is assumed to be constant. Hence as salinity drops, it is sensible to expect the water profile to grow larger and slower. Figure 6.3 agrees with this intuition.

In figure 6.3, the changing behaviour of the shock height and shock speed is the effect of an imbibition curve of the oil relative permeability k_n^I changing in time according to s_{nr} . Different imbibition curves imply different k_n values for the same levels of saturation (figure 6.4). Low oil saturations that could not be

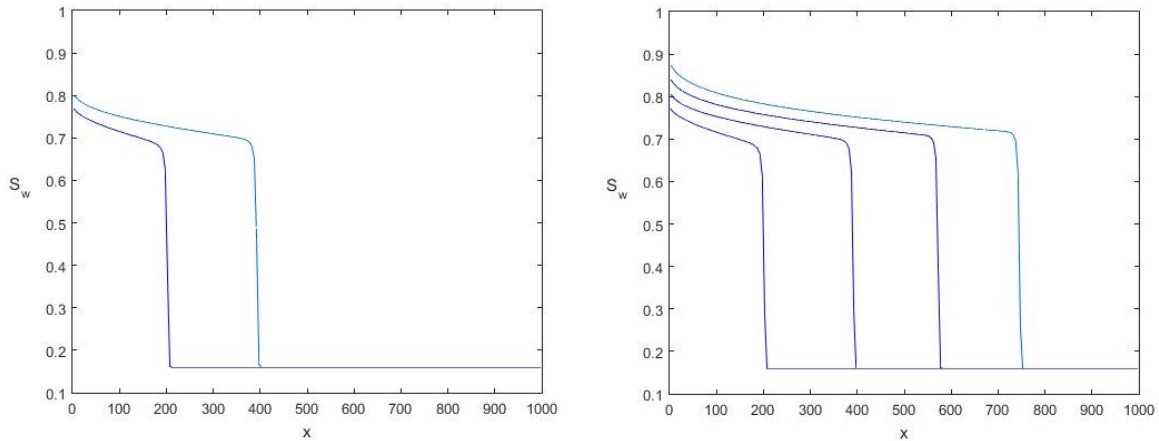


Figure 6.3: Water saturation profile for a water flood with salinity changing over time. As it advances through the reservoir, the shock speed and height varies with the salinity.

pushed by the incoming water front suddenly gain mobility, thanks to the shift in the curve k_n^I , and can now be displaced by the shock wave.

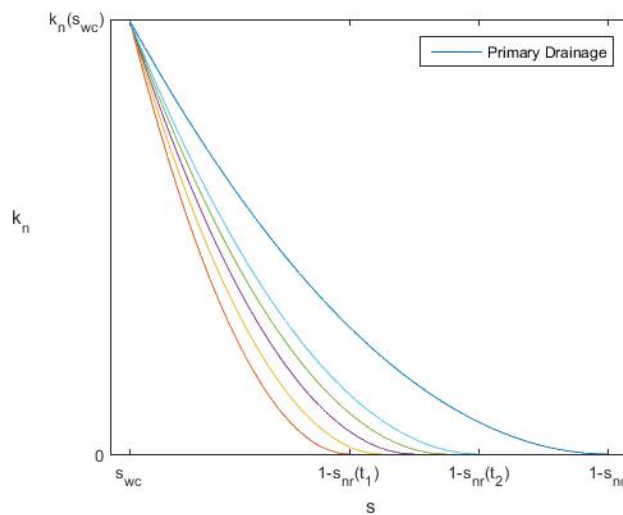


Figure 6.4: Relative permeability bounding curves for a system with varying salinity. The shape and position of the primary imbibition curve k_n^I depends on residual oil saturation $s_{nr}(t)$.

Figure 6.4 shows an example of a time depending bounding curve, where only the primary imbibition curve is affected by a decreasing parameter s_{nr} . However both bounding curves may vary in a number of ways, as in the examples listed in section 7.2.2.

For any hysteresis models, any changes on the bounding curves affect the whole system. By definition, these models require the previous history of the system to be effective. Hence it is essential that history is preserved even as the system changes in time. The question then becomes how to translate the historical information that governs the system at one time step into the next time step.

Three different methods of interpreting these time dependent bounding curves are shown in the next section. It is also argued why one of these methods is more suited for the models of Killough and Carlson, while the other better accommodates the Scanning Hysteresis Model.

6.2. TIME DEPENDENCY OF SCANNING CURVES

In the models presented in this document, all scanning curves are interpolated or otherwise determined by the bounding curves. When including time-dependent bounding curves into a hysteresis model, it is necessary to specify how scanning curves will also change in time, and they must do so according to the history of the system.

6.2.1. KILLOUGH AND CARLSON

As the bounding curves shift with time, figure 6.5, Land's constant C needs to be computed at each time step, hence equation (4.9) becomes:

$$C(t) = \frac{1}{s_{nr}^{max}(t)} - \frac{1}{s_{ni}^{max}(t)}$$

where $s_{nr}^{max}(t)$ and $s_{ni}^{max}(t)$ are the end points of the imbibition curve at time t .

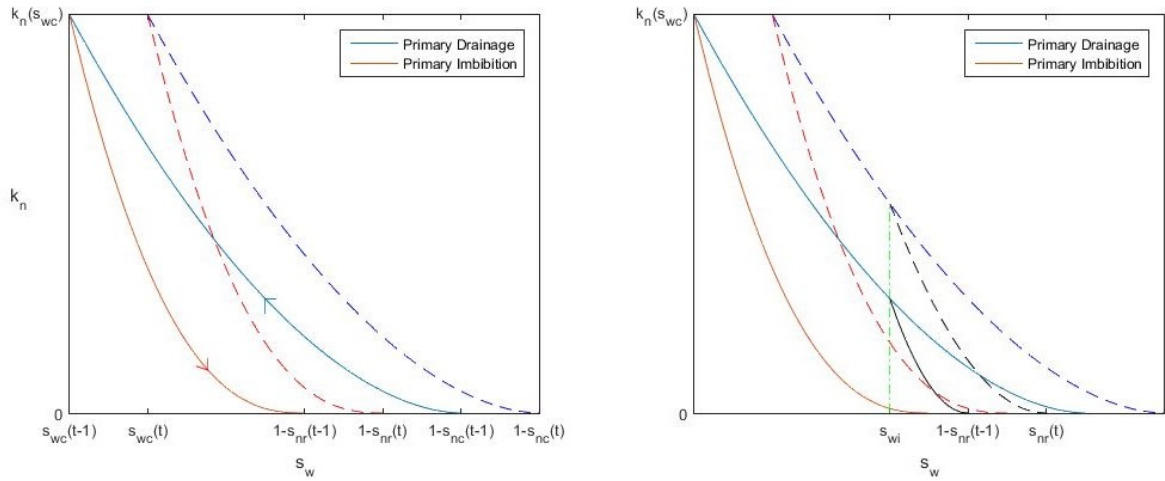


Figure 6.5: Time dependent relative permeability curves after one time step. The scanning curve (black) spanning at s_{wi} at time t^{n-1} must be redefined at the next time step t^n .

Scanning curves must also be determined at each time step. Let

$$k_n^S(s, s_{wi}, t^{n-1})$$

represent a scanning curve starting at point s_{wi} at time t^{n-1} . In the next time step, it is assumed reversal point s_{wi} remains constant, in order to keep track of the system's history. However Land's constant does not, hence the end point s_{nr} associated to s_{wi} (equation (4.3)) becomes

$$s_{nr}(t) = \left(C(t) + \frac{1}{s_{wi}} \right)^{-1}$$

The scanning curve at the new time step has two end points: $(s_{wi}, k_n^D(s_{wi}, t^n))$ and $(s_{nr}(t^n), 0)$. The saturation of the next time step $s(t^n)$ is evaluated in the new scanning curve $k_n^S(s, s_{wi}, t^n)$ (figure 6.6).

Notice that even if saturation does not change significantly over a time step, relative permeability k_n may change. Hence the oil phase may gain or loose mobility while remaining at the same level of saturation. In figure 6.6, if we assume $s(t^n) = s(t^{n-1})$, saturation remains constant over time yet its permeability is increased thanks to the new scanning curve.

In both models of Killough and Carlson, historical reversal saturation s_{wi} remains constant in order to predict the new scanning curves. This is one way of keeping track of the model's history.

However, this reasoning follows from the fact that both models are based on Land's theory of trapping. According to Land, scanning curves depend entirely on oil trapping, and trapping depends solely on reversal

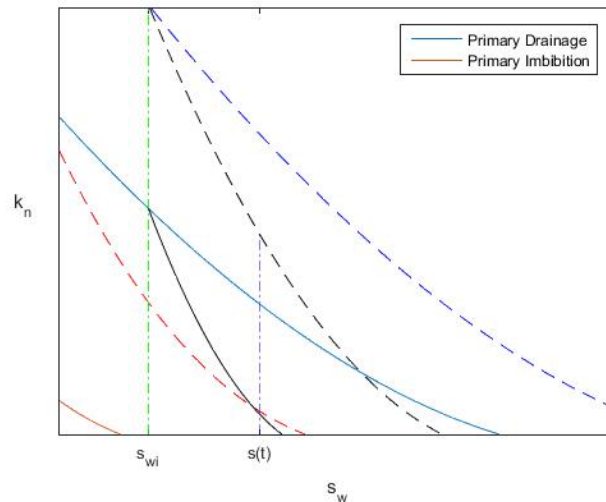


Figure 6.6: Zooming in on figure 6.5 shows saturation $s(t)$ evaluated in the new scanning curve (pointed black).

saturation s_{wi} by Land's equation (4.3). If Land's equation is assumed to hold at all times, it is sensible to conclude that scanning curves depend solely on the historical reversal points.

On the other hand, for a model that does not follow Land's reasoning, like SHM, this is not the only way to predict how scanning curves change in time. We will see there is at least two ways to go about this.

6.2.2. SCANNING HYSTERESIS MODEL

The main function of parameter π in SHM is that it serves as a relation between the two end points of every scanning curve. This relation is given by the two parametrizations $\pi^D(s)$ and $\pi^I(s)$, and the equation

$$\pi^D(s_{wi}^{(1)}) = \pi^I(s_{wi}^{(2)}) \tag{6.2}$$

always holds, where $s_{wi}^{(1)}$ and $s_{wi}^{(2)}$ denote the two end points of the scanning curve.

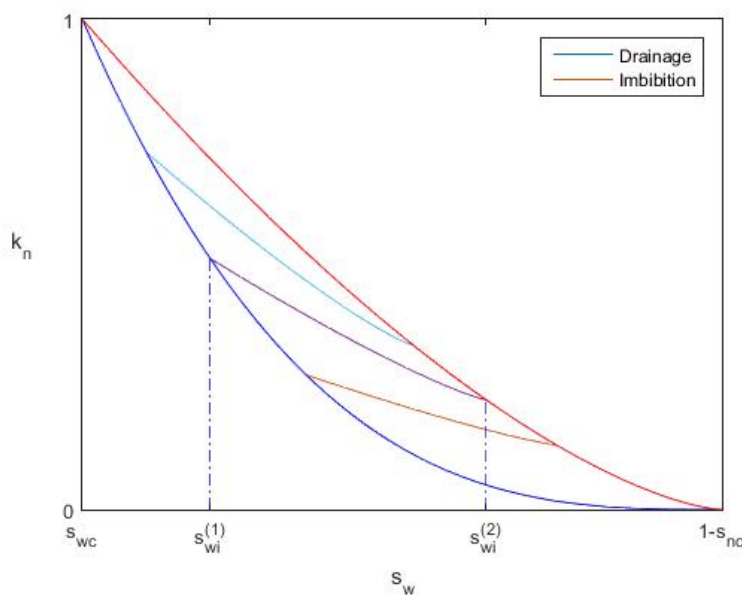


Figure 6.7: Scanning curves for the SHM model. The two ending points of any particular scanning curve, $s_{wi}^{(1)}$ and $s_{wi}^{(2)}$, are related by equation (6.2).

Parametrizations π^D and π^I are determined implicitly from

$$k_n^D(s) = k_n^S(s, \pi^D(s)) \quad \text{and} \quad k_n^I(s) = k_n^S(s, \pi^I(s)) \quad (6.3)$$

Both sets of equations (6.2) and (6.3) must hold at all times. As bounding curves change with time, by equation (6.3) parametrizations π^D and π^I may also change in time.

In Land's theory, it is sensible to keep track of historical reversal saturation $s_{wi}^{(1)}$. Alternatively, SHM offers the option of keeping track of history through parameter π . Let us show both methods.

OPTION 1

Assume a drainage process reversed at $s_{wi}^{(1)}$. Option 1 consists on remembering reversal saturation $s_{wi}^{(1)}$ to keep track of the system's history. Using (6.2), we can always obtain the other end point

$$s_{wi}^{(2)} = (\pi^I)^{-1}(\pi^D(s_{wi}^{(1)}))$$

and hence the rest of the scanning curve. Allowing parametrizations $\pi^D = \pi^D(s, t)$ and $\pi^I = \pi^I(s, t)$ to vary with time but fixing $s_{wi}^{(1)}$ yields different end points for the scanning process

$$s_{wi}^{(2)}(t) = \pi^I(\cdot, t)^{-1}(\pi^D(s_{wi}^{(1)}, t)) \quad (6.4)$$

and therefore also different scanning curves every time step. As before, saturation at the new time step $s(t)$ is evaluated in the new scanning curve $k_n^S = k_n^S(s(t), \pi(t))$, where

$$\pi(t) = \pi^D(s_{wi}^{(1)}, t) = \pi^I(s_{wi}^{(2)}(t), t) \quad (6.5)$$

for $s(t) \in [s_{wi}^{(1)}, s_{wi}^{(2)}(t)]$.

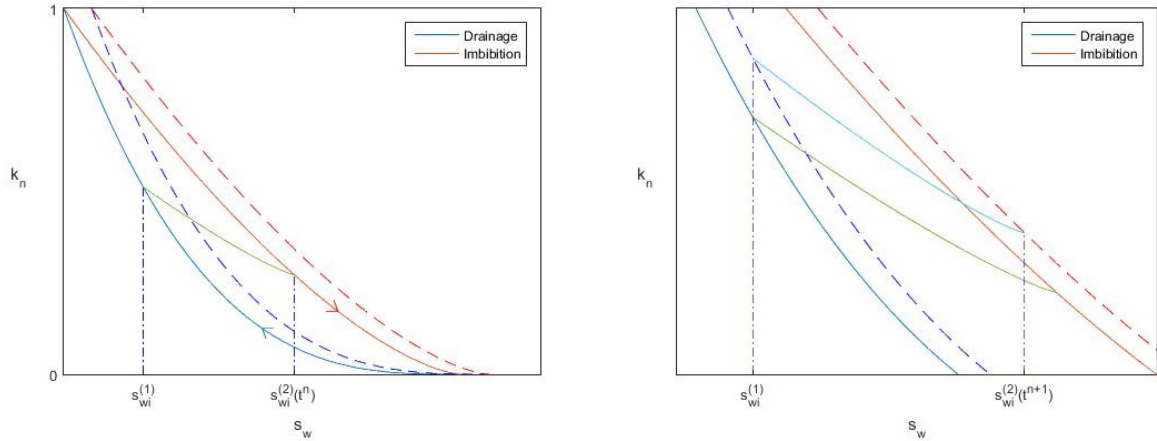


Figure 6.8: The bounding curves have shifted after one time step. The new scanning curve is determined by fixing the reversal point $s_{wi}^{(1)}$. The ending point of the new scanning curve $s_{wi}^{(2)}(t^{n+1})$ is given by (6.4).

Figure 6.8 shows a system where the residual oil saturation s_{nr} increases over time. Both bounding curves shift slowly to the left, which in turns affects parametrization π^D and π^I .

In this example, while the system is in scanning mode, point $s_{wi}^{(1)}$ remains constant while $s_{wi}^{(2)}$ decreases gradually, by property of equation (6.4). The value of π associated with the scanning curve also changes. Indeed, by equation (6.5), a varying function π^D and constant saturation $s_{wi}^{(1)}$ produce a time dependent parameter $\pi(t)$.

OPTION 2

The last example proposed fixing the value of $s_{wi}^{(1)}$ in order to maintain history. An alternative is to use parameter π as the memory instead. Assume a drainage process is reversed at saturation $s_{wi}^{(1)}$ and time t . Then a scanning curve is generated with a π value of

$$\pi = \pi^D(s_{wi}^{(1)}, t)$$

Once π has been selected this way, it shall remain fixed for the entire scanning process. As time goes on and parametrizations π^D and π^I change, we can recover the two end points of the new scanning curve, $s_{wi}^{(1)}(t)$ and $s_{wi}^{(2)}(t)$, by solving the implicit equations

$$\pi = \pi^D(s_{wi}^{(1)}, t) \quad \text{and} \quad \pi = \pi^I(s_{wi}^{(2)}, t) \quad (6.6)$$

This method also yields a different scanning curve every time step. However, now it is parameter π which serves as the memory of the scanning curve, by remaining constant during the scanning process. In contrast, the starting point of the scanning curve $s_{wi}^{(1)}(t)$ now changes over time, as we have assumed it no longer represents the history of the system.

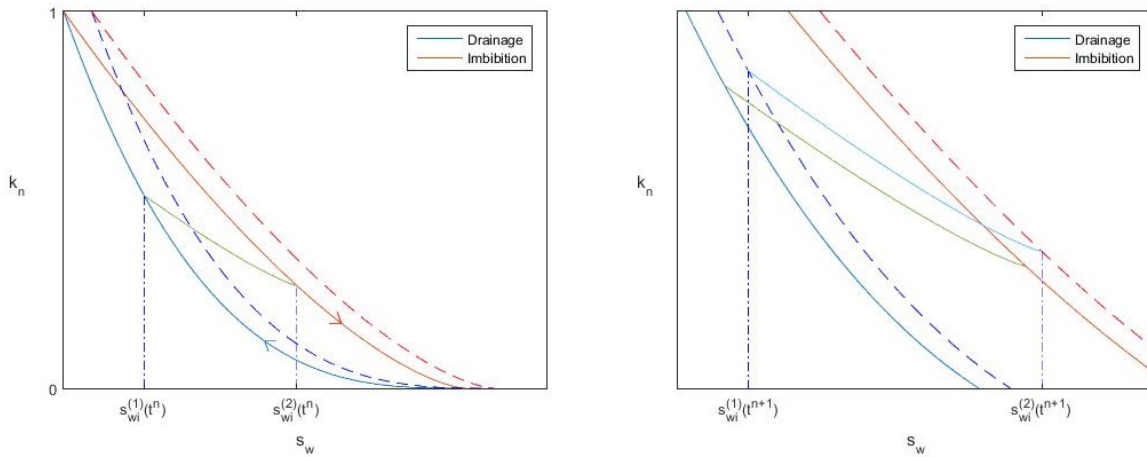


Figure 6.9: In option 2, the new scanning curve is determined by fixing value $\pi = \pi^D(s_{wi}^{(1)}(t^n))$. The two end points of the new scanning curve at time t^{n+1} are given by (6.6).

Notice that the variables (s, π) can be seen as a parametrization of the graph space (s, k_n) , where the coordinate transformation $\pi(s, k_n(s))$ is defined by equations (6.3). When a reversal occurs, at saturation s_{wi} , a point in the graph $(s_{wi}, k_n(s_{wi}))$ is set as the memory of the scanning curve. This point has a parametrization (s_{wi}, π_i) , $\pi_i = \pi(s_{wi}, k_n(s_{wi}))$, which is also historical.

Hence, the difference between option 1 and option 2 is which one of the two coordinates of historical point (s_{wi}, π_i) is chosen to be remembered.

Realizing this, it is possible to build an algorithm that traces the information to the new time step by going not only in one of the two directions s or π of the plane, but rather, all the different directions resulting from the possible combinations of these two coordinates.

6.2.3. OPTION 3

In the previous examples, the effect of historic data in the new bounding curves can be determined by following at least one of its two coordinates, e.g. s_{wi} or π .

In the same fashion, for instance in Killough's model, historical point $(s_{wi}, k_n(s_{wi}))$ can be remembered by its historical permeability $k_n(s_{wi})$. This means fixing value $k_n(s_{wi})$ and adapting the new scanning curve to also begin at this coordinate.

This also creates a functional time-dependent hysteresis model. However its physical interpretation is entirely different from that shown in section 6.2.1. In option 1, the shifting scanning curve is assumed to always begin at saturation s_{wi} , and the scanning process is only considered finished after this saturation value has been surpassed again.

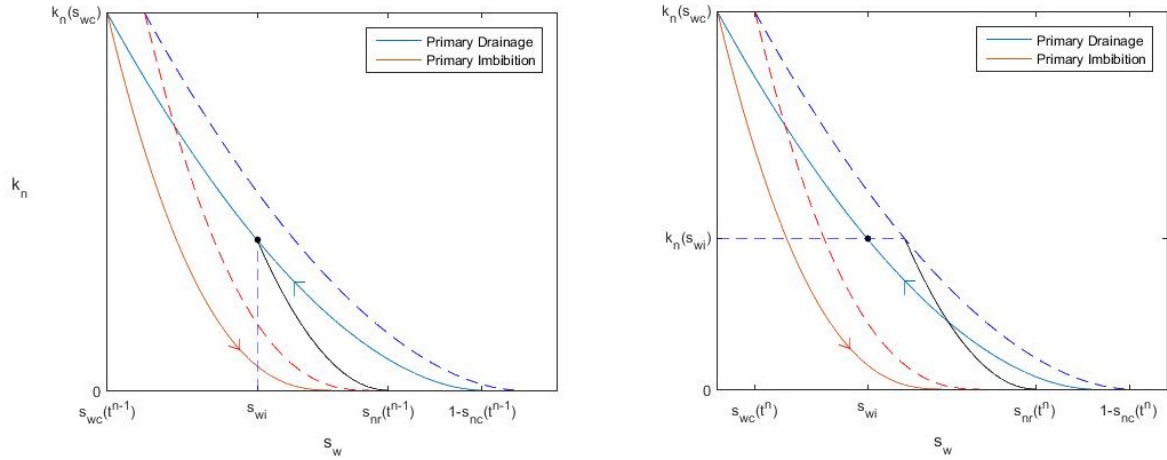


Figure 6.10: In option 3, the starting point s of the new scanning curve is given by equation $k_n^D(s, t) = k_n(s_{wi})$. The new residual saturation $s_{nr}(t)$ depends on this new reversal saturation.

In option 3, on the other hand, the present scanning curve begins with a fixed k_n value, and it can only be exited after this particular oil permeability has been achieved again. This reasoning carries a clear implicit meaning: trapping, the process that defines scanning curves, begins when oil permeability is diminished, and the effects of trapping remain until the same oil permeability is regained.

This is not the argument posed by Land as described in chapter 4. Land's reasoning proposes the change in oil saturation as the main condition driving oil trapping, and he argues that the trapping will continue to be present for as long as historical oil saturation is not regained.

Clearly, option 1 is coherent with models based on Land's theory, while option 3 does not carry the same physical meaning. Still, option 3 may yet be proven to be consistent with some other physical hysteresis model, either already existent or yet to be proposed.

6.2.4. CAPILLARY PRESSURE

The same treatment befalls capillary pressure when faced with time dependent bounding curves. As an example consider the model from Kleppe *et al.*

Assume the drainage curve is reversed at gas saturation s_{gi} . Then the scanning curve starting at this point is built by taking the section of the imbibition curve contained in the interval $[s_{gr}^{max}, s_g^*]$, and scaling it to fit in the interval $[s_{gr}, s_{gi}]$, as in figure 6.11. Here, s_g^* is the saturation satisfying

$$k_n^D(s_{gi}) = k_n^I(s_g^*)$$

and s_{gr} is determined by s_{gi} through equation (4.13):

$$s_{gr} = \frac{s_{gi}}{s_g^{max}} s_{gr}^{max} \quad (6.7)$$

For a time dependent model, however, end point saturations such as s_{gr}^{max} may vary over time. Hence equation (6.7) becomes:

$$s_{gr}(t) = \frac{s_{gi}}{s_g^{max}(t)} s_{gr}^{max}(t) \quad (6.8)$$

Assume only the imbibition curve shifts over a time step, as in figure 6.12, then saturation $s_g^*(t)$ can be retrieved from equation

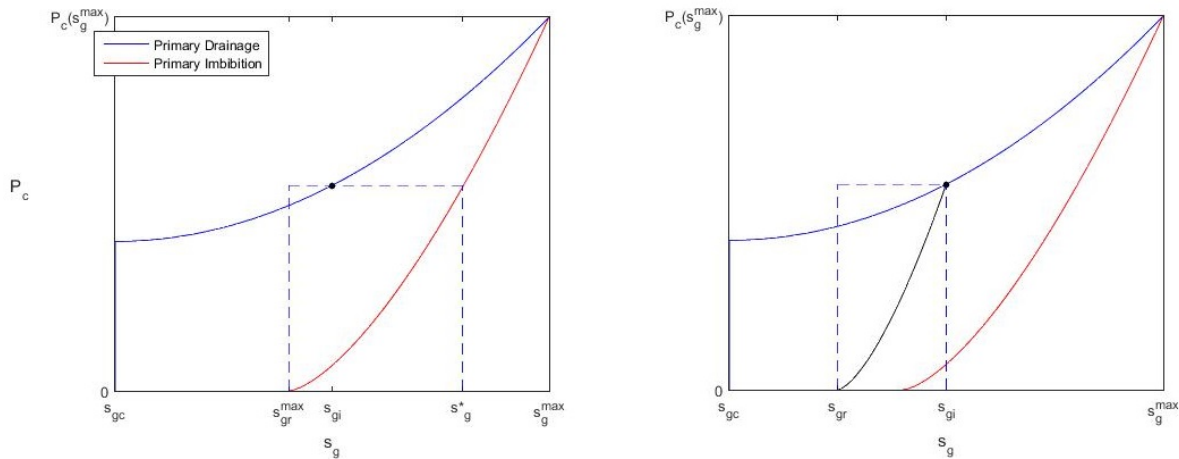


Figure 6.11: Drainage process reversed at gas saturation s_{gi} . The resulting scanning curve is built by scaling the section of the imbibition curve that lies in interval $[s_{gr}^{max}, s_g^*]$ into the interval $[s_{gr}, s_{gi}]$.

$$k_n^D(s_{gi}) = k_n^I(s_g^*(t), t)$$

Now, at the new time step t^n , the section of the new imbibition curve $k_n^I(\cdot, t^n)$ contained in the interval $[s_{gr}^{max}(t^n), s_g^*(t^n)]$ is scaled down to interval $[s_{gr}(t^n), s_{gi}]$, as in figure 6.12.

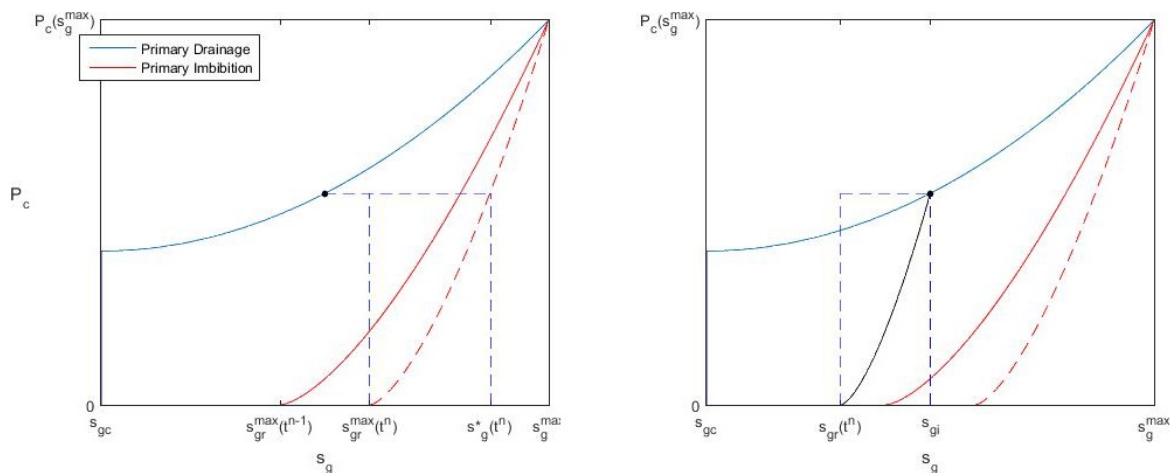


Figure 6.12: Imbibition curve has shifted over time. The new scanning curve at time t is built by scaling the section of the new imbibition curve that lies in interval $[s_{gr}^{max}(t), s_g^*(t)]$ into the interval $[s_{gr}(t), s_{gi}]$.

Notice how in this example it is not necessary to translate historical point s_{gi} into the new time step, since the drainage curve does not change over time. This example was purposely chosen to show the behaviour of capillary pressure under time dependency, without having to discuss the different methods of translating information. A similar analysis of such methods results as in the relative permeability case.

In the next section, however, we will see a unifying methodology that encompasses options 1, 2 and 3, independently of the model considered.

6.3. GENERAL METHODOLOGY

So far we have seen at least three different ways of translating history through time. In option 1, fixing saturation s_{wi} meant translating the historical point $(s_{wi}, k_n(s_{wi}, t^n))$ to the new point $(s_{wi}, k_n(s_{wi}, t^{n+1}))$. This is equivalent to moving vertically to find the new bounding curve $k_n(\cdot, t)$, as in figure 6.5.

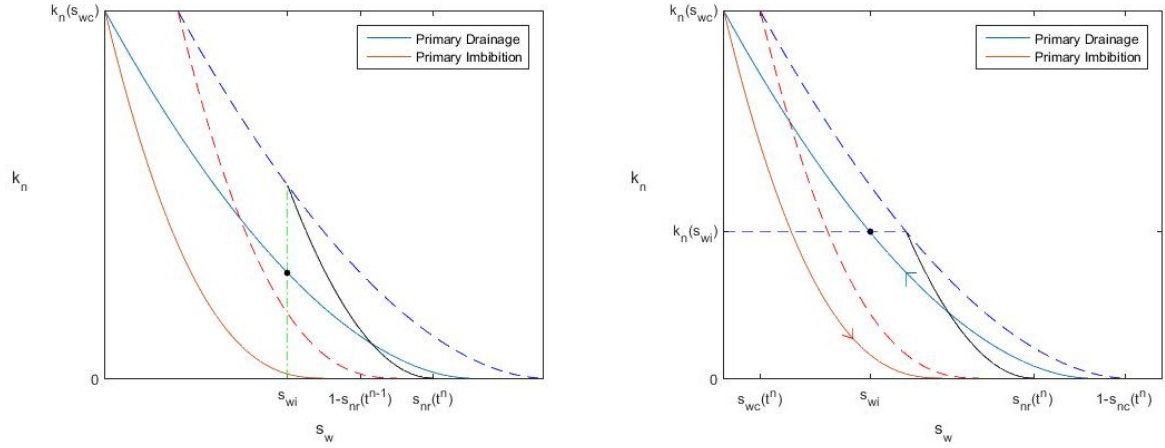


Figure 6.13: In option 1 (left), reversal saturation s_{wi} is fixed in time and used to determine the new scanning curve (figure 6.5). In option 3 on the other hand (right), reversal permeability $k_n(s_{wi})$ is considered constant over time (figure 6.12).

In option 3, historical relative permeability $k_n(s_{wi}(t^n), t^n)$ was fixed in order to find the new historical reversal saturation, i.e. saturation $s_{wi}(t^{n+1})$ which satisfies

$$k_n(s_{wi}(t^{n+1}), t^{n+1}) = k_n(s_{wi}(t^n), t^n)$$

This leads to the new historical point $(s_{wi}(t^{n+1}), k_n(s_{wi}(t^{n+1}), t^{n+1}))$, where the second coordinate is the same as in the previous historical point $(s_{wi}(t^n), k_n(s_{wi}(t^n), t^n))$. Hence the historical point has moved horizontally to the new bounding curve, as in figure 6.12.

These two methods of moving historical information represent but two directions of the graph space (s, k_n) . Clearly, there exist an infinite number of directions in which information can be moved in order to be used in a different bounding curve. In fact, option 2 presents one of such alternatives.

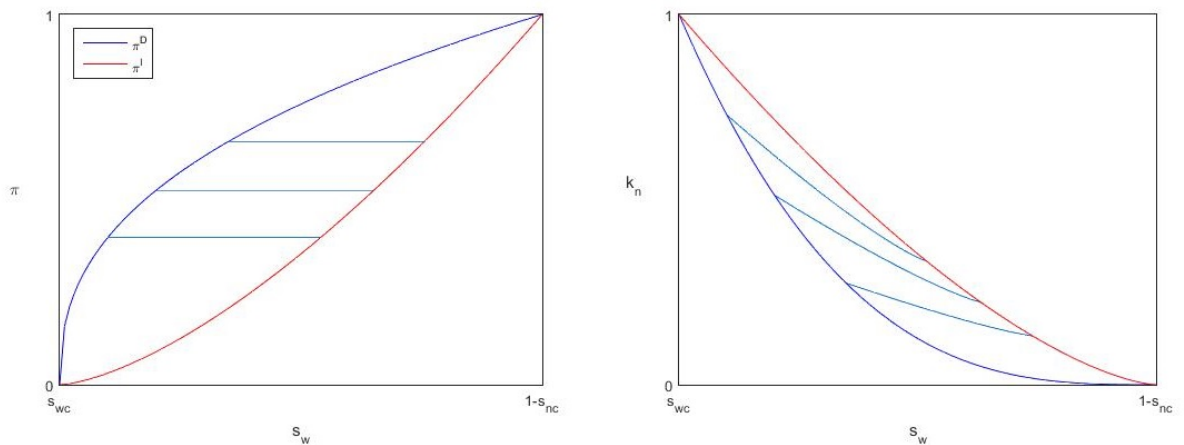


Figure 6.14: Parametrization π as a function of water saturation s_w (left). The constant values of π in the (s_w, π) graph correspond to the scanning curves of the SHM model (right).

Indeed, the space (s, π) acts as a parametrization of the graph space (s, k_n) , where the coordinate transformation $\pi(s, k_n)$ is defined by equations (6.2) and (6.3). Each value of π represents a specific curve in the

original graph space (s, k_n) . Moving along the π axis, as in figure 6.14, is equivalent to following the curve it represents in the original graph space (s, k_n) .

Hence fixing parameter π to translate information, as shown in option 2, is equivalent to follow the direction of the curve it represents, which is neither in the s or k_n axis, but a clear third trajectory.

This reasoning holds for every hysteresis model. Historical information must be translated into the new system. Since bounding curves in the system shift on the graph space, translating previous information always involves shifting historical points as well. By the nature of functions k_n and P_c , the graph spaces (s, k_n) and (s, P_c) are two dimensional and any direction in which data can move is forcefully a curve defined by a relation between two variables: saturation s (of any given phase) and its associated function k_n or P_c .

Parametrization π in option 2 is merely an example of such a relation. Parametrizations $\pi^D(s)$ and $\pi^I(s)$ are governed by equations (6.3) which is an assumed relation between s and k_n . These relations describe a set of curves spanning the entire graph. In fact they describe the scanning curves, which is their main purpose, but they also define paths for historical information to follow through time.

Hence options 1, 2 and 3, while having fundamentally different physical interpretations, describe the same method of handling historical information: translating the information in the graph space to a new location where it can be used by the new system, e.g. moving it to find the reversal point in the new bounding curve. The difference lies on which direction information travels as time goes on.

OTHER MODELS AND PARAMETRIZATIONS

It is possible for models to use other parameters to try and describe hysteresis, as long as they do not impose crippling restrictions on the model. Parametrization π in SHM works well because it is defined through measurements, and by definition it causes the model no conflict to include these additional constraints. Thus, for different models using other parameters, relations imposed by their parametrizations may also produce useful trajectories for information to follow, if they result in meaningful physical interpretations.

For three-phase systems, the methodology will be the same if the variable of interest, for instance k_n , is a function of only one saturation, hence defining a two-dimensional graph space (s, k_n) . In the model of Larsen & Skauge, section 4.5, relative permeabilities k_n are evaluated on constrained trajectories as defined in figure 4.7, which can be followed through the use of only one phase saturation. Thus the graph of k_n in this case is described by only two coordinates.

7

NUMERICAL IMPLEMENTATION

7.1. NUMERICAL ALGORITHMS

Some of the necessary algorithms to simulate our hysteresis models are presented in this chapter, along with the numerical considerations that may arise when implementing them. After this first discussion of IMPES and implicit methods, the rest of the algorithms presented in this section were written by the author of this document.

7.1.1. IMPES vs FIM

For simplicity, all simulations shown so far have been produced using the IMPES method. However this method treats relative permeabilities and capillary pressure explicitly, which compromises stability, specially when considering more than one spatial dimension.

DISCONTINUOUS DERIVATIVES

Using fully implicit methods improves stability but requires special considerations. Recall equation (3.24):

$$\mathbf{T}^{n+1} \mathbf{P}^{n+1} + \mathbf{D}^{n+1} (\mathbf{S}^{n+1} - \mathbf{S}^n) = \mathbf{Q}$$

and the associated Newton's method defined by the iterations (3.25):

$$\mathbf{F}^{(v)} (\mathbf{X}^{(v+1)} - \mathbf{X}^{(v)}) = -\mathbf{f}^{(v)}$$

where $\mathbf{X} = \begin{pmatrix} \mathbf{P} \\ \mathbf{S} \end{pmatrix}$. Then terms in matrix $\mathbf{F} = \begin{pmatrix} f_i \\ x_j \end{pmatrix}$ contains derivatives of the form

$$\frac{\partial \lambda_n}{\partial s_w} \quad \text{and} \quad \frac{\partial P_c}{\partial s_w}$$

We have seen from section 5.2.2 that moving from a scanning curve to the primary drainage curve produces a continuous function k_n that is not smooth everywhere. Specifically, the derivative $\frac{\partial k_n}{\partial s_w}$ is discontinuous at reversal point s_{wi} . Similarly for the capillary pressure models, at any historical saturation $s_{wi}^{(k)}$ derivatives are different from the left and right side.

However Newton's method may diverge if the derivative is discontinuous at the root. Even if the derivative is bounded and continuous in the neighbourhood of a reversal point s_{wi} , the method may still fail to converge if $s_w^{n+1} = s_{wi}$. Therefore it is necessary to consider an alternate method as the solution approaches a reversal point.

While explicit methods like IMPES are not affected by this, the stability of any explicit method greatly decreases as one expands the model into the 2D and 3D scenarios. For implicit methods, on the other hand, the

problem of discontinuous derivatives does not scale with dimension, as these depend only in saturation. Furthermore this problem is simply a limitation on Land's theory. In fact, it is sensible to expect future hysteresis models to account for smooth physical behaviour of the hysteretic variables.

Finally, notice how these discontinuities appear in every hysteresis model except for one. The model of Kleppe *et al* for capillary pressure does not consider any transitions from scanning curve to bounding curves, hence the derivative remains constant for the whole duration of any imbibition or drainage process.

HISTORY FOR ITERATIVE METHODS

On every time step t^n , the hysteresis models must evaluate mobilities and capillary pressures at the newest available saturation s_w^n . Clearly, the models must also react to the new saturation, in case any reversals have occurred.

For any iterations occurring between time steps, however, history must not be allowed to be changed by every iteration $s_w^{(v)}$, since they may oscillate while moving towards the solution s_w^{n+1} . Only the final iteration $s_w^{(v)} = s_w^{n+1}$ is representative of the history of the model. Care must be taken when evaluating in every iteration, so history is not altered incorrectly.

7.1.2. SCANNING CURVES ALGORITHM

As described in chapter 4, the models of Carlson and Killough for describing relative permeability hysteresis are both based in Land's theory of oil trapping. In both models, the bounding curves are used as input and the scanning curves are interpolated or otherwise obtained from these curves.

Let us recall the behaviour of such scanning curves. For both models, the primary drainage curve could only be followed during drainage and only when no oil had been trapped. As soon as the saturation direction was reversed, an imbibition curve was created from the point of flow reversal ($s_{wi}, k_n(s_{wi})$) until the maximum water saturation ($1 - s_{nr}, 0$) due to the residual oil saturation s_{nr} , which depends on s_{wi} .

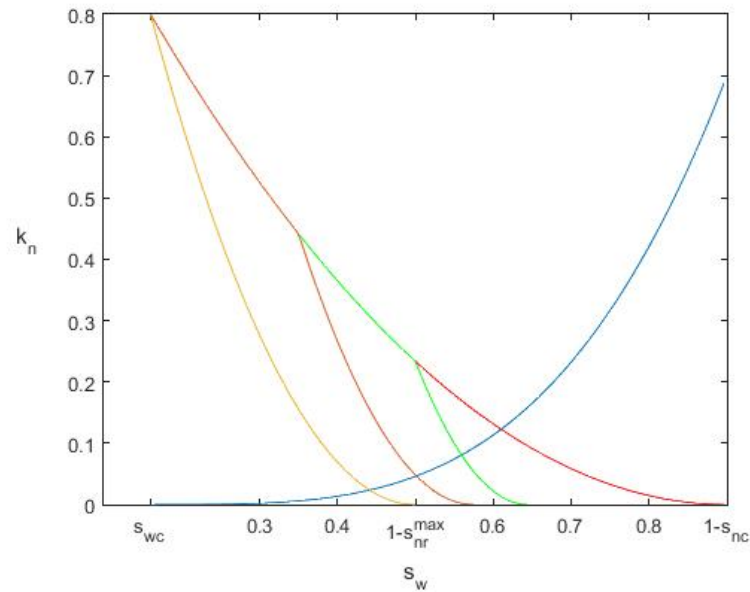


Figure 7.1: Scanning curves for the oil relative permeability according to Land's theory. Different reversal points s_{ni} produce different residual oil saturations s_{nr} . The curve for water relative permeability is also shown (blue).

Residual saturation for each scanning curve is predicted by Land's equation (4.3):

$$s_{nr} = \left(C + \frac{1}{s_{ni}} \right)^{-1} \quad (7.1)$$

where $s_{ni} = 1 - s_{wi}$. Oil relative permeability k_n would follow this new curve until such a time when the water

saturation is drained past the point s_{wi} , moment when k_n follows the primary drainage curve again. The system continues to use the primary drainage curve until a new reversal occurs and a new value of s_{wi} is established.

An algorithm to reproduce either Killough or Carlson's model would be:

```

if s(t) > swi
    k_{n}(s(t)) = k_{n}^{S}(s(t), swi)
else
    if s(t) < s(t-1)
        k_{n}(s(t)) = k_{n}^{D}(s)
    else
        swi = s(t-1)
        k_{n}(s(t)) = k_{n}^{S}(s(t), swi)

```

This states that if saturation s_w is above reversal point s_{wi} , then the system follows the scanning curve determined by s_{wi} . If saturation is below this point, then we are in the primary drainage curve. In this case, we are allowed to continue to follow the primary drainage curve only if saturation continues to drop, otherwise a new scanning curve is created using the last state $s_w(t^{n-1})$ as the new reversal point.

Notice that we only need the primary imbibition curve k_n^I to determine Land's constant C . Once C is known, by (7.1), every other scanning curve k_n^S , including k_n^I , can be computed as a function of water saturation s_w and the reversal point s_{wi} .

STORAGE

This algorithm requires comparison of the current water saturation $s(t^n)$ with the previous state $s(t^{n-1})$ in order to determine the direction of the change. Also, it requires the last given value of s_{wi} in order to determine when the process leaves a scanning curve and returns to the primary drainage curve. The value of s_{wi} is updated whenever we leave the curve k_n^D . Furthermore, this is required for every point in the grid, which results in two additional vectors to be stored at all times.

This is specially important when considering numerical schemes, since most transport simulators require only the state at the previous time step $\lambda_n(s(t^{n-1}))$ in order to compute the new state $s(t^n)$. However, to compute mobility λ_n at time step t^{n-1} , saturations at times t^{n-1} and t^{n-2} would be required if one wishes to include the effect of hysteresis. Hence hysteresis forces us to store our numerical solution at least two time steps behind.

THE SHM

Similarly, to compute the value of $k_n(s(t^n))$ using the Scanning Hysteresis Model, storage would be needed for both the previous state $s(t^{n-1})$ and the reversal point s_{wi} , for each point in the grid. Alternatively to storing s_{wi} , one could choose instead to update parameter π , which entirely determines which scanning curve is visited upon a reversal. This also involves a vector of real parameters $\pi \in [0, 1]$ to be stored in memory.

7.1.3. CAPILLARY PRESSURE

In chapter 5 capillary pressure was ignored since the Buckley-Leverett solution for equation (2.11) assumes $\frac{\partial}{\partial x} P_c = 0$. This condition greatly simplifies our numerical schemes and allows us to compare with the analytical solution, but does not allow for capillary pressure hysteresis to take part in the model. For any numerical scheme, however, any function $P_c(s_w)$ is easily incorporated into our model, for instance as described for IMPES in section 3.2.

As in the relative permeability hysteresis scenario, each time step requires at least the saturation states from the two previous time steps in order to determine the changes in direction of flow. As before, each time a scanning curve is created it is necessary to store the reversal saturation s_{wi} in memory during the duration of the scanning process.

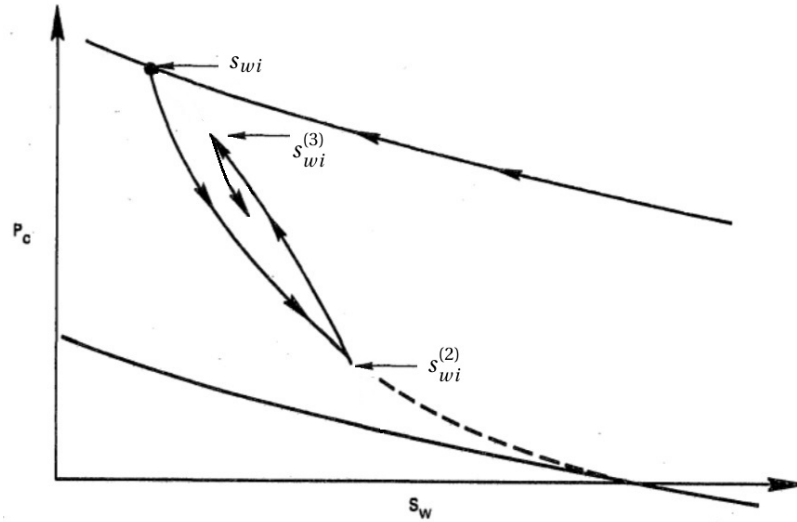


Figure 7.2: A first scanning process started at s_{wi} . A scanning curve starting at $s_{wi}^{(2)}$ and reversed again at point $s_{wi}^{(3)}$, generating a third scanning curve which ends at the original reversal point s_{wi} .

For Killough's capillary pressure model, however, a second reversal occurring while still in scanning state will generate a process that depends on the new reversal point $s_{wi}^{(2)}$ and the original one s_{wi} . Both need to be remembered for the duration of the second scanning curve. Moreover, a third reversal resulting in a third scanning curve would require an additional storage value for $s_{wi}^{(3)}$.

Let us describe an algorithm for computing P_c scanning curves. Assume a function P_c^S such that

$$P_c^S = P_c^S(s, s_{wi}^{(i)}, s_{wi}^{(i-1)})$$

and which gives the value (at saturation s) of the scanning curve which spans from the last remembered reversal point $s_{wi}^{(i)}$ to the second last reversal point $s_{wi}^{(i-1)}$.

The vector $s_{wi} = (s_{wi}^1, \dots, s_{wi}^{i-1}, s_{wi}^i)$ contains the reversal points in the order they appeared, and can increase size if a new reversal occurs, or decrease if a scanning curve is completely traversed and two reversal points can be forgotten. The direction of a scanning curve can be determined from the difference $s_{wi}^{(i)} - s_{wi}^{(i-1)}$. For instance the bounding curves P_c^D and P_c^I would be given, respectively, by

$$P_c^D(s) = P_c^S(s, 1 - snc, swc)$$

$$P_c^I(s) = P_c^S(s, swc, 1 - snc)$$

An algorithm to keep track of any new scanning curves that may appear and their respective reversal points is as follows. To be initialized it requires at least two reversal points $s_{wi} = (s_{wi}^1, s_{wi}^2)$ for the extreme

points of the bounding curves, and a boolean parameter **direction** which keeps track of the last flow direction in order to compare it to the direction of the new time step.

```

if direction == sign(s(t)-s(t-1))
    if direction.*s(t) >= direction.*swi(i-1)
        Pc(s(t)) = Pc^{S}(s(t),swi(i),swi(i-1))
    else
        swi = swi(1:i-2)
        i = i-2
        Pc(s(t)) = Pc^{S}(s(t),swi(i),swi(i-1))
else
    direction = -direction
    swi = [swi, s(t-1)]
    i = i+1
    Pc(s(t)) = Pc^{S}(s(t),swi(i),swi(i-1))

```

This algorithm checks first if direction is not reversed. If not, then k_n must follow the present scanning curve, until its end, at $s_{wi}^{(i-1)}$. When this happens, it means a scanning cycle is completed and the last two reversal points are forgotten. If on the other hand, saturation is reversed, then a new reversal point is remembered and a new scanning curve is assigned to it.

For simplicity, this algorithm fails if the systems reaches the end of a bounding curve, since at this point the size of vector s_{wi} drops bellow 2. This is easily fixed by adding a few more lines to update vector s_{wi} whenever the system reaches one of its two extreme points.

In theory reversals could continue to occur in such a way that an indefinite number of reversal points need to be stored. Also, the order of the points is also important, since any point $s_{wi}^{(k)}$ can only be forgotten after its scanning process has been completed. Indeed, since the last scanning process is the first one to be completed and similarly the first scanning process is the last one to be completed, reversal values can only be forgotten in opposite order as they are stored. Luckily this requirement could possibly be ignored if it is unlikely that many reversal processes happen so close together. .

TIME DEPENDENT MODEL

As with the other models, when including time dependent bounding curves into Killough's model for capillary pressure, history of the system must translated from one the present time step into the next. As seen in section 6.2, there are several ways to do this.

However for Killough's P_c model a great number of historic reversal points may be stored. At very time step, all historical information must be adapted, even if not every reversal point is used to compute the scanning curves at every time step.

7.1.4. LAND'S CONSTANT

Equation (7.1) gives us a nice relation between the reversal oil saturation s_{ni} and the expected residual oil s_{nr} . This model makes sense for sensible values of s_{ni} but fails when it approaches s_{nc} , i.e. if the primary drainage is reversed too soon. Indeed, from figure 7.1 one would expect the corresponding value of s_{nr} for when $s_{ni} = s_{nc}$ to be also $s_{nr} = s_{nc}$, however this is not satisfied for most values of C .

This does not mean, however, that C is uniquely determined or that it is the same for every reservoir. On the contrary, trapping mechanics vary from reservoir to reservoir and it is through Land's constant C that we can keep track of different hysteresis scenarios.

Hence C is allowed to have different values other than the one that satisfies $s_{nc} = (C + s_{nc}^{-1})^{-1}$, which is only $C = 0$, since it allows our model to make sense for most values of $s_{ni} \in [s_{nc}, 1 - s_{wc}]$. Rather, a small fix is proposed to deal with the problems that arise when s_{ni} is close to s_{nc} . This involves the use of a continuous (an preferably convex) function $g(s_n)$ such that

$$g(s_{nc}) = h \quad \text{and} \quad g(1 - s_{wc}) = 0$$

where

$$h = s_{nc} - (C + s_{nc}^{-1})^{-1}$$

Function $g(s_n)$ is then added to the definition of s_{nr} , so that equation (7.1) becomes

$$s_{nr} = \left(C + \frac{1}{s_{ni}}\right)^{-1} + g(s_{ni}) \quad (7.2)$$

This small modification leaves most values of s_{nr} almost unchanged while modifying the ones close to s_{nc} . By doing this, the consistency of our model is guaranteed.

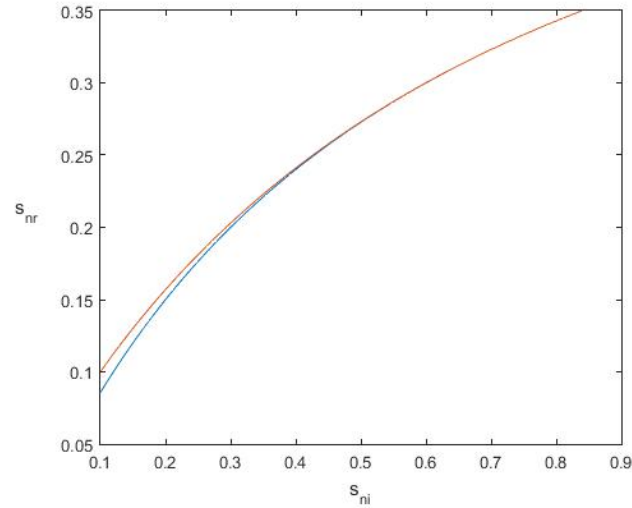


Figure 7.3: Residual oil saturation s_{nr} as a function of reversal oil saturation s_{ni} by equation (7.1) (blue) and the modified values given by equation (7.2) (red), for a Land's constant of $C = \frac{5}{3}$.

Notice that this issue arises from the limitations of Land's theory, since Land's relation (7.1) is merely an approximation and it is not expected to behave properly when faced with extreme values. This supports the argument that well-established physical models for hysteresis are still required in order to generate accurate simulations.

7.1.5. EXTENDED BOUNDING CURVES

When considering time dependent bounding curves, it is wise to extend the relative permeability curves as constants outside the domain $[s_{wc}, 1 - s_{nc}]$, as in figure 7.4.

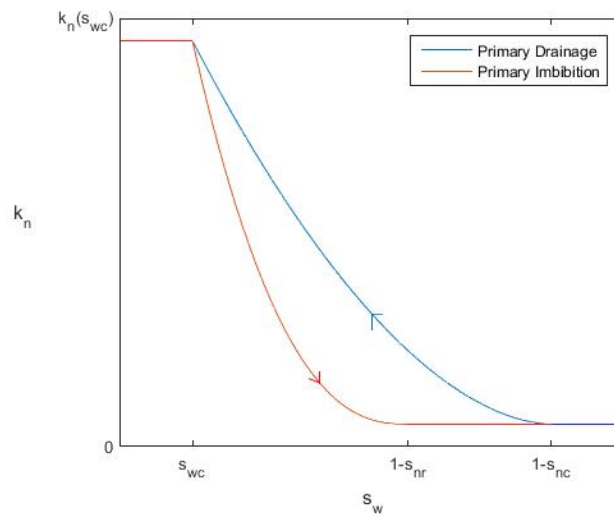


Figure 7.4: Relative permeability bounding curves extended constantly outside their natural domain.

This is important for the consistency of the model. Figure 7.5 shows an example of a system where the saturation $s(t^n) = s(t^{n+1})$ remains constant over a time step but the bounding curves shifts, leaving the saturation $s(t^{n+1})$ outside the domain $[s_{wc}(t^{n+1}), 1 - s_{nc}(t^{n+1})]$.

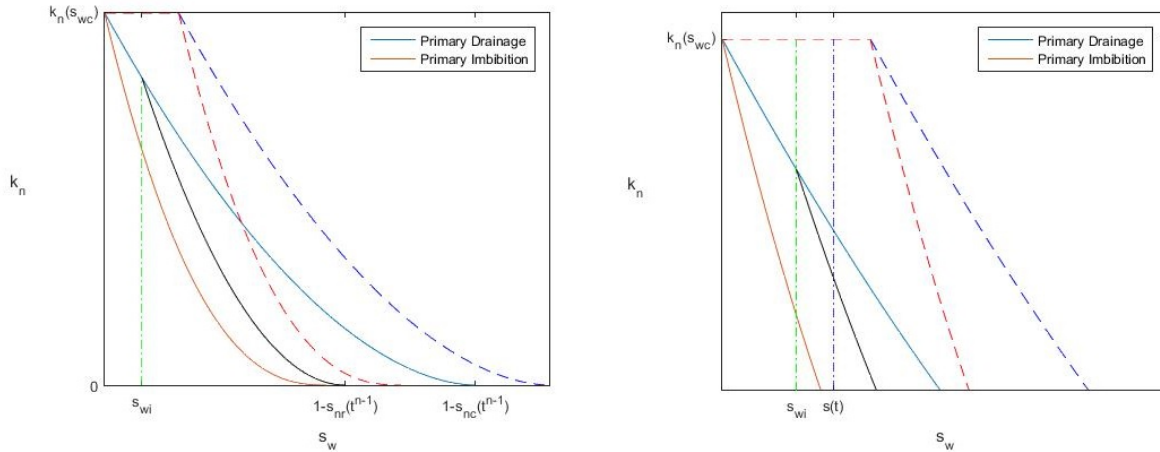


Figure 7.5: Historical saturation s_{wi} being tracked over the new time step, landing outside the natural domain of the bounding curves.

By extending the relative permeability functions as in figure 7.4, one can compute the gain in oil permeability experienced by saturation $s(t^n)$ due to the shift of the bounding curves.

7.2. NUMERICAL EXAMPLES

This chapter, together the previous one, propose algorithms to simulate time-dependent hysteresis models, and show some of the practical considerations that arise when implementing them. To see the effect of these ideas on the numerical solutions, and to test the robustness of the algorithms, results of said simulations are presented in this section.

Consider again the example from section 6.1. An imbibition process was presented where the salt content in water varies over time, changing the bounding relative permeability functions k_n^D and k_n^I . The main feature driving this example is the change in residual saturation. Let us make use of this feature a while longer.

7.2.1. SHARP SALINITY DROP

Figure 6.3 in the original example presented a salinity level that dropped continuously over time. Consistent with the reasoning of Buckley Leverett, section 5.1, this resulted in a water front with an increasingly higher shock wave and a rarefaction wave that included increasing values of water saturation. The water front also reduced its speed as the shock height augmented, following assumption (2.6) on constant total velocity.

To test our algorithms in an extreme scenario, consider the improbable case of salt content suddenly dropping everywhere in the reservoir, as well as in the incoming water entering through the boundary. This results in a sharp, abrupt change in salinity and, following Jerauld, Webb & Lin [13], in the maximum residual oil saturation s_{nr}^{max} . Assume this happens not at the start of imbibition but sometime in the middle of the process.

For the models of Killough and Carlson, this implies a sharp shift for the imbibition curve. Figure 7.6 shows the result of simulating such scenario:

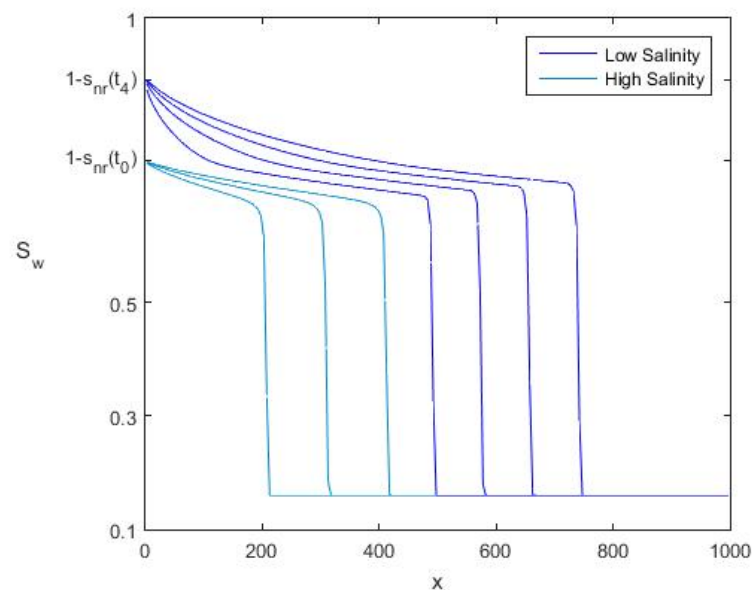


Figure 7.6: Water saturation profile for an imbibition process at different times $t_k = k \cdot t_1$. Salinity profile is piecewise constant and it is reduced drastically at time t_4 .

As expected, the receding s_{nr}^{max} gives way to higher values of water saturation entering the reservoir. The shape of the waterfront changes similarly as it does in figure 6.3, however this time the change happens almost instantly instead of gradually. Figure 7.7 shows the water saturation profile moments after the salinity has dropped, to illustrate how fast the system adapts to the new parameters.

For the models of Killough and Carlson, it has been argued why option 1 is the most sensible method to treat history over time. All examples in this section are produced using option 1 on Killough's relative permeability model.

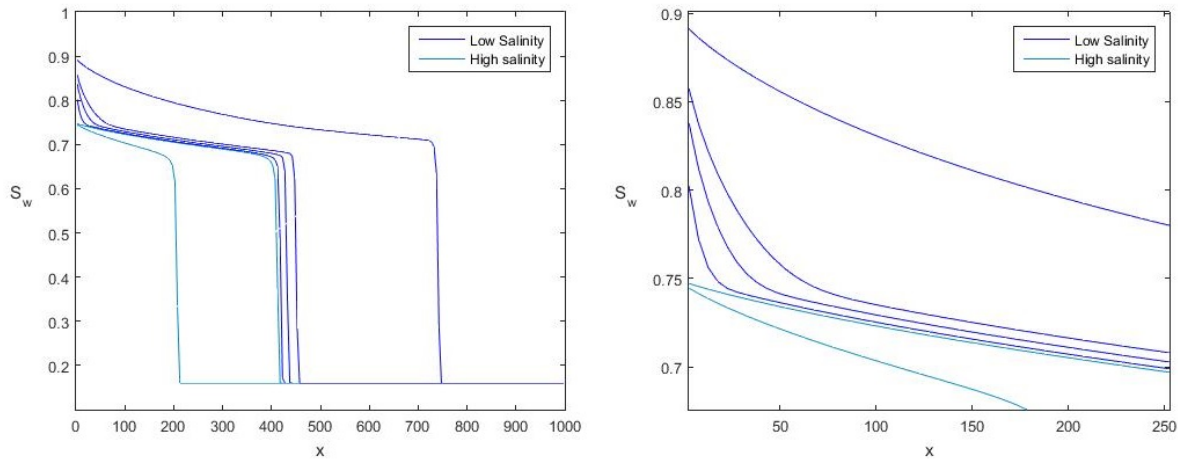


Figure 7.7: Water saturation profile as described in figure 7.6. Several profiles occurring right after the salinity drop are shown to illustrate the quick change in the water front.

As explained in section 2.3.2, the saturation values consisting of the rarefaction wave, i.e. the values above the shock saturation, follow characteristic curves which are straight lines in the (x, t) plane. For each saturation s in the rarefaction wave, its characteristic velocity, i.e. the slope of its characteristic line, is given by the derivative of the fractional flow f in equation (2.12).

This velocities are constant as long as f does not change. In this scenario, saturation values s that used to be "static", i.e. that did not propagate in x over time, suddenly gain non zero velocity $f'(s)$ thanks to the shift in the flow function f .

This means that most part of the rarefaction wave in the solution in figure 7.7 was completely static until the salinity drop, when it gained full speed, as opposed to the solution in figure 6.3 where it accelerated gradually over time.

In these particular examples, the final profile of both figures 6.3 and 7.6 at final time t_8 is the same, simply because one example had salinity lowered linearly from t_0 to t_8 , while the other had a jump from initial to final salt saturation at exactly half the time t_4 , hence the average speed for both processes is the same.

7.2.2. GRADUAL SALINITY INCREMENT

Let us produce the opposite example where salt content is increased over time. Like before, such a scenario is improbable and merely used for illustrating the behaviour of numerical solutions.

An increment in salinity implies higher residual oil saturation and reduced oil relative permeability. The solution must then consist of an accelerating waterfront with a reducing shock height:

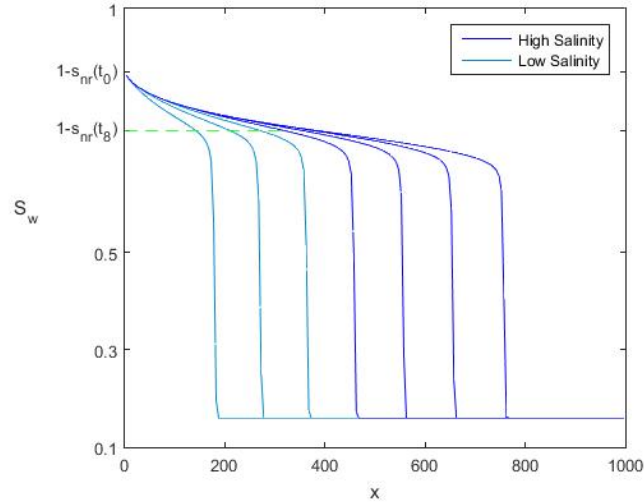


Figure 7.8: Water saturation profile for an imbibition process with gradually increasing salinity. The shock wave reduces in height and gains speed as time goes on.

As before the rarefaction wave moves at velocities $f'(s)$ determined by the derivative of the fractional flow f . Notice how, even though the residual oil saturation grows, disabling the advance of certain values of water saturation, the high water saturation values already achieved at previous time remain. Hence at any positive time t , the solution consist of three parts: a shock wave, consisting of the values below shock saturation $s_k(t)$, a rarefaction wave, for the values between $s_k(t)$ and $1 - s_{nr}(t)$, and finally a static part for values above $1 - s_{nr}(t)$.

This last part is formed by the saturations s that used to be part of the rarefaction wave but gradually lost their oil relative permeability, and hence their characteristic velocity $f'(s)$, until becoming permanently fixed when $1 - s_{nr}(t) \leq s$. The length l of the static part of the solution, in the spatial coordinate x , at any given time t is given by

$$l(\tilde{t}) = \int_0^{\tilde{t}} f'(1 - s_{nr}(t)) dt \quad (7.3)$$

where

$$\frac{1}{\tilde{t}} \int_0^{\tilde{t}} f'(1 - s_{nr}(t)) dt$$

is the average speed of the highest moving water saturation until time \tilde{t} . Clearly, the volume under the static part of the solution can no longer contribute to oil recovery.

7.2.3. SHARP SALINITY SURGE

Let now the change in salinity take place suddenly as in example 7.2.1, this time in the form of a sharp increase rather than a drop. The jump in residual oil saturation signifies a big shift (to the left) of the imbibition curve in Killough's hysteresis model. The Buckley Leverett solution dictates that the water profile must quickly adapt to its new shape, as determined by the new fractional flow function f . Figure 7.9 clarifies this phenomenon:

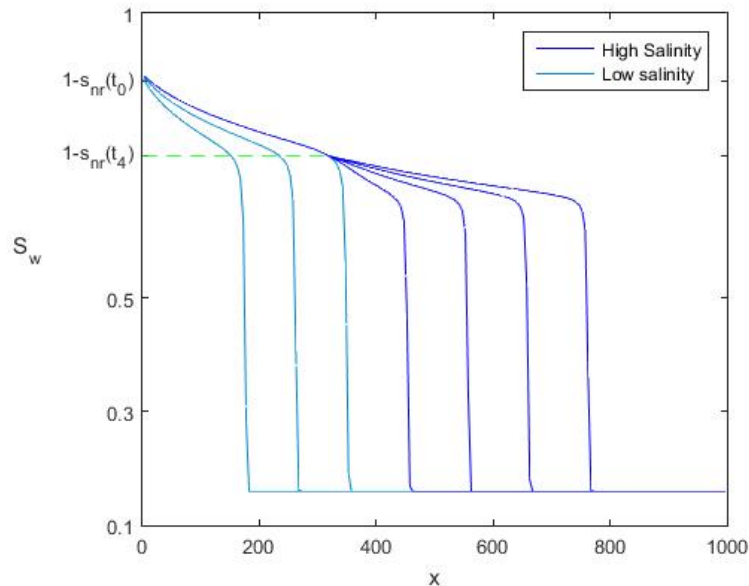


Figure 7.9: Water saturation profile for an imbibition process at different times $t_k = k \cdot t_1$, with a sudden increase in salinity at t_4 . The shock wave experiences a sharp shape shift at this time.

The solution also features a static part after the salinity rises at time t_4 . The static part of the solution only exists in the section of the reservoir that was already traversed by the waterfront at time t_4 . Equation (7.3) again gives the length of the static section, which in this case is constant: $l = t_4 \cdot f'(1 - s_{nr}(t_0))$.

As in example 7.2.1, the sudden change in salinity forces the solution to adapt its shape almost instantly. A closer look to the solution moments after the salinity rise let us see this transformation:

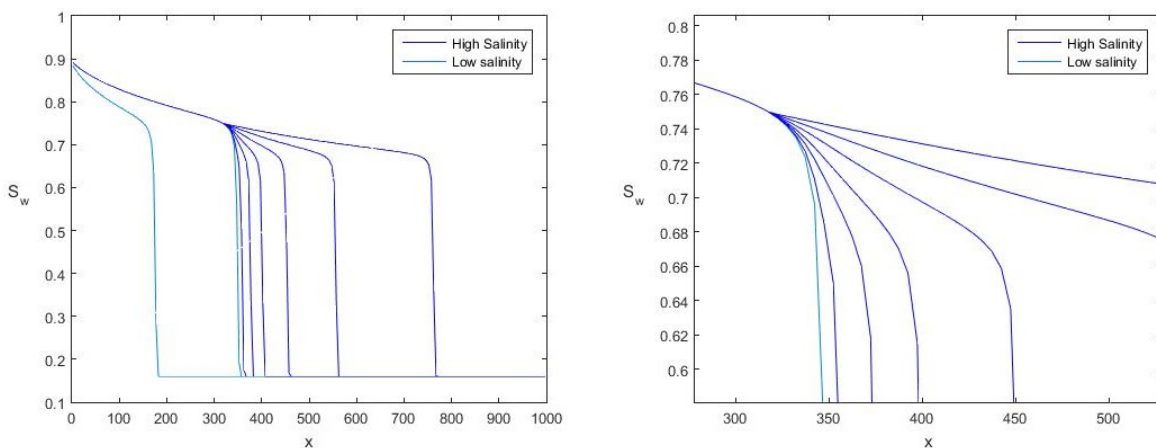


Figure 7.10: Water saturation profile as described in figure 7.9. Several profiles occurring right after the salinity rise are shown to illustrate the quick change in the water front.

8

OVERALL REMARKS

8.1. CLASSIFICATION OF HYSTERESIS MODELS

The models for relative permeability and capillary pressure hysteresis are all based on different ideas, each one behaves distinctly and requires particular considerations to be implemented. A summary of the models presented in this work and their properties is presented in this section.

BY INPUT

All of the hysteresis models assume known bounding curves and all predictions are produced using this information. Realistic measurements of relative permeability and capillary pressure are needed in the construction of the bounding curves for the models to be reliable. In the case of Killough and Carlson, correct estimation of Land's constant C is central to their methodology.

For the Scanning Hysteresis Model an additional parametrization π is required. This often comes in the form of functions $\pi^D(s)$ and $\pi^I(s)$. This parametrizations depend on the bounding curves and estimations of at least one scanning curve. Meaningful parametrization of these functions is essential for the SHM to be effective.

BY REVERSIBILITY OF THE SCANNING CURVES

The relative permeability models of Carlson, Killough and the SHM consider retraceable scanning curves. This means that reversals in the saturation flow do not affect the system unless they happen while on the bounding curves, i.e. past the values of the historical reversal points. According to these models, flow reversals occurring during scanning state do not modify the history of the system. This reasoning implies that not every drainage-imbibition cycle will exhibit hysteresis.

For the P_c models of Kleppe *et al* and Killough, scanning curves, like bounding curves, are meant to be followed in a specific direction. Any reversal results in a new scanning curve in the new direction. Hence any imbibition-drainage cycle is subjected to hysteresis, no matter how short it may be.

BY REVERSIBILITY OF THE SYSTEM

For Killough's P_c model and the scanning hysteresis model, any full imbibition-drainage process creates a closed loop, i.e. the starting point of the cycle is also the ending point. This return to the original point makes possible to revisit any path previously taken. Moreover, any point in the graph can be revisited by choosing a proper path, no matter the history of the system.

This is not the case for the relative permeability models of Carlson, Killough, and the P_c model of Kleppe *et al*. Trapping creates new scanning curves and it also prevents some scanning curves from being revisited. In these models, the maximum historical oil saturation s_{ni} drives the system and determines the expected residual oil saturation s_{nr} . Since the maximum historical saturation does not decrease, neither does the maximum historical s_{nr} , hence any scanning curve corresponding to a smaller residual oil saturation $s'_{nr} < s_{nr}$ is no longer considered.

	Relative Permeability			Capillary Pressure	
	Killough	Carlson	SHM	Killough	Kleppe <i>et al</i>
Required Input	Drainage curve and s_{nr}^{max}	Drainage curve and s_{nr}^{max}	Bounding curves & parametrization π	Drainage and imbibition curves	Drainage and imbibition curves
Creates a new Scanning Curve upon Reversal	Only while on drainage curve	Only while on drainage curve	Only while on either one of the bounding curves	Always	Always
Reversibility of the System	Residual oil saturation s_{nr} cannot decrease	Residual oil saturation s_{nr} cannot decrease	Any scanning curve can be revisited	Any scanning curve can be revisited	Residual oil saturation s_{nr} cannot decrease
Requires Inverse Functions	Not required	Not required	Requires to solve either x or y from $\pi^D(x) = \pi^I(y)$	Not required	Requires to solve x from $Pc^I(x) = Pc^D(y)$
Recommended Method for translating History	Option 1	Option 1	Option 3	-	Option 1

Figure 8.1: Comparison of hysteresis models by their properties.

8.2. CLASSIFICATION OF TIME-DEPENDENT HYSTERESIS MODELS

BY CHOICE OF HISTORIC DATA

Section 6.2 shows more than one method of interpreting history on a time-dependent system. For any model that depends strongly on oil trapping such as Carlson, Killough and Kleppe *et al*, it is sensible to use maximum oil saturations as historical information, since this is the main variable driving trapping according to Land's theory.

For a model such as SHM, which has a specific parameter π solely devoted to keep track of history, it is practical to extend its functionality to include time dependent parametrizations $\pi^D(s, t)$ and $\pi^I(s, t)$.

As shown before, these are by far not the only choices for keeping information. Any other model seeking to be realistic is allowed to adapt their scanning curves in a way that is coherent with the physical model on which they are based.

BY COMPUTATIONAL COST

In section 6.2.2 it is explained how to update scanning curves in the new time step using historical parameter π . This involves solving equation (6.6) every time step, which is a non linear equation and computationally expensive. If parametrizations π^D and π^I and their inverses are known analytically then the cost is significantly reduced.

Same applies for the model of Kleppe *et al*, where saturation s' needs to be solved from equation

$$P_c(s_{wi}) = P_c^\delta(s')$$

where $\delta = D, I$ represents one of the bounding curves. As before, an analytical expression for the bounding curves and their inverses is convenient. However, bounding curves are based on empirical data and analytical expressions are not always available.

BY TIME DEPENDENCY OF PARAMETERS

Different types of possible time dependency for the hysteresis models are listed here.

1. All relative permeability and capillary pressure hysteresis models are based on bounding curves limited by parameters s_{wc} , s_{nr}^{max} and s_{nc} . These parameters may be subjected to time dependency by other factors,

for instance lower salinity may reduce residual oil, as in section 6.1. Changes in these parameters forcefully change the behaviour of bounding curves.

2. The shape and scale of bounding curves may also be altered by other variables corresponding to the porous medium, or the chemistry of the fluids themselves.

3. The scanning curves in a model such as Killough's are interpolated from the bounding curves. The choice of how to interpolate this scanning curve may also vary over time.

4. In the Scanning Hysteresis Model, for instance, parametrizations π^D and π^I may also change over time, even if the bounding curves remain constant. This change in parametrizations directly affect the shape and length of the scanning curves.

8.3. FINAL REMARKS

In this document, some basic tools to model systems with hysteresis have been shown, as well as a small introduction to the behaviour of their solutions.

To this purpose, several hysteresis models have been revised, for both relative permeability and capillary pressure, and their similarities and advantages have been compared. The fundamental differences between the models are evidence of a physical background that is still under development.

Furthermore, the question of how these models behave under the influence of time depending bounding curves has been posed. An incipient approach to this question has been followed, by proposing new algorithms capable of adopting this feature. For every case, it was shown that the historical data of the system was central to the accuracy of time dependent models.

The interpretation of history in a time dependent system is not trivial. As we have seen, there is more than one way to translate historical information into a new time step, as well as several ways in which the model can vary over time, e.g. as listed in section 7.3.

A methodology was described that generalizes the different methods of keeping track of history. The question of how to translate information over time becomes a question of which trajectories does it follow. Trajectories can be categorized by meaningful parametrizations, and different paths represent fundamentally different physical interpretations.

The methods described in chapter 6 are robust enough to accommodate all of these examples. However the choice of method to adapt the scanning curves must be sensible, it must seek to follow the chosen physical model and be consistent with empirical data. All of these consideration will be central as more physical models arise and give way to better hysteresis models looking to increase precision.

BIBLIOGRAPHY

- [1] K. Aziz and A. Settari, *Petroleum reservoir simulation* (Chapman & Hall, 1979).
- [2] R. J. LeVeque, *Finite volume methods for hyperbolic problems*, Vol. 31 (Cambridge university press, 2002).
- [3] M. R. Todd and W. J. Longstaff, *The development, testing, and application of a numerical simulator for predicting miscible flood performance*, *Journal of Petroleum Technology* **24**, 874 (1972).
- [4] J. A. Larsen and A. Skauge, *Methodology for numerical simulation with cycle-dependent relative permeabilities*, *SPE Journal* **3**, 163 (1998).
- [5] J. E. Killough, *Reservoir simulation with history-dependent saturation functions*, *Society of Petroleum Engineers Journal* **16**, 37 (1976).
- [6] F. M. Carlson, *Simulation of Relative Permeability Hysteresis to the Nonwetting Phase*, in *SPE Annual Technical Conference and Exhibition* (Society of Petroleum Engineers, 1981).
- [7] C. S. Land, *The Optimum Gas Saturation for Maximum Oil Recovery from Displacement by Water. Paper SPE 2216 presented at the Fall Meeting of the Society of Petroleum Engineers of AIME, Houston, 29 September–2 October*, (1968).
- [8] B. Plohr, D. Marchesin, P. Bedrikovetsky, and P. Krause, *Modeling hysteresis in porous media flow via relaxation*, *Computational Geosciences* **5**, 225 (2001).
- [9] R. E. Gladfelter and S. P. Gupta, *Effect of fractional flow hysteresis on recovery of tertiary oil*, *Society of Petroleum Engineers Journal* **20**, 508 (1980).
- [10] E. M. Braun and R. F. Holland, *Relative permeability hysteresis: Laboratory measurements and a conceptual model*, *SPE Reservoir Engineering* **10**, 222 (1995).
- [11] C. E. Schaerer, D. Marchesin, M. Sarkis, and P. Bedrikovetsky, *Permeability hysteresis in gravity counterflow segregation*, *SIAM Journal on Applied Mathematics* **66**, 1512 (2006).
- [12] J. Kleppe, P. Delaplace, R. Lenormand, G. Hamon, and E. Chaput, *Representation of capillary pressure hysteresis in reservoir simulation*, in *SPE Annual Technical Conference and Exhibition* (Society of Petroleum Engineers, 1997).
- [13] G. R. Jerauld, K. J. Webb, C.-Y. Lin, and J. C. Seccombe, *Modeling low-salinity waterflooding*, *SPE Reservoir Evaluation & Engineering* **11**, 0 (2008).
- [14] K. M. Furati, *Effects of relative permeability history dependence on two-phase flow in porous media*, *Transport in Porous Media* **28**, 181 (1997).
- [15] R. C. MacDonald, *Methods for numerical simulation of water and gas coning*, *Society of Petroleum Engineers Journal* **10**, 425 (1970).
- [16] D. W. Peaceman, *Fundamentals of Numerical Reservoir Simulation*. 1977, .
- [17] E. E. Templeton, R. F. Nielsen, and C. D. Stahl, *A study of gravity counterflow segregation*, *Society of Petroleum Engineers Journal* **2**, 185 (1962).
- [18] F. M. Van Kats and C. J. Van Duijn, *A mathematical model for hysteretic two-phase flow in porous media*, *Transport in Porous Media* **43**, 239 (2001).
- [19] PetroWiki, *PEH relative permeability and capillary pressure*, (2007).